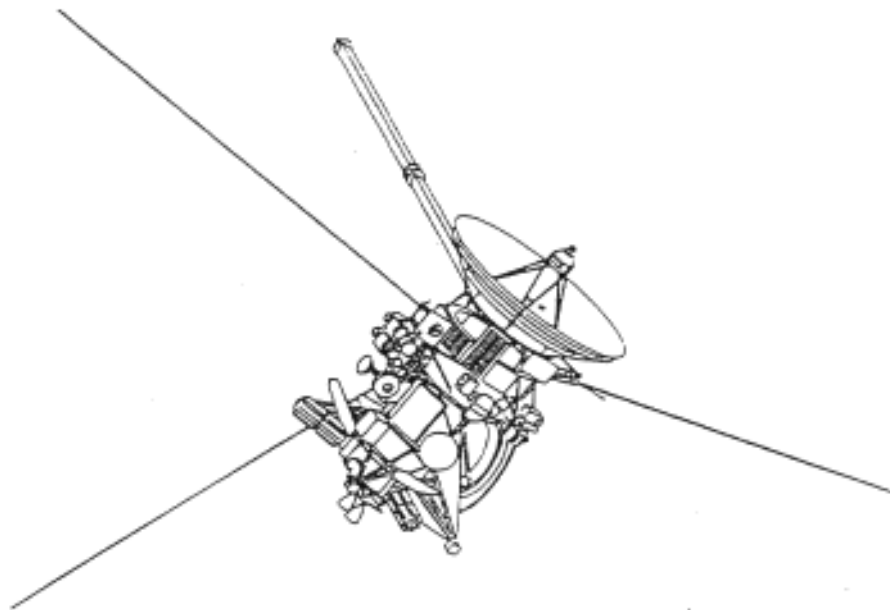


699-70-3-Sup

# Cassini Earth Swingby Plan Supplement



19 May 1997

**JPL**  
Jet Propulsion Laboratory  
California Institute of Technology

JPL D-10178-3

## CONTENTS

0. OVERVIEW .....	0-1
0.1 INTRODUCTION.....	0-1
0.2 WHY CASSINI WILL NOT IMPACT THE EARTH.....	0-2
0.2.1 Why Cassini Will Not Impact The Earth During the Short-Term .....	0-3
0.2.2 Why Cassini Will Not Impact The Earth During The Long-Term .....	0-4
0.3 METHODOLOGY.....	0-6
0.4 EARTH IMPACT PROBABILITY ASSESSMENT .....	0-9
0.5 SUMMARY .....	0-9
1. INTRODUCTION.....	1-1
1.1 PURPOSE OF THIS SUPPLEMENT.....	1-1
1.2 ORGANIZATION OF THE SUPPLEMENT .....	1-1
2. METHODOLOGY.....	2-1
2.1 INTRODUCTION.....	2-1
2.2 FAILURE MODE ANALYSIS.....	2-4
2.3 SHORT-TERM IMPACT PROBABILITY .....	2-6
2.4 LONG-TERM IMPACT PROBABILITY.....	2-7
2.5 EARTH IMPACT PROBABILITY ASSESSMENT .....	2-9
3. FAILURE MODES .....	3-1
3.1 METHODOLOGY.....	3-1
3.1.1 Introduction .....	3-1
3.1.2 Estimate Uncertainties .....	3-1
3.1.3 Summary of Results .....	3-3
3.2 DELTA-V INDUCING FAILURES .....	3-3
3.2.1 Micrometeoroid-Induced Failures.....	3-3
3.2.2 Additional Failure Mode Analysis.....	3-25

3.3	INTERNAL SPACECRAFT FAILURES .....	3-27
3.3.1	Internal Bus Probability of Failure.....	3-27
3.3.2	Bayesian Corection Factor to Bus Micrometeoroid Failure.....	3-29
3.4	INCREASED MICROMETEOROID SHIELDING .....	3-30
3.4.1	Changes in Spacecraft Design to Reduce Failure Probabilitied Due to Micrometeoroid Impact .....	3-31
3.5	PROBABILITY OF NO RECOVERY ( $P_{NR}$ ).....	3-33
4.	SHORT-TERM EARTH IMPACT PROBABILITY.....	4-1
4.1	INTRODUCTION.....	4-1
4.2	MANEUVER STRATEGY .....	4-1
4.3	NAVIGATION MODELS.....	4-9
4.4	SHORT-TERM IMPACT PROBABILITY COMPUTATIONS	4-9
4.5	ENTRY ANGLE AND ENTRY LATITUDE COMPUTATIONS.....	4-9
4.6	EARTH IMPACT PROBABILITIES .....	4-10
5.	LONG-TERM EARTH IMPACT PROBABILITY.....	5-1
5.1	INTRODUCTION.....	5-1
5.2	METHOD .....	5-1
5.2.1	Trajectory Design Strategy .....	5-6
5.2.2	Monte Carlo Case Formulation .....	5-8
5.3.3	Orbital Geometry Required For Impact.....	5-9
5.3	RESULTS.....	5-15
5.3.1	Uncertainty Analysis.....	5-16
5.3.2	Long-Term Earth Impact Probability.....	5-17
5.3.3	Influence of Trajectory Characteristics on Long-Term Earth Impact Probability .....	5-21

5.4 Conclusions .....	5-25
6. EARTH IMPACT PROBABILITY ASSESSMENT.....	6-1

## LIST OF FIGURES

Figure 0-1	Simplified Logic Tree for Portraying Short-Term Earth Impact Threat (T) .....	0-7
Figure 0-2	Simplified Logic Tree for Portraying Long-Term Earth Impact Threat (T) .....	0-8
Figure 0-3	Primary Mission Probability Density Function.....	0-10
Figure 0-4	Primary Mission Complementary Cumulative Probability .....	0-10
Figure 0-5	Secondary Mission Probability Density Function.....	0-11
Figure 0-6	Secondary Mission Complementary Cumulative Probability .....	0-11
Figure 2-1	Earth Impact Probability Assessment Methodology.....	2-2
Figure 3-1	Micrometeoroid Evaluation Program Process .....	3-6
Figure 3-2	TRASYS Modeling of Cassini.....	3-7
Figure 3-3	Representative Test Configuration and Projectile .....	3-9
Figure 3-4A	Range Test Results for the S2, E2 Matrix Standard MLI.....	3-11
Figure 3-4B	Range Test Results for the S2, E2 Matrix Using Beta MLI .....	3-11
Figure 3-5A	Test Results Examining Shield Spacing Bet $\beta_{\text{Cloth}}$ and $\beta_{\text{MLI}}$ .....	3-13
Figure 3-5B	Crater Depth Distribution as a Function of Incident Particle Mass.....	3-14
Figure 3-5C	Rough Estimate of the Probability of No Damage to Ti Plate and the Probability of Perforation of Ti Plate .....	3-15
Figure 3-6	Results of Higher Velocity Calculations Which Determine Critical Mass vs. Velocity at 2, 10 and 18 Inch Spacing .....	3-18
Figure 3-7	Probability of Tank Failure from Venus-20 Days to Earth Flyby .....	3-20

Figure 3-8	Calculated Probabilities for Possible Scenario Paths Result from Micrometeoroid Damage to Propellant Tanks.....	3-21
Figure 3-9	Spacecraft $\Delta V$ Magnitude and Direction as a Result of Micrometeoroid Induced Tank Failure .....	3-23
Figure 3-10	Total Probability of Failure vs. Time from Launch .....	3-29
Figure 3-11	Original S/C Blanket Configuration.....	3-30
Figure 3-12	Modified S/C Blanket Configuration for Micrometeoroid Protection .....	3-32
Figure 3-13	Probability of No Recovery Logic.....	3-33
Figure 3-14	Probability of No Recovery Ground Error Component .....	3-35
Figure 3-15	Probability of No Recovery 77 to 2 Days Before Earth Flyby, Primary Mission .....	3-36
Figure 4-1	Cassini Primary Mission VVEJGA Trajectory-Earth B-Plane.....	4-6
Figure 4-2	Cassini Secondary Mission VVEJGA Trajectory-Earth 1 B-Plane.....	4-6
Figure 4-3	Cassini Secondary Mission VVEJGA Trajectory-Earth 2 B-Plane.....	4-8
Figure 4-4	Primary Mission: Complementary Cumulative Probability Distribution.....	4-14
Figure 4-5	Primary Mission: Probability Density Function .....	4-15
Figure 4-6	Primary: Probability vs. Entry Angle.....	4-16
Figure 4-7	Primary: Entry Angle Cumulative Probability .....	4-16
Figure 4-8	Primary Mission: Entry Latitude Probability Distribution.....	4-17
Figure 4-9	Secondary-E1: Complementary Cumulative Probability .....	4-18
Figure 4-10	Secondary-E1: Probability Density Function .....	4-19
Figure 4-11	Secondary-E1: Probability vs. Entry Angle .....	4-20

Figure 4-12	Secondary-E1: Entry Angle Cumulative Distribution .....	4-20
Figure 4-13	Secondary-E1: Entry Latitude Probability Distribution .....	4-21
Figure 4-14	Secondary-E2: Complementary Cumulative Probability .....	4-22
Figure 4-15	Secondary-E2: Probability Density Function .....	4-23
Figure 4-16	Secondary-E2: Probability vs. Entry Angle .....	4-24
Figure 4-17	Secondary-E2: Entry Angle Cumulative Distribution .....	4-25
Figure 4-18	Secondary-E2: Entry Angle Latitude Distribution .....	4-25
Figure 5-1	Orbital Geometry and Phasing Required For Earth Impact .....	5-4
Figure 5-2	Process for Computing Long-Term Earth Impact Probability for Each Mission .....	5-6
Figure 5-3	Spacecraft and Earth Orbit Intersection Geometry .....	5-14
Figure 5-4	Range of Planet Motion for Which Intersection is Possible .....	5-14
Figure 5-5	Long-Term Earth Impact Probability Density Function for Primary Mission .....	5-19
Figure 5-6	Long-Term Earth Impact Complementary Cumulative Distribution for Primary Mission .....	5-19
Figure 5-7	Long-Term Earth Impact Probability Density Function for Secondary Mission .....	5-20
Figure 5-8	Long-Term Earth Impact Complementary Cumulative Distribution for Secondary Mission .....	5-20
Figure 6-1	Primary Mission Probability Density Function .....	6-2
Figure 6-2	Primary Mission Complementary Cumulative Probability .....	6-2

Figure 6-3	Secondary Mission Probability Density Function .....	6-3
Figure 6-4	Secondary Mission Complementary Cumulative Probability .....	6-3

## LIST OF TABLES

Table 3-1	Spacecraft Components, Ground Induced Error and Flight Software Failure Probabilities and $\Delta V$ Effects.....	3-37
Table 3-2	Estimates of Critical Incident Particle Mass .....	3-49
Table 4-1	Primary Mission - Venus to Earth Maneuver/Event Profile .....	4-3
Table 4-2	Secondary Mission - Venus to Earth 1 Maneuver/Event Profile .....	4-5
Table 4-3	Secondary Mission - Earth 1 to Earth 2 Maneuver/Event Profile .....	4-5
Table 4-4	TCM Execution Errors ( $3\sigma$ ) .....	4-9
Table 4-5	$1\sigma$ Orbit Determination Uncertainty in B-Plane Position .....	4-10
Table 4-6	Short-Term Mean Earth Impact Probabilities.....	4-13
Table 5-1	Dominant Contributors to $N_{CRX}/N_{CASE}$ and $P_{I/CRX}$ Uncertainties.....	5-17

## OVERVIEW

### 0.1 INTRODUCTION

The Cassini mission requires trajectories that use planetary swingbys to achieve the necessary energy and orbit shaping to reach Saturn. The proposed baseline or primary trajectory for Cassini is a Venus-Venus-Earth-Jupiter-Gravity-Assist (VVEJGA) transfer to Saturn. The launch period for this opportunity extends from October 6 to November 15, 1997. As the name implies, the VVEJGA trajectory makes use of four gravity-assist planetary swingbys between launch from Earth and arrival at Saturn. This use of planetary gravity assists reduces launch energy requirements, compared to other Earth-Saturn transfer modes, and allows the spacecraft to be launched by the Titan IV (SRMU)/Centaur. Direct Earth-Saturn transfers with this launch vehicle are not possible for Cassini.

The baseline plan calls for the Cassini spacecraft to use Radioisotope Thermoelectric Generators (RTGs) to supply electrical power. Therefore, precautions must be taken to ensure that an inadvertent reentry into the Earth's atmosphere, defined for this report as Earth impact, does not occur in the course of performing the Earth swingby. The situation is analogous to previous missions where navigation techniques and mission operations were designed to ensure either Earth impact avoidance (Galileo mission to Jupiter) or Mars protection from microbiological contamination (Mariner and Viking missions to Mars).

Design precautions must also be taken to preclude Earth impact resulting from loss of control of the spacecraft during interplanetary cruise. If the spacecraft were to drift in its orbit around the Sun, Earth impact could result decades to millennia later after many spacecraft orbits around the Sun.

To ensure that an accidental Earth impact is not a credible event, the Cassini Project has levied a design requirement in its Project Policies and Requirements Document that the probability of Earth impact be less than one in a million. To satisfy this requirement an assessment of the Earth impact probability has been performed. The probability of Earth impact is presented as a probability distribution over the model uncertainty rather than a worst-case value. The advantage of such an approach is to provide information about the uncertainty of the estimation of the Earth impact probability. The above requirement is interpreted to be that the expected value of the Earth impact probability, from injection to 100 years beyond the time of spacecraft failure, shall not exceed  $10^{-6}$ .

In November 1993 the Cassini Earth Swingby Plan was documented in Volume 3 of the "Cassini Program Environmental Impact Statement Supporting Study". Included was a quantitative assessment

of the probability of Earth impact for both the primary mission and the backup mission (March 19 to April 4, 1999 launch opportunity) that showed that the  $10^{-6}$  requirement was satisfied.

Since publication of the Earth Swingby Plan, more analysis has taken place which has resulted in additional blanketing and shielding being added to the spacecraft, and additional bias being incorporated into the spacecraft's trajectory to maintain the  $10^{-6}$  requirement. Also, the secondary mission (November 28, 1997-January 11, 1998 launch opportunity) has been analyzed. A trajectory biasing strategy for the secondary mission has been selected that satisfies the Earth swingby requirement. Earth impact probabilities for the backup mission opportunity have not been updated. Our previous analysis indicates that the Earth swingby requirement can be satisfied for a smaller  $\Delta V$  penalty than was used for the secondary mission.

In this supplement the updated analyses for both the primary and secondary missions are presented. This supplement, combined with the Earth Swingby Plan, provides the documentation that the Earth swingby requirement is being satisfied.

## 0.2 WHY CASSINI WILL NOT IMPACT THE EARTH

The Cassini mission is being designed so that the probability of an inadvertent Earth reentry is less than one in a million. Achieving this has been more than a mathematical exercise. A number of features have been incorporated into the design of the Cassini spacecraft, how the spacecraft is flown and monitored, and in the design of the interplanetary trajectory to enable Cassini to safely swing by the Earth and to avoid any future Earth impacts for at least 100 years.

Inadvertent Earth reentry by Cassini is examined during two distinct time regimes since the methodology used to study each time regime is quite different. The first time regime is a short-term time frame during which failures before Earth swingby could result in an Earth-impacting trajectory. These failures could be in the spacecraft, in the ground-control system, or induced by the environment (e.g., micrometeoroid impact). The second time regime is a long-term time frame in which a failure has disabled Cassini, leaving it to drift, possibly in an Earth-crossing heliocentric trajectory. These failures are usually spacecraft system internal failures. Inadvertent Earth reentry up to 100 years beyond the time of spacecraft failure is considered.

It is important to realize that a spacecraft failure does not automatically mean that Cassini will reenter the Earth's atmosphere either at the Earth swingby or at a much later date. For the short-term time frame, the failure must cause a change to the spacecraft's velocity of exactly the required magnitude and direction to place it on an impacting trajectory. Even then, it may be possible to take corrective action to place the spacecraft on a non-impacting trajectory. For the long-term time frame, the gravitational effects of the planets must alter the spacecraft's trajectory such that impact occurs sometime

within the next 100 years. Long-term Earth impact requires very specific spacecraft orbital geometry and phasing, which are intentionally avoided during design of the interplanetary trajectory. In order for Earth impact to occur in either the short or long-term time regime, an unlikely chain of events must occur, and the probability of these events has been minimized by design.

#### 0.2.1 WHY CASSINI WILL NOT IMPACT THE EARTH DURING THE SHORT-TERM

A key to achieving low impact probability for the short-term time frame is to bias the interplanetary trajectory so that hitting the Earth requires an unexpected change in the spacecraft's velocity. Up until the last 20 days before Earth swingby, the trajectory is biased so that Cassini will pass by the Earth at a distance of many tens of thousands of kilometers. The trajectory bias is reduced in increments as Cassini approaches Earth swingby. That way, if Cassini is permanently disabled prior to the last bias removal maneuver, 6.5 days before Earth swingby, there is an extremely high probability that Cassini will safely pass the Earth at a far distance.

Due to the trajectory bias, any spacecraft, ground system, or environmentally-induced failure that does not cause a  $\Delta V$  is not a concern for inadvertent reentry during the Earth swingby. If a failure prior to the last Venus swingby results in a  $\Delta V$ , it is very difficult for Cassini to impact the Earth. As Cassini approaches Earth, the likelihood of an inadvertent  $\Delta V$  causing Earth impact becomes larger. After the last Venus swingby, the minimum  $\Delta V$  required to reach Earth is about 12 m/s. This minimum  $\Delta V$  decreases to around 1.6 m/s, 6.5 days before Earth swingby as the trajectory bias is removed. Given the mass of Cassini, the only energy sources on the spacecraft that could cause a  $\Delta V$  greater than 1.6 m/s are related to the pressurized tanks and lines of the propulsion system. Therefore, the biasing strategy focuses the issue of inadvertent reentry on propulsion system failures that cause a  $\Delta V$  greater than 1.6 m/s.

An unplanned  $\Delta V$  attributable to the spacecraft propulsion system could result from a rupture or leak in a pressurized portion of the system or a stuck-open valve during one of the four orbit correction burns during the period between the Venus and Earth swingbys. Experience has shown that such failures occur principally when the state of the system is changed by command : an engine firing, a valve opening, or a repressurization. Therefore, to minimize this risk for the Cassini Earth swingby, the spacecraft is placed in a benign state for most of the cruise between Venus and Earth. This is achieved by isolating that portion of the propulsion system used to pressurize the propellant and oxidizer tanks. This mode of operation, in which the propulsion system operates on residual tank pressure only, is known as Slowdown. There have been no catastrophic propulsion system failures when operating in a slowdown state.

If a failure were to occur, Cassini has an autonomous fault-protection system designed to sense a propulsion system failure and terminate the inadvertent burn. If the fault protection system could not limit the resultant  $\Delta V$  (a propulsion system leak or stuck valve), the failure would have to cause a  $\Delta V$  greater than the required maneuver in a direction that could cause Earth impact. In addition, Cassini is tracked continuously during this critical period and could be commanded to miss Earth unless the redundant propulsion systems or some part of the command system has failed as well. Therefore, inadvertent Earth reentry requires an unlikely sequence of failures during a limited period of time.

The only propulsive maneuvers during the cruise period between Venus and Earth will be the four required trajectory correction maneuvers, which are needed to remove the trajectory bias and achieve the desired swingby altitude. The propulsive system failures observed in the past generally occurred during burns. For Cassini, however, these burns will be performed with the system in blowdown mode. This will avoid repressurization and the need to fire pyro valves which were the conditions implicated in the failure of the Mars Observer spacecraft. Also, the propulsion system will have been used in this mode at least 6 times prior to the second Venus swingby which will provide ample data to confirm the stability and reliability of the system.

The minimum Earth swingby altitude is 800 km for Cassini and is only used for several days during the first half of the launch period. For days in the second half of the launch period the Earth swingby altitude increases to between 1200 and 1800 km. The Galileo spacecraft performed two successful Earth swingbys with closest approach for the second Earth swingby at 303 km. The higher Cassini swingby altitude helps reduce the probability of Earth impact to less than one in a million.

#### 0.2.2 WHY CASSINI WILL NOT IMPACT THE EARTH DURING THE LONG-TERM

A key to achieving a low Earth impact probability for the long-term time frame is to bias the interplanetary trajectory such that the post-failure-spacecraft trajectory is initially far from Earth's orbital distance and remains so during the next 100 years. Many segments of the trajectory do not require biasing to achieve low impact probability, since many post failure trajectories naturally do not pass near Earth's orbit.

The long-term impact probability is a function of the interplanetary trajectory characteristics of the spacecraft at failure and during the next 100 years. For failure during much of the interplanetary cruise, the realm of resulting spacecraft trajectories naturally have characteristics which ensure a very low probability of long-term Earth impact. For failure times which result in trajectories with a higher long-term Earth impact probability, the interplanetary trajectory was modified, often at the expense of additional propellant, by redesigning the nominal swingby aimpoints. Modification of the swingby aimpoints was done

in conjunction with the short-term analysis, since the swingby aimpoints influence both the short and long-term Earth impact probability.

In order for long-term Earth impact to take place, a series of low probability events must occur. In order for any chance of Earth impact, the spacecraft must be present in the solar system. For nearly all failures during the second half of the interplanetary cruise on both the primary and secondary missions, the spacecraft is ejected from the solar system by the strong Saturn gravity assist, precluding any possibility of Earth impact. For failures on the Jupiter to Saturn leg of the primary mission, the Jupiter gravity assist raises the spacecraft orbit periapsis (closest approach distance to the Sun) well above the distance of the Earth from the Sun precluding any possibility of Earth impact. The periapsis radius remains above this initial value for the duration of the long-term analysis. Therefore, gravity assists by the massive outer planets virtually assure that failures during the last 72% of the primary and last 50% of the secondary interplanetary cruise do not result in Earth impact.

To compute the probability of long-term Earth impact for spacecraft orbits which do cross Earth's orbital distance after failure, the number of passages of the spacecraft through the Earth torus are counted. The Earth torus is the volume swept out by the Earth as it orbits the Sun. The spacecraft may be on an Earth torus-crossing orbit at the failure time or may eventually be put on one by orbital perturbations. For each passage through the torus, the probability that both the Earth and spacecraft occupy the same portion of the torus at the same time is then evaluated.

The initial proximity of the spacecraft trajectory to the torus after failure is an indication of the likelihood of long-term Earth impact. Some trajectory segments of the interplanetary cruise which cross Earth's orbital distance naturally do not pass within the vicinity of Earth's torus during a 100 year time period, and thus the probability of long-term Earth impact on these segments is very low. For failures which result in crossings in the vicinity of the Earth torus, swingby aimpoints are designed such that most trajectories remain far away from the Earth torus and stay far away over the next 100 years. Some torus crossings over 100 years are unavoidable since aimpoint dispersions can be quite large and at least one leg of the trajectory is targeted for an Earth swingby. When deemed necessary, aimpoints were modified in an iterative manner using the short-term aimpoints as initial values. Care was taken to ensure that the short-term impact probability was not increased.

Other aimpoint design strategies were also employed to reduce torus crossings thereby lowering Earth impact probability. For example, on the Earth-1 to Earth-2 leg of the secondary mission, the inclination of the spacecraft orbit with respect to the Earth's orbital plane was increased from near zero to  $0.2^\circ$  by expending

additional  $\Delta V$  at the large deep space maneuver. This inclination change decreases the likelihood of passing through the Earth torus in the event of a spacecraft failure.

In order for Earth impact to occur at a torus passage, at the time the spacecraft crosses the Earth torus, the Earth and spacecraft must occupy the same space in the torus at the same time - another highly unlikely event since the Earth's diameter is about 5 orders of magnitude smaller than its orbital circumference. The probability that the Earth is in the proper position in the torus for impact is quite small and on the order of  $10^{-5}$ .

### 0.3 METHODOLOGY

As discussed in Subsection 0.2, an inadvertent Earth reentry by Cassini could occur during two distinct time regimes. The first time regime is a short-term time frame during which failures before Earth swingby could result in a Earth-impacting trajectory. The second time regime is a long-term time frame in which a failure has disabled Cassini, leaving it to drift possibly in an Earth-crossing heliocentric trajectory. Inadvertent Earth reentry up to 100 years beyond the time of spacecraft failure is considered.

The approach to calculating the short-term probability of inadvertent reentry is shown in Figure 0-1. The "failure logic tree" identifies those combinations of events needed to cause Earth reentry. This logic tree shows that there are two paths that lead to inadvertent Earth reentry. The first path portrays the scenario where the mission appears to be proceeding normally, when, in fact, the spacecraft is on an impacting trajectory due to an undetected navigation model error. Ground system procedures eliminate this as a credible scenario for Earth impact.

The second path portrays the scenario where there has been a failure which has resulted in a  $\Delta V$  being imparted to the spacecraft. Inadvertent reentry occurs if the failure  $\Delta V$  places the spacecraft on an Earth impacting trajectory and a trajectory correction maneuver is not possible. The Earth swingby analysis requires that all spacecraft, ground system or environmentally induced failures that could cause a change in velocity be identified. For each failure mode, design approach, test data, flight experience, and engineering judgment are used to estimate the 10, 50, and 90% failure probabilities or to generate probability distributions. For each of these failure modes, the resultant velocity distributions are calculated and used to determine the probability of Earth impact if a failure occurs. These impact probabilities are combined with the failure probabilities and the probability of recovery for each failure. A thousand Monte Carlo runs calculate the probability distributions for Earth impact.

The approach to calculating the long-term probability of inadvertent reentry is shown in Figure 0-2. This "failure logic tree" illustrates the combination of events required for long-term Earth

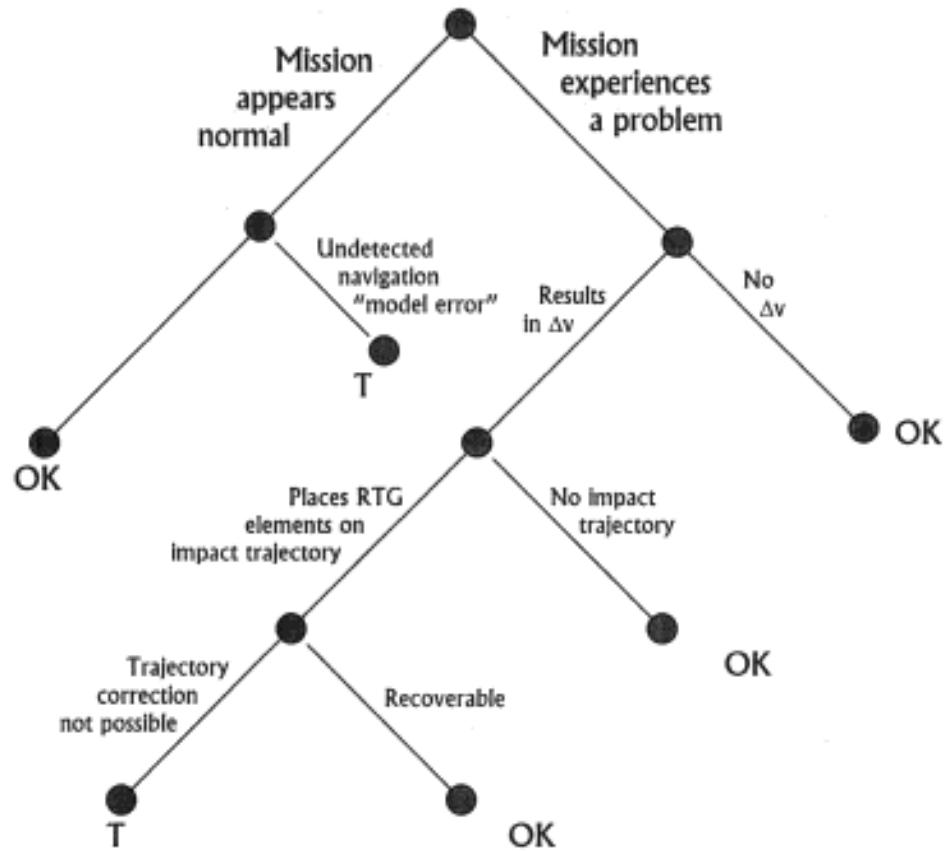


**Figure 0-1. SIMPLIFIED LOGIC TREE FOR PORTRAYING SHORT-TERM EARTH IMPACT THREAT (T)**

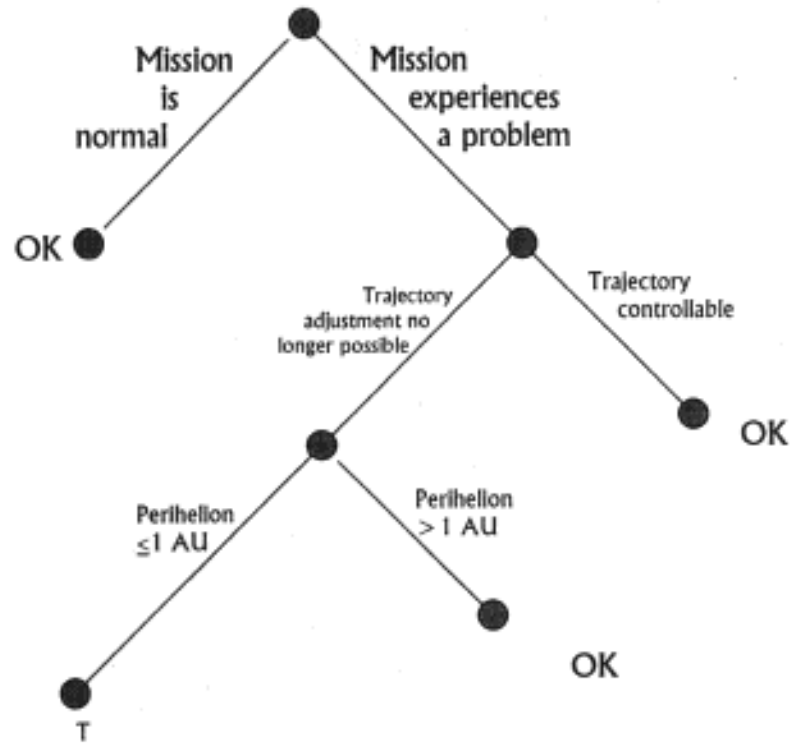


**Figure 0-2. SIMPLIFIED LOGIC TREE FOR PORTRAYING LONG-TERM EARTH IMPACT THREAT (T)**

impact. If the spacecraft becomes uncommendable before Saturn orbit insertion and does not impact the Earth during a targeted swingby, there is still a remote possibility that long-term perturbations to the orbit could cause the spacecraft to eventually reencounter the Earth. The probability of long-term Earth impact depends on the heliocentric trajectory of the spacecraft resulting from the failure and its evolution over the next 100 years caused by third-body gravitational perturbations. The trajectory perihelion must be less than or equal to the Earth's orbit to allow the possibility of the spacecraft trajectory intercepting the Earth's torus.

Because of the difficulty of analytically predicting the third-body effects on the spacecraft trajectory, numerical predictions of Cassini orbits were made from the trajectory and velocity statistics for possible spacecraft failures. These were projected 100 years to give the probable number of Earth orbit torus crossings. For each crossing the probability of Earth intercept was calculated using a modification of existing theory that has been used in orbit lifetime analysis of asteroids and comets. Since a single trajectory propagation would not be representative of the range of possible spacecraft trajectories that could result given a failure at any time during interplanetary cruise, a Monte Carlo analysis was performed using thousands of trajectories considering a wide range of failure times.

#### 0.4 EARTH IMPACT PROBABILITY ASSESSMENT

The Project requirement on the Earth Swingby Plan is that the probability of Earth impact be less than or equal to one in a million ( $10^{-6}$ ). A number of parameters can be used to describe the characteristics and interpretation of a probability density function (p.d.f.) or of a complementary cumulative probability curve. The "expected value" of a random variable is expressed by the mean of the probability distribution. Thus, the Project requirement that the probability of Earth impact be less than or equal to  $10^{-6}$  has been considered met when the mean of the assessed probability distribution is less than or equal to  $10^{-6}$ .

The total Earth impact probability distribution is the probabilistic sum of the short-term and long-term Earth impact probability distributions. A 1,000-trial Monte Carlo simulation was used to perform this probabilistic summation. The p.d.f.s and complementary cumulative probabilities for the primary and secondary trajectories are presented in Figures 0-3 through 0-6. The mean values of these distributions are  $7.6 \times 10^{-7}$  for the primary trajectory and  $8.3 \times 10^{-7}$  for the secondary trajectory. Since the mean of both distributions is less than  $10^{-6}$ , the Earth swingby requirement is satisfied for both missions.

#### 0.5 SUMMARY

The Cassini mission satisfies the Earth swingby requirement that the mean probability of inadvertent reentry into the Earth's

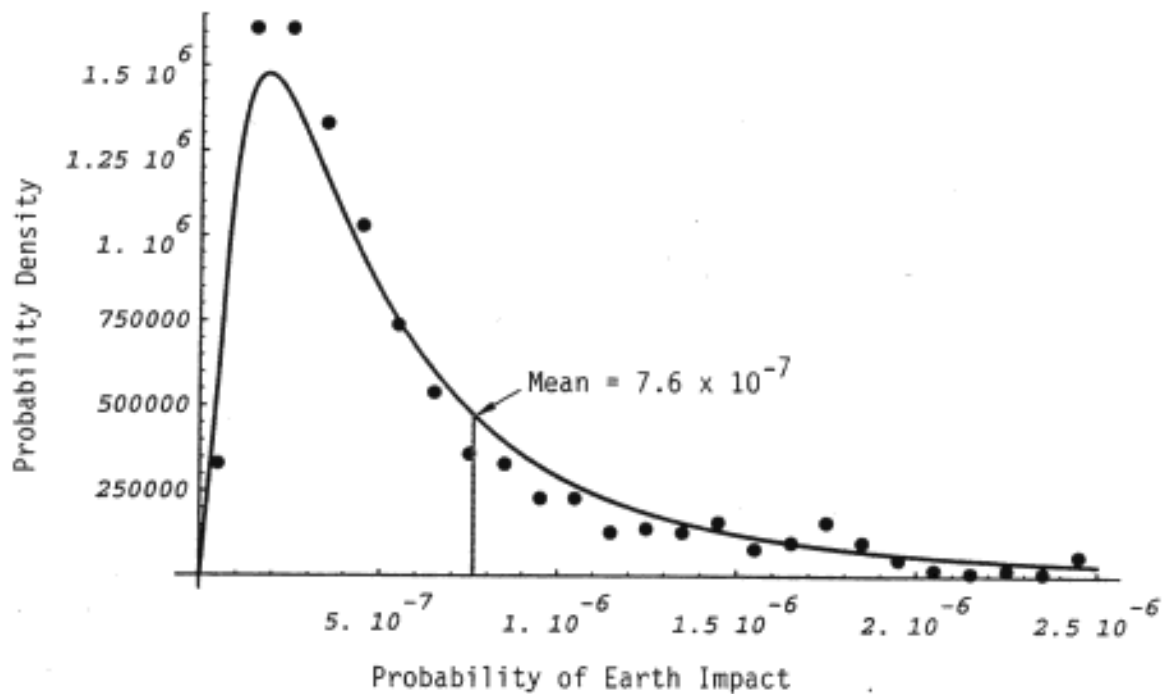


Figure 0-3 Primary Mission Probability Density Function

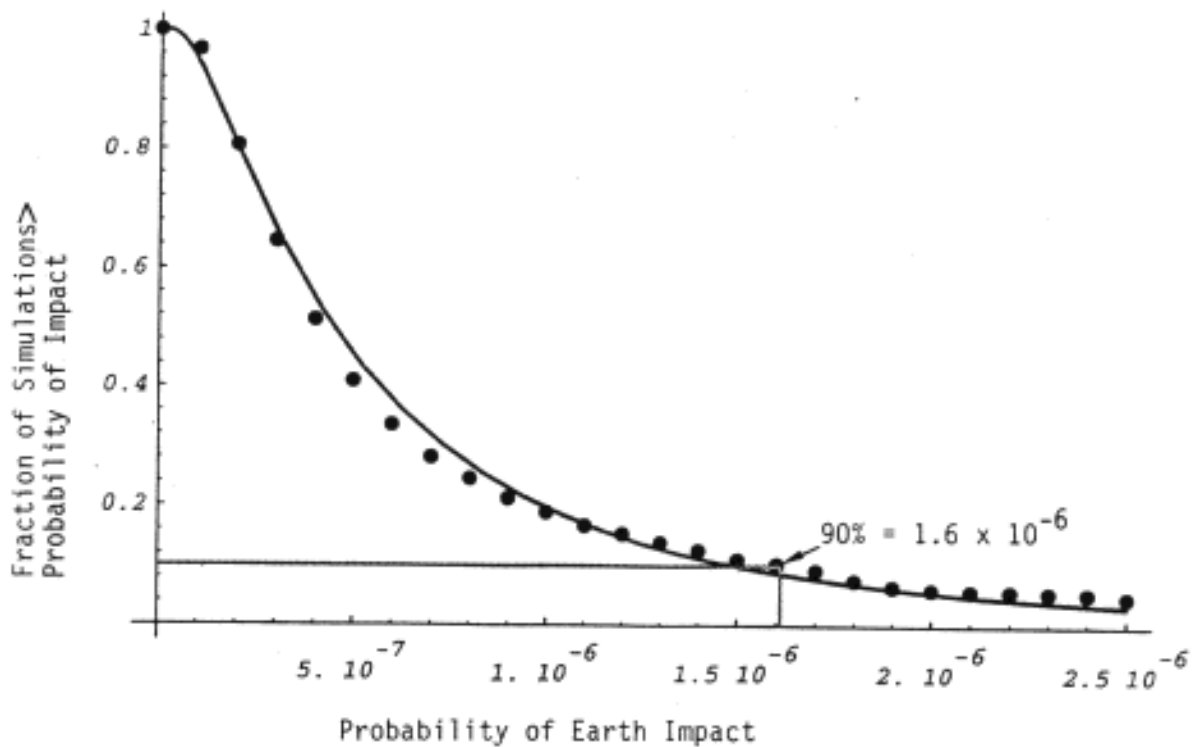


Figure 0-4 Primary Mission Complementary Cumulative Probability

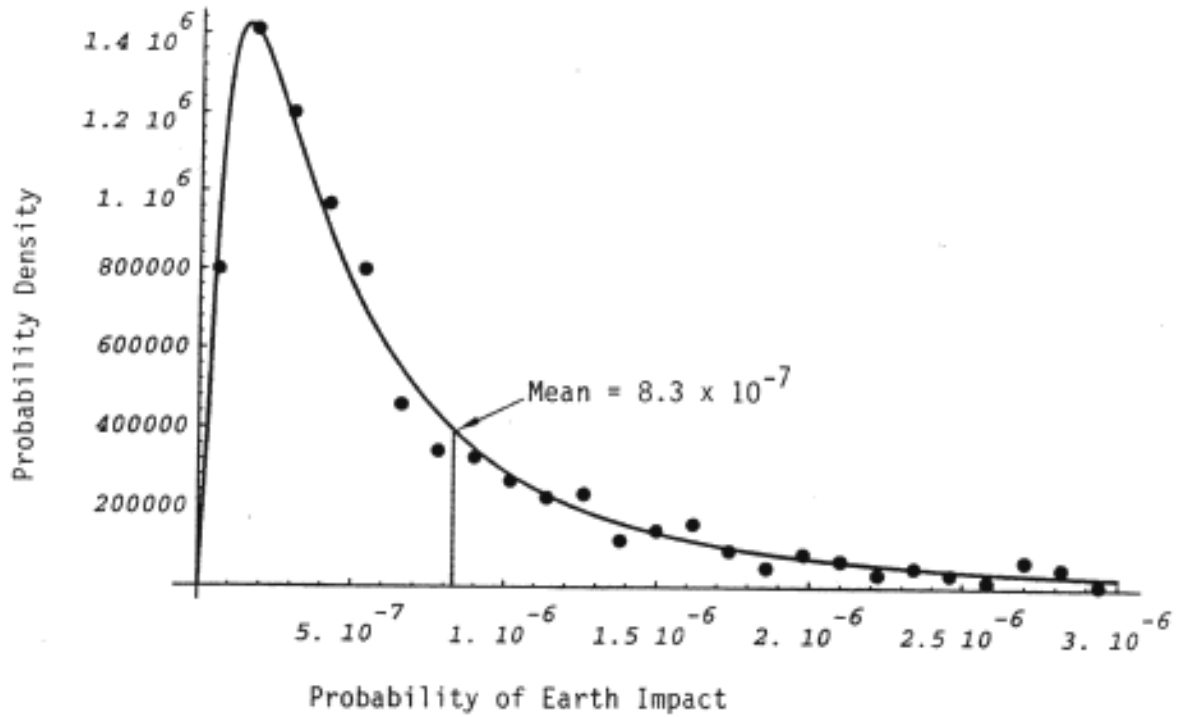


Figure 0-5 Secondary Mission Probability Density Function

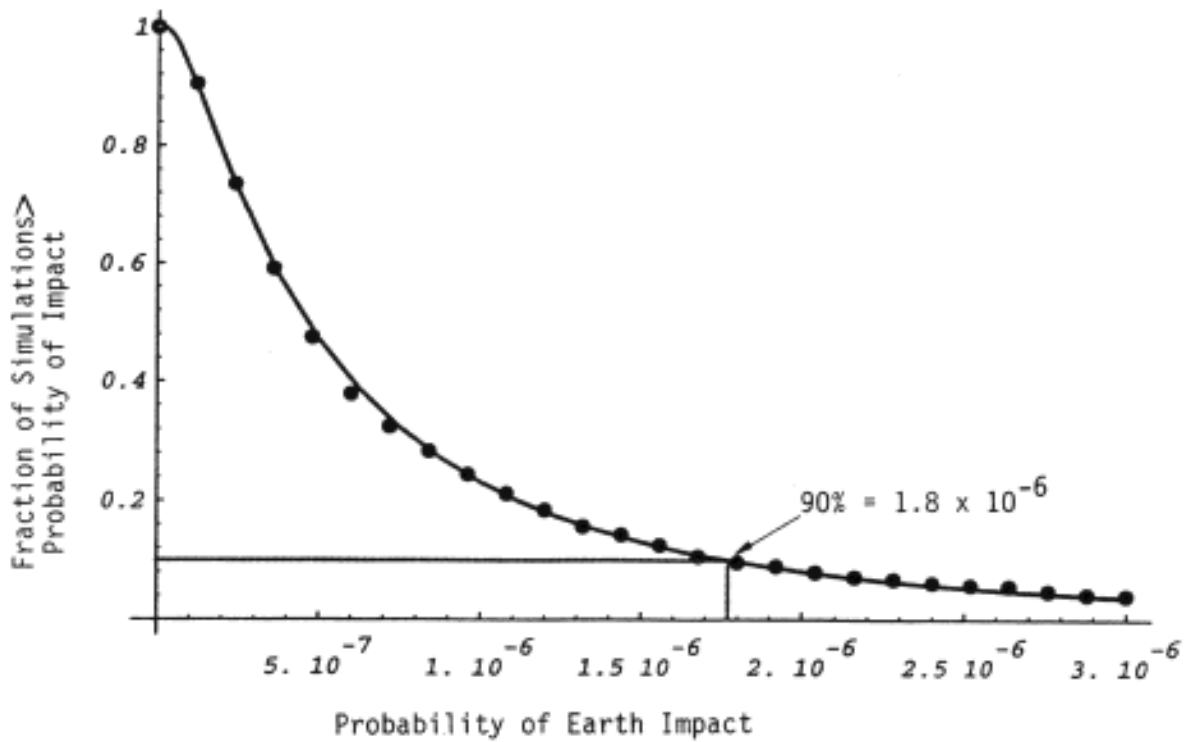


Figure 0-6 Secondary Mission Complementary Cumulative Probability

atmosphere be less than one in a million. Both short and long-term time frames are considered. The basic design of the spacecraft is robust, with redundancy in most hardware and software subsystems and built-in fault detection and correction for many classes of problems.

The trajectory biasing strategy assures that it is extremely unlikely for the spacecraft to be placed on an Earth-impacting path . After the second Venus swingby, Cassini can only impact the Earth if there is a failure that imparts a  $\Delta V$  greater than between 1.6 and 12 m/s in exactly the proper direction. Cassini is placed in a benign state prior to Earth swingby with minimal propulsion system commands to reduce the probability of failures that can provide a  $\Delta V$ . During this critical Earth swingby period, Cassini will be tracked continuously so that the ground system can independently detect and correct any  $\Delta V$ s that might result in an Earth impact trajectory.

The interplanetary trajectory is also designed to minimize the probability of Earth impact for a 100 year time period commencing at spacecraft failure. For failures during cruise which tend to place the spacecraft on a trajectory which crosses near the Earth torus, the swingby aimpoints were designed to insure that most post-failure trajectories were biased away from the vicinity of the Earth torus for at least 100 years past failure. Aimpoint design was performed in conjunction with the short-term biasing strategy. Failures during many portions of interplanetary cruise naturally result in trajectories which do not contribute to Earth impact probability. Gravity assists by the massive outer planets virtually assure that failures during the last 72% of the primary and last 50% of the secondary interplanetary cruise do not result in long-term Earth impact.

## SECTION 1

### INTRODUCTION

#### 1.1 PURPOSE OF THIS SUPPLEMENT

In November 1993 the Cassini Earth Swingby Plan was documented in Volume 3 of the Cassini Program Environmental Impact Statement Supporting Study. Included was a quantitative assessment of the probability of Earth impact for both the primary mission and the backup mission (March 19 to April 4, 1999 launch opportunity) that showed that the  $10^{-6}$  requirement was satisfied.

Since publication of the Earth Swingby Plan, more analysis has taken place which has resulted in additional blanketing and shielding being added to the spacecraft and additional bias being incorporated into the spacecraft's trajectory to maintain the  $10^{-6}$  requirement. Also, the secondary mission (November 28, 1997-January 11, 1998 launch opportunity) has been analysed. A trajectory biasing strategy for the secondary mission has been selected that satisfies the Earth swingby requirement.

In this supplement the updated analyses for both the primary and secondary missions are presented. This supplement, combined with the Earth Swingby Plan, provides the documentation that the Earth Swingby requirement is being satisfied.

#### 1.2 ORGANIZATION OF THE SUPPLEMENT

The supplement begins with an overview of the Earth swingby analysis. This overview is intended to provide in a single section, a complete summary of the process used to calculate the Earth impact probabilities. A top-down discussion explains how the design of the Cassini spacecraft and mission enables the Earth swingby requirement to be satisfied.

The methodology for determining Earth impact probabilities is given in Section 2. The single basic defining equation for Earth impact probability is presented. The application of this equation to both the short-term and long-term Earth impact probabilities is discussed. The calculation of probability density functions for Earth impact probabilities using Monte Carlo techniques is also presented.

Section 3 provides an update to the failure mode analysis used in the Earth impact probability calculations. Most of the new work has been in the area of micrometeoroid-induced failures, the delta-Vs resulting from these failures and the actions taken to better protect the spacecraft from micrometeoroid impacts. Eleven new low probability failure modes were incorporated into the models and minor changes were made to

several existing failure modes. None of these changes have significantly affected the Earth impact probabilities.

The updated maneuver design strategy for navigating the Cassini spacecraft safely past the Earth is presented for the primary and secondary trajectories in Section 4. The contribution of each of the failure modes to the total short-term Earth impact probability is detailed.

The Earth impact probability over time periods much greater than the nominal trajectories is called the long-term impact probability and is treated in Section 5. The time period examined for the long-term impact probability of a disabled spacecraft is 100 years.

The total Earth impact probability is the statistical combination of the short-term and long-term impact probabilities. This is presented in Section 6 as a probability distribution function that accounts for uncertainties in both the process and mathematical models used in the process.

## SECTION 2

### METHODOLOGY

#### 2.1 INTRODUCTION

In order that an accidental Earth impact not be a credible event, the Cassini Project has levied a design requirement in its Project Policies and Requirements Document that the probability of Earth impact be less than one in a million. For this study, Earth impact is defined as reentry at an entry angle greater than or equal to 7 degrees at a reference entry altitude of 122 km (76 ml). The 7 degree entry angle boundary not only includes cases where Cassini would directly reenter the Earth's atmosphere, but also includes those cases where Cassini would skip off the Earth's atmosphere and lose enough energy to return and reenter the Earth's atmosphere at a later time. Entry angles of less than 7 degrees result in trajectories that skip off the atmosphere with sufficient energy to escape the Earth's gravitational influence. The probability of Cassini skipping off the atmosphere and reencountering the Earth in the next 100 years is several orders of magnitude less than the one in a million requirement. This is due to the skip scenario being somewhat a combination of both short-term and long-term impact scenarios.

To satisfy the Earth swingby requirement, an assessment of the Earth impact probability has been performed. The probability of Earth impact is presented as a probability density function over the model uncertainty. The advantage of such an approach is to provide information about the uncertainty of the estimation of the Earth impact probability. The above requirement is interpreted to be that the expected value (mean) of the Earth impact probability from injection to 100 years beyond the date of spacecraft failure shall not exceed  $10^{-6}$ .

The overall methodology for determining Earth impact probability is given in Figure 2-1. The Earth impact probability is composed of short-term and long-term components. The short-term component is the contribution resulting from the navigation of the Earth swingbys for a given trajectory. The long-term component is the contribution due to a disabled spacecraft drifting in orbit about the Sun that could reencounter the Earth sometime in the next 100 years.

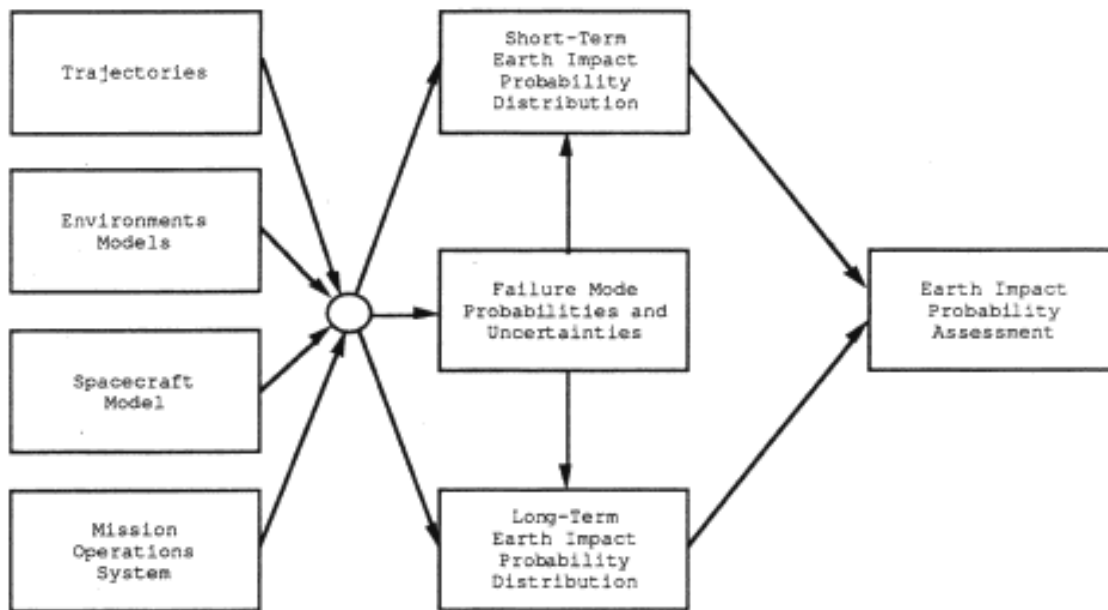


Figure 2-1 Earth Impact Probability Assessment Methodology

An important defining equation for Earth impact probability is as follows:

$$P_I = \sum_i P_F(i) * P_{I/F}(i) * P_{NR}(i)$$

where

- $P_I$  = probability of Earth impact
- $P_F(i)$  = probability of failure for ith failure mode
- $P_{I/F}(i)$  = probability of a resultant Earth impact trajectory given an occurrence of the ith failure mode
- $P_{NR}(i)$  = probability of no recovery given the failure mode and the time to impact - this probability is conditional on the occurrence of the failure and on the spacecraft being on an impact trajectory resulting from the failure

This equation illustrates several important concepts. First is that there are a number of failure modes that contribute

to Earth impact probability. One objective of this study is to identify all these failure modes. The  $P_{I/F}$  and  $P_{NR}$  terms acknowledge that most failures do not place the spacecraft on an impacting trajectory nor affect the capability to achieve a successful and safe Earth swingby. An example is the Galileo high gain antenna anomaly that resulted in only a partial deployment of the antenna before reaching the second planned Earth swingby. This failure did not prevent the precise delivery of the Galileo spacecraft at the second Earth swingby.

To keep the short-term impact probability acceptably low, a trajectory biasing strategy is used to reduce  $P_{I/F}$ . During most of Cassini's inner solar system journey, the spacecraft is on a trajectory that, without further maneuvers, would miss the Earth by tens of thousands of kilometers. The spacecraft is placed on a trajectory passing through the required Earth swingby point 6.5 days prior to the encounter. To keep the long-term impact probability acceptably low, the swingby aimpoints are designed such that the spacecraft is on a trajectory that, without further maneuvers, crosses through the ecliptic plane far from Earth's orbital distance and remains so during the next 100 years. Modification of the swingby aimpoints is done in conjunction with the short-term analysis, since the swingby aimpoints influence both the short and long-term Earth impact probability.

The  $P_{NR}$  term in the impact probability equation factors in the spacecraft's ability to recover and successfully apply a corrective maneuver after a failure. If a failure does not completely incapacitate the spacecraft, then the normal course of action is to modify the spacecraft configuration to compensate for the failure, accurately determine the spacecraft trajectory and, if required, command a recovery sequence to correct the trajectory and avoid Earth impact. For the long-term analysis, only those failures which would cause the spacecraft to become unmaneuverable with no chance of recovery are appropriate. The  $P_{NR}$  term is therefore always equal to 1 for the long-term analysis.

The failure mode analysis for this study considered three types of failures; environmentally induced spacecraft failures, spacecraft failures, and ground-induced errors. These failures may impart a velocity change to the spacecraft, thus altering its trajectory. For an Earth impacting trajectory to result from a velocity change, the velocity change must be of sufficient magnitude and in the necessary direction.

Earth-impacting trajectories can also result from uncertainties in the normal operation of the spacecraft and navigation system. For example, the actual velocity change achieved during a maneuver will differ slightly from the desired change. Likewise, the actual state (position and velocity) of the spacecraft will differ slightly from the state estimated by the navigation system. Both of these uncertainties, if large enough and uncorrected, could conceivably lead to Earth impact. These are

not failures, but expected variations in the operation of the systems. However, such variations are always quickly identified and corrected because of the continuous tracking coverage of the spacecraft during the critical Earth swingby period.

The Earth impact probability is evaluated for two trajectories. The first trajectory is the proposed baseline Venus-Venus-Earth-Jupiter-Gravity-Assist (VVEJGA) trajectory. The launch period for this trajectory is from October 6 to November 15, 1997. The trajectory for the opening day of the launch period was selected for evaluation of the short-term impact probability, since the Earth swingby is at the minimum allowed swingby altitude of 800 km (497 ml). Trajectories for days later in the launch period with swingby altitudes greater than 800 km have lower short-term Earth impact probabilities. The long-term impact probability is not sensitive to launch day. The long-term impact analysis was performed for launch on October 9 and is representative of all launch days.

The second trajectory considered in this study is the secondary Venus-Earth-Earth-Gravity-Assist (VEEGA) trajectory. The launch period for this opportunity is from November 28, 1997 to January 11, 1998. The opening day of the launch period was selected for evaluation for both the short-term and long-term impact probabilities. The second Earth swingby altitude of 1000 km is constant across the launch period, and the first Earth swingby altitude is at its minimum value, above 2000 km, on the opening day. It is therefore concluded that the Earth impact probability has very little launch day dependence for this opportunity, with the opening day tending to be the highest.

## 2.2 FAILURE MODE ANALYSIS

In general, all failures can be classified into three categories: environmentally induced failures, internal spacecraft failures, and ground induced failures. These failures can result either in an anomalous  $\Delta V$ , which might place the spacecraft on an Earth impacting trajectory, or may prevent the spacecraft from being recovered after inadvertently being placed on an Earth impact trajectory.

For most of the failure modes identified, three estimates of the probability of occurrence are provided. The first estimate is the best estimate and represents the most accurate estimation of the failure rate. There is believed to be a 50-50 chance of the real value being higher or lower than the best estimate. The other two values attempt to quantify the uncertainty associated with the best estimate. The 90 percentile value represents the value that is believed to have a 90% chance of being greater than the true value. It is thus a conservative estimate of the failure probability. The 10 percentile value represents the non-conservative end of the uncertainty. There is only a 10% chance that the true value will be below the 10

percentile value. There are also some uncertainties in the  $\Delta V$  estimates associated with some failures. A similar process was used to quantify these uncertainties. Probability distributions were used instead of 10,50,90 values for the dominant failure mode contributors such as micrometeoroid induced failures, internal spacecraft failures (long-term analysis), and pyro valve failures. Probability distributions were also used for the  $\Delta V$ s resulting from tank ruptures.

Micrometeoroid-induced tank rupture is a failure mode that contributes significantly to the short-term Earth impact probability. The spacecraft design does include components to provide protection from micrometeoroids, but there are particles with sufficiently high energies to damage the spacecraft. A rupture of a propellant or a pressurant tank will cause an anomalous  $\Delta V$ , and cause loss of spacecraft commendability or spacecraft incapacitation. A micrometeoroid impact on the electronic bus structure will impart only a negligible  $\Delta V$ , but may cause loss of spacecraft commendability. Other failure modes include stuck-open thruster valves, main engine valve failures, accelerometer failures, main engine gimbal actuator failures, and anomalous Sun search due to stellar reference unit or inertial reference unit failures. AACS and CDS flight software coding errors are the spacecraft software contributors to Earth impact probability.

Loss due to spacecraft system internal failures is the dominant failure mode for the long-term Earth impact probability. These failures include design and implementation errors, common-mode failures, cascading failures, electronic parts failures, hardware failures, and software errors.

Ground-induced errors are errors made on the ground by the spacecraft controllers, which are then sent to the spacecraft and executed. Two categories of ground induced errors are erroneous ground commands and navigation design errors. Since all validity checks are done on the ground, if an erroneous  $\Delta V$  command is transmitted, it will be executed. An error in one of the parameters for a planned maneuver during the design process prior to the sequence generation cycle is an example of a navigational design error. Multiple, independent checks and reviews are held to reduce the likelihood of a faulty ground command being executed by the spacecraft to an insignificant occurrence.

The failure modes analysis also includes a calculation of the probability of no recovery. For catastrophic failures, which preclude the execution of subsequent maneuvers, the value of  $P_{NR}$  is set to 1. In particular,  $P_{NR}$  is 1 for all of the failures involved in the long-term impact probability.

For those failures that put the spacecraft on an impacting trajectory, but do not preclude the execution of subsequent maneuvers, the key determining factor as to whether the spacecraft could in fact be maneuvered off the impacting trajectory is the time left before swingby, not the cause of the

initial failure. Failure modes were identified for several time periods and probability estimates were made for each, to be used for all recoverable failures causing the spacecraft to go on an impacting trajectory.

### 2.3 SHORT-TERM IMPACT PROBABILITY

The primary objective of the navigation strategy between launch and the Earth swingby is to satisfy the Earth impact probability requirement while delivering the spacecraft to the necessary Earth swingby aimpoint. To calculate the probability of Earth impact requires a knowledge of three factors: the failure probabilities and associated  $\Delta V$ s, the uncertainties in the navigation process, and the characteristics of the spacecraft trajectory. For the purpose of defining an Earth swingby navigation strategy, steps have been taken to minimize the effect of spacecraft failures and navigation uncertainties. The navigation strategy focuses on specifying and controlling the spacecraft trajectory conditions given the failure probabilities and navigation uncertainties.

In general, the impact probability decreases as the swingby altitude increases, so that impact avoidance requirements could be satisfied by simply raising the swingby altitude. However, specific swingby conditions are needed to shape the trajectory, and the spacecraft cannot carry sufficient propellant to replace this effect (except possibly for a very small bias). Fortunately, there is enough propellant to bring the trajectory in towards the Earth in several steps before the swingby.

The technique is to partition the trajectory into segments. The trajectory on each segment is targeted to swingby conditions that yield an acceptable impact probability under the conditions expected during that segment. Due to the navigational uncertainties and trajectory dynamics, this strategy allows at least the final segment to be targeted to the desired swingby conditions. Prior segments are targeted to biased aimpoints that, if uncorrected, have higher swingby altitudes. The trajectory segments are joined by required spacecraft maneuvers. Prior to launch, analysis is performed to determine both the duration and swingby conditions for each segment. After launch, the spacecraft is controlled to meet these conditions.

The following general method is used to calculate the short-term Earth impact probability for both the primary and secondary trajectories. For each failure mode it is necessary to compute the probability of impact given failure. Given values for three confidence levels (10%, 50%, and 90%) for navigation uncertainties (consisting of orbit determination and execution errors) and three variations of failure  $\Delta V$ ; the impact probability given failure is computed along the trajectory at either maneuvers or discrete time steps, depending upon the failure mode. The

result is nine variations of fractional impact probability as a function of time.

In order to generate a p.d.f. for the short-term Earth impact probability, a Monte Carlo simulation was performed with random selections from each of the three terms ( $P_{I/F}$ ,  $P_F$ , and  $P_{NR}$ ) required to calculate Earth impact probability. For the probability of impact given failure ( $P_{I/F}$ ), a random selection is made from one of the nine fractional impact probability vectors. The probability of failure ( $P_F$ ) is sampled at three discrete probability levels, 10%, 50%, and 90%, representing the best estimate of the failure probability and the upper and lower values, or a continuous distribution is sampled. The probability of not being able to accomplish a recovery maneuver ( $P_{NR}$ ) is also sampled at the 10%, 50%, and 90% probability levels.

The Monte Carlo process simulates the results for a large number of missions. Each simulated mission is broken down into a number of time steps. After sampling each of the three individual factors, they are multiplied together to obtain a probability of impact,  $P_I$ , for the failure mode during the time interval. These individual impact probabilities are then summed over both the duration of the mission segment and across all of the failure modes to obtain the total distribution of the probability of impact for the mission segment.

#### 2.4 LONG-TERM IMPACT PROBABILITY

The short-term impact analysis establishes that the probability of Earth impact during a targeted Earth swingby is extremely small. However, if the spacecraft becomes uncommandable during interplanetary cruise and does not impact the Earth or Venus during a targeted swingby, there is still a remote possibility that long-term perturbations to the orbit could cause the spacecraft to eventually reencounter the Earth. The long-term analysis computes the probability of Earth impact at a non-targeted swingby for a period of 100 years commencing at the time of spacecraft failure.

To compute the probability of Earth impact, a knowledge of the spacecraft failure probabilities, the uncertainties in the navigation process, and the long-term motion of the spacecraft is required. Only those failures which cause the spacecraft to become uncommandable with no chance of recovery are appropriate for the long-term analysis. The probability of no recovery ( $P_{NR}$ ) is therefore equal to 1. The long-term impact probability is a function of the interplanetary trajectory characteristics of the spacecraft at failure and the evolution of the spacecraft orbit, due to third-body gravitational effects, over the next 100 years. Therefore, the design of swingby aimpoints must consider not only the short-term impact probability, but also the behavior of the post-failure trajectory over the next 100 years.

The following method is used to compute the long-term Earth impact probability for both the primary and secondary trajectories. Since a single trajectory propagation would not be representative of the range of possible spacecraft trajectories that could result given a failure at any time during interplanetary cruise, a Monte Carlo analysis was performed using thousands of trajectories considering a wide range of failure times. The primary and secondary Cassini trajectories were each evaluated using ~6000 failure cases which are sufficient to sample each swingby aimpoint dispersion at least several hundred times. Associated with each case is an initial spacecraft orbital state, which is perturbed by navigation uncertainty. Since  $\Delta V$ s are only associated with several percent of the long-term failure cases and past analysis has shown them to have a negligible effect on long-term impact probability, the effects of micrometeoroid induced  $\Delta V$ s were ignored in the calculations of initial spacecraft orbital states. Each initial spacecraft state is then propagated for 100 years in the analysis.

Spacecraft failure probabilities were used to compute a probability distribution of failure ( $P_F$  term) representative of the entire interplanetary cruise for each mission. The failure probability distribution was obtained by randomly sampling the cumulative failure probability distributions as many times as required until ~6000 failure times during cruise were obtained.

To determine the probability of Earth impact given a failure,  $P_{I/F}$ , use was made of a large body of work refined over the past forty years to estimate the probability of impact by Earth-crossing asteroids. In this method, the number of passages of the spacecraft through the torus swept out by the Earth as it orbits the Sun are used to compute the probability of Earth impact. For an impact to occur, the spacecraft must cross through the Earth torus and, at the time of the crossing, the Earth must be at a position within the torus to cause impact. The term  $P_{I/F}$  is computed as the product of two terms: 1) the expected number of torus crossings by the spacecraft per Monte Carlo case ( $N_{CRX} / N_{CASE}$ ) and 2) the probability that the Earth occupies the same portion of the torus as the spacecraft at the time the spacecraft crosses the torus ( $P_{I/CRX}$ ).

The number of torus crossings for all Monte Carlo cases were computed by propagating the initial conditions for each case using a high-precision numerical integration program and counting each passage through the Earth torus. Numerical integration was used rather than the analytical model for long-term orbital motion used by most Earth-crossing asteroid analyses since the analytical expressions proved inadequate for the Cassini time frame and orbital characteristics. An uncertainty on the number of torus crossings per case was determined, and a distribution for this term constructed (assuming a normal distribution).

Standard Earth-crossing asteroid theory was applicable and therefore used to compute the  $P_{I/CRX}$  term. The value of  $P_{I/CRX}$  is slightly different for each torus crossing, and thus an average value was used to compute a best estimate value for the entire mission. An uncertainty in the value of  $P_{I/CRX}$  was estimated and a distribution for this term constructed assuming a log-normal distribution. The distributions for the  $N_{CRX}/N_{CASE}$  and  $P_{I/CRX}$  terms were combined with the distribution for the  $P_F(i)$  term to yield a p.d.f. for the long-term Earth impact probability,  $P_I$ .

## 2.5 EARTH IMPACT PROBABILITY ASSESSMENT

The Project requirement on the Earth Swingby Plan is that the probability of Earth impact be less than or equal to one in a million ( $10^{-6}$ ). A number of parameters can be used to describe the characteristics and interpretation of a p.d.f. (or of a complementary cumulative probability curve). The "expected value" of a random variable is expressed by the mean of the probability distribution. Thus, the Project requirement that the probability of Earth impact be less than or equal to  $10^{-6}$  has been considered met when the mean of the assessed probability distribution is less than or equal to  $10^{-6}$ .

The total Earth impact probability distribution is the probabilistic sum of the short-term and long-term Earth impact probability distributions. A 1000-trial Monte Carlo simulation was used to perform this probabilistic summation. The mean of the total Earth impact distribution was compared to  $10^{-6}$  to determine that the Project Earth impact requirement was satisfied for both the primary and secondary trajectories.

## SECTION 3

### FAILURE MODES

#### 3.1 METHODOLOGY

##### 3.1.1 Introduction

This section updates the failure modes reported in Volume 3: Cassini Earth Swingby Plan, November 18, 1993. Most of the new work has been in the area of micrometeoroid induced failures, the  $\Delta V$ s resulting from these failures and the actions taken to better protect the spacecraft. Eleven new low probability failure modes were incorporated into the models and minor changes were made to several existing failure modes but none of these changes has had any significant effect on the Earth impact probabilities. The remaining failure modes involving the Ground System, flight software and spacecraft components remain the same. There are five subsections: 1) Methodology, 2) Delta-V Inducing Failures, 3) Internal Spacecraft Failures, 4) The Increased Micrometeoroid Shielding of Cassini, 5) Probability of No Recovery.

##### 3.1.2 Estimate Uncertainties

The probability of failure ( $P_F$ ) was estimated for each failure mode using a combination of historical test data (where available), analysis (where appropriate), and informed judgments by experienced engineers.

The uncertainties in predicted  $P_{FS}$  were quantified by providing three estimates of the  $P_F$  for each failure mode with the exception of Pyro Valve Failure, Micrometeoroids-Induced Tank Failure and Internal Bus Failure whose uncertainties were expressed in the form of probability distribution functions. The best estimate of the  $P_F$  is assigned as  $P_{F.50}$  and is defined as the point at which there is believed to be a 50-50 chance of the real  $P_F$  being higher or lower than the  $P_{F.50}$  estimate. The  $P_{F.50}$  value is thus the median value of the predicted range of probabilities. The two additional values are used to quantify the uncertainty associated with the best estimate. The 90 percentile value,  $P_{F.90}$ , represents a conservative upper estimate and the 10 percentile value,  $P_{F.10}$  represents an unconservative lower estimate. The real  $P_F$  has only a 10 percent chance of being higher than  $P_{F.90}$  and only a 10 percent chance of being lower than  $P_{F.10}$ .

Three points were considered sufficient to describe the uncertainties associated with most of the failure modes. Because there were a large number of inputs to the calculations used to

predict the probability distribution of Earth impact, it was expected that the final probability distribution would be well-populated in both tails by the choice of extreme uncertainty values for several inputs. However, it was decided to model the uncertainties in the dominant failure modes as continuous distributions. When the effects of these distributions are removed from the final probability calculations, the remaining distribution of points shows that the choice of three points to describe model uncertainty does in fact provide a filled-out distribution.

The placement of the three uncertainty points (10%, 50%, 90%) was chosen so that all of the points contribute significantly to the result. Each point is sampled 30%, 40% and 30% of the time, respectively, to regenerate the standard deviation of a normal distribution with arithmetically spaced point values, or the logarithmic spread of a log normal distribution with geometrically spaced point values. This choice also gave the experts providing the quantitative failure information familiar confidence levels upon which to base their uncertainty estimates.

A similar process was used to quantify the uncertainties associated with most  $\Delta V$  estimates. The best estimate of the  $\Delta V$  produced by a failure,  $\Delta V_{BE}$ , was assessed by determining what physical process would most likely occur, and then determining the  $\Delta V$  that would result from that process. The amount of uncertainty associated with the  $\Delta V$ s of each failure mode can thus be assessed by examining its three values. Well-understood and predictable failure modes have a narrow range of predicted values, and less well-understood or less predictable modes have broader ranges.

Because micrometeoroid-induced propellant tank failure is among the dominant contributors to short-term Earth impact probability and the resultant  $\Delta V$  distributions are difficult to estimate, a Monte Carlo simulation was used for all failures of the propellant and pressurant tanks. Extensive study and analysis was conducted to refine the understanding of the possible results of micrometeoroid impact to the Cassini Propulsion Module Subsystem (PMS). Using this data, refined simulations were developed and run to calculate the uncertainties in the probabilistic occurrences of each possible outcome. For each case the impulse imparted to the spacecraft, the angular orientation of the impulse vector with respect to the spacecraft and the time duration of the event were calculated. Equations of motion of a free body under the influence of disturbance forces were used to estimate the resultant  $\Delta V$  magnitude and direction that would be imparted to the spacecraft.

Uncertainties in the predicted micrometeoroid failure rates were estimated using a Monte Carlo simulation based on the following equation:

$$F_{123} = f_1 * (1/f_2)^{1.2} * f_3$$

The dimensionless sub-factor  $f_1$  accounts for the effect of the uncertainty influence which is discussed in paragraph 3.2.1.6. The dimensionless sub-factor  $f_2$  accounts for the effect of the uncertainty in critical mass which is discussed in paragraph 3.2.1.5.2. The exponent is derived from the models discussed in paragraph 3.2.1.6. The dimensionless sub-factor  $f_3$  accounts for the effect of the scale-up of critical mass with velocity which is discussed in paragraph 3.2.1.5.3 (Reference 3-1).

### 3.1.3 Summary of Results

Table 3-1, in the back of this section, is a summary of most of the spacecraft component failure modes included in the study. Detailed analysis was obtained to update the stuck open thruster valve and stuck open main engine valve (Reference 3-2). Accelerometer failure, main engine gimbal actuator failure, AACs flight software error, CDS flight software error, anomalous sun search, erroneous ground initiation of a TCM and navigation design error remain the same (Reference 3-3). The remainder of the failures in the table resulted from analysis conducted since the last publishing. Discussion of failure modes not included in Table 3-1 can be found below: (1) Micrometeoroid-Induced Tank Failures, paragraph 3.2.1; (2) Internal Bus Failures, paragraph 3.3.1, and (3) No-recovery/ Ground Error Component, paragraph 3.5.

## 3.2 DELTA-V INDUCING FAILURES

Failures that will induce an unplanned or anomalous  $\Delta V$  to the spacecraft are discussed. These failures include those caused by micrometeoroids, spacecraft failures, and ground system failures. Some of these failures will also cause loss of spacecraft commandability.

### 3.2.1. Micrometeoroid-Induced Tank Failures

During the Cassini Swingby Review, in January '95, Johnson SFC micrometeoroid experts expressed an opinion that MLI blankets might not provide adequate micrometeoroid protection for the Cassini Spacecraft. Subsequent to this review a short series of tests were performed at Johnson SFC that confirmed the opinions of Johnson SFC experts. JPL then initiated a micrometeoroid evaluation program that included additional testing, computer modeling, increased shielding, and identification of alternative trajectories (covered in Section 4) with increased biasing away from the Earth.

#### 3.2.1.1 Micrometeoroid Evaluation Program Overview

Analysis identified the Cassini structures most sensitive to micrometeoroid impact. In particular, the large surface area (approximately 10 m<sup>2</sup>) of the Cassini propellant tanks

and an extremely low allowable probability of failure required for Earth swingby led to the design of a comprehensive micrometeoroid shielding system.

The initial Cassini protective shields were reviewed and one worst case configuration was selected and tested at NASA Johnson. Particles from micrograms to 432 mg composed of soda lime, iron, aluminum and polyethylene were accelerated to velocities near 6 km/s. These substances were selected to represent the range in expected composition of the interplanetary micrometeoroid population--soda lime glass for silicates, iron for iron micrometeoroids, and polyethylene for cometary-derived "CHON" particles. These tests indicated that the proposed configurations did not adequately protect the Cassini tanks (based on the initial tank perforation criteria). It was determined that further design and testing would be necessary to achieve the desired levels of protection. The tests also confirmed that soda lime glass was the best test particle from a simulated micrometeoroid standpoint in that it better represented the expected mechanical impedance of the majority of the interplanetary particles of concern to Cassini.

The Cassini design is based on the classic "Whipple Shield" approach--the first line of defense in this approach being the spacecraft thermal blankets which are intended to break up the impacting particles and spread the debris out into an expanding cloud. The thermal blankets were in turn spaced varying distances (2.5 to 18 inches) off of a secondary shield behind which the tanks were placed. This approach is expected to be particularly effective in stopping particles with velocities above 10 km/s--the primary velocity range of interest to Cassini. Limited test results were available for micrometeoroid damage at velocities above 10 km/s so the test results have to be scaled up using the results of hydrocode analysis. Given the importance of these shields to the survival of Cassini, it was deemed necessary to validate the models and shielding configurations by conducting a series of hypervelocity impact tests at the NASA Ames Vertical Gun Facility. The tests provided a basis for determining the amount of damage that particles of various masses would produce in the Ti6Al4V-STA propellant tank walls and filament wound Helium tank walls after passing through the various blanketing shield configurations.

The experimental evaluation program described herein had two goals. The first goal was to develop data which characterized the damage created in the critical components of the spacecraft by particles of various masses impacting at 5-6 km/s. These data were used to estimate the maximum particle mass which did not cause critical damage to the spacecraft. After early ballistic test results indicated that the existing spacecraft was inadequately protected, the scope of the evaluation program was expanded to include the evaluation of improved shielding.

The second goal was to support the development and "tuning" of the hydrocode models so they could be used to predict the effects at higher velocities.

JPL experimentally evaluated the level of protection afforded by the spacecraft for its critical components (tanks and main engine nozzles) against the impact from hypervelocity particles which they might encounter during the mission. Electronic bays were shielded by single surface Aluminum shear plates and were amenable to analysis using "NASA SP-8042 Penetration Formula. from NASA document "Meteoroid Damage Assessment,. dated May 1970. The major micrometeoroid particle threat to the spacecraft was estimated to be a range of particle masses from 1 mg to 100 mg which possess a distribution of velocities 5-40 km/s. The mass range of interest would have been tested over the desired velocity range; however, physical limitations on achievable particle launch velocities limited the test velocities to a maximum of 5-6 km/s. Computer models (hydrocodes) were used to predict the damage done to the spacecraft at particle impact velocities greater than 5-6 km/s. Confidence in the use of this numerical modeling approach for estimating the damage done at high velocities is dependent on satisfactory " tuning " of the models to agree with the experimental data measured at 5-6 km/s. However, since correlation between the hydrocode model predictions and experimental data was not as high as desired. Conservative bounding limits were used.

In order to simulate the spacecraft shielding configurations, a test matrix of target configurations was developed. This matrix enabled efficient evaluation of the protection levels provided in the critical spacecraft areas. The testing approach maintained a nearly constant impact velocity and varied the impacting particle mass to determine the amount of damage produced by each mass in each of the target configurations evaluated. Analysis methods and models were developed to interpret and extrapolate the data trends in order for estimates of the critical incident particle masses to be made for all defined spacecraft areas.

The original plan was to allow partial penetration of the tank walls by a micrometeoroid in order to remove some of the conservatism in the analysis. However, in order to do this the behavior of pressurized tank walls needed to be thoroughly understood. A study was conducted to measure the dynamic fracture toughness of the titanium tank alloy under the dynamic conditions that would be experienced following a micrometeoroid impact. Based on this study, rough estimates of the dynamic crack initiation criteria for the pressurized and unpressurized titanium tanks were made. These estimates indicated that the pressurized tank may withstand micrometeoroid crater depths of up to 10 to 30% of the tank wall thickness before failing, but it became apparent that considerable additional effort would have to be expended in order to validate this. After review of the experimental results a decision was made to conservatively define "critical particle

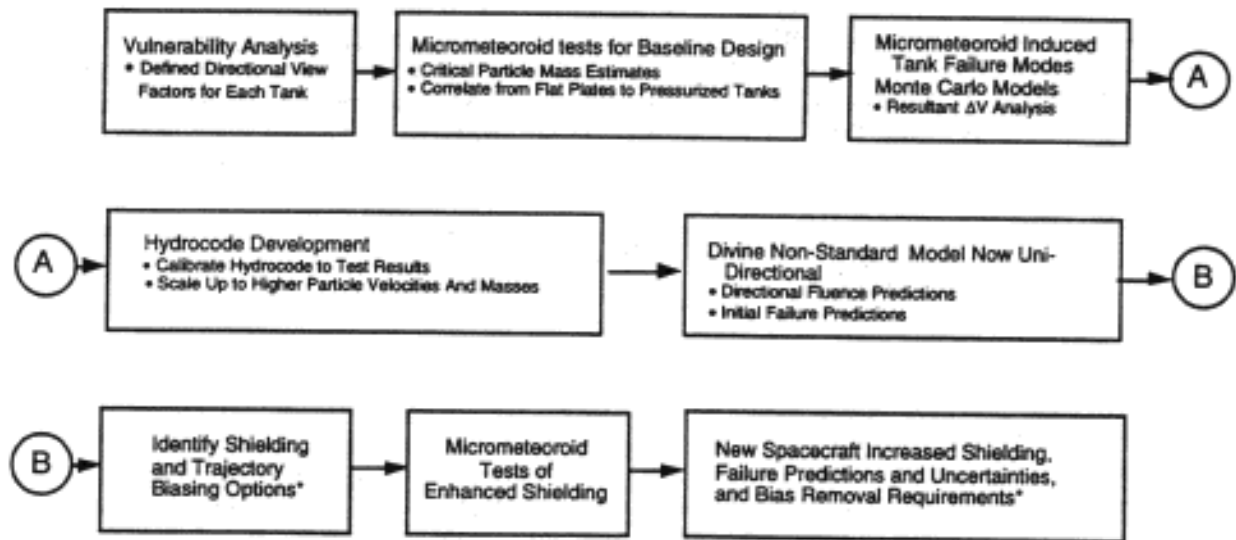
mass" as that mass which causes "no-damage to the tank wall" (Reference 3-4).

### 3.2.1.2 Micrometeoroid Evaluation Program Process

Figure 3-1 documents the process followed in evaluating and improving the protection against micrometeoroids. Significant iteration occurred between the various engineering activities and much was done in parallel.

In this evaluation process the spacecraft configurations were defined by nodes, solid angles and view factors. Mean critical mass estimates were derived from test results. Included in this process were steps taken to test the spacecraft baseline design and correlate flat plate test results to pressurized tanks. Tank failure modes were evaluated and resultant  $\Delta V$ s were estimated. Hydrocode was developed in order to define critical mass variability with velocity. These parameters were then input to the Divine Model to calculate tank failure probabilities. Results of this analysis were used to identify and verify new shielding configurations. In addition to increasing the shielding, the data were provided to support separate evaluations of trajectory biasing options and bias removal requirements (discussed in Section 4).

**Figure 3-1 Micrometeoroid Evaluation Program Process**

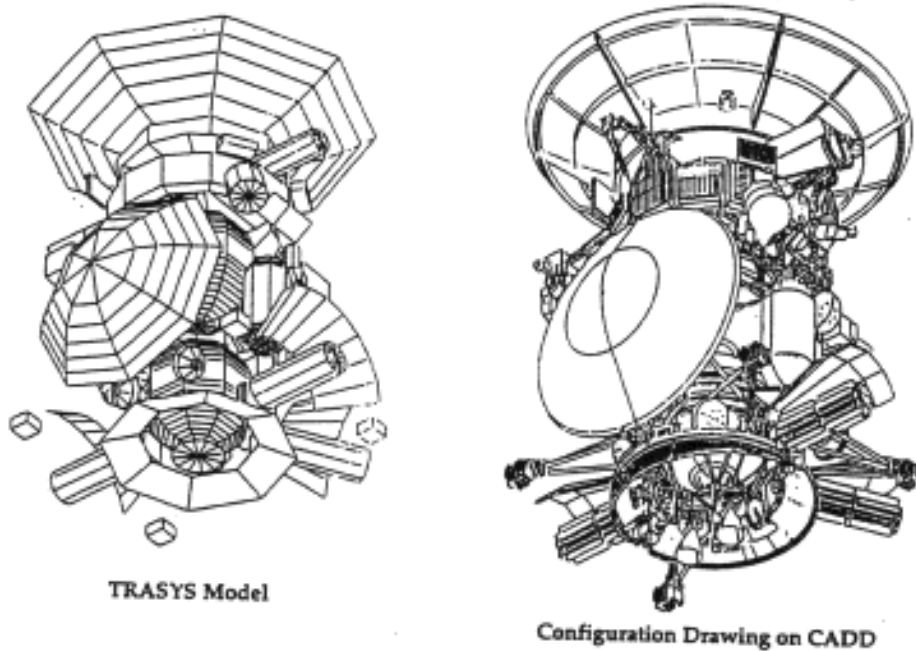


\*Note: Trajectory Biasing Options are covered in Section 4.

### 3.2.1.3 Spacecraft Vulnerability Analysis/Geometric Modeling

The spacecraft was modeled geometrically in order to calculate the fluence that can impact the tanks. View factors were calculated for each node from a number of angular positions around the spacecraft. Appropriate critical masses were then calculated for every view factor for each node. The vulnerable areas were defined using eighteen shielding configurations, ninety-six nodes, and ninety view factors. The view factors were estimated using a thermal radiation view factor program called TRASYS. Each bipropellant tank was modeled as forty nodes, the hydrazine tank was modeled as eight nodes, and the Helium tank was modeled as eight nodes. The model is shown in Figure 3-2.

Figure 3 - 2 TRASYS Modeling of Cassini (Nodal, View Factor, Vulnerability, Analysis)



In order to calculate effective view factors the model was run in two configurations. The first configuration consisted of the tanks and what are called "perfect" blocker surfaces. These "perfect" blocker surfaces include the Huygens Probe, the Bus, and the RTGs. These items are considered "perfect" blocker surfaces since their high density results in the ability to protect the tanks from very large micrometeoroids. The second configuration contained the tanks, the perfect blockers, and the semi-perfect blockers (HGA, instruments, engineering assemblies, RTG shades, PIA panels, PCA panels, etc.) which are not as dense as the "perfect" blockers but do provide a significant amount of protection to the tanks.

By comparing the results from the two configurations the percent of fluence impinging on the semi-perfect blockers can be calculated. These values and the appropriate critical masses were then input to the Divine micrometeoroid fluence model to calculate micrometeoroid tank failure probabilities (Reference 3-5).

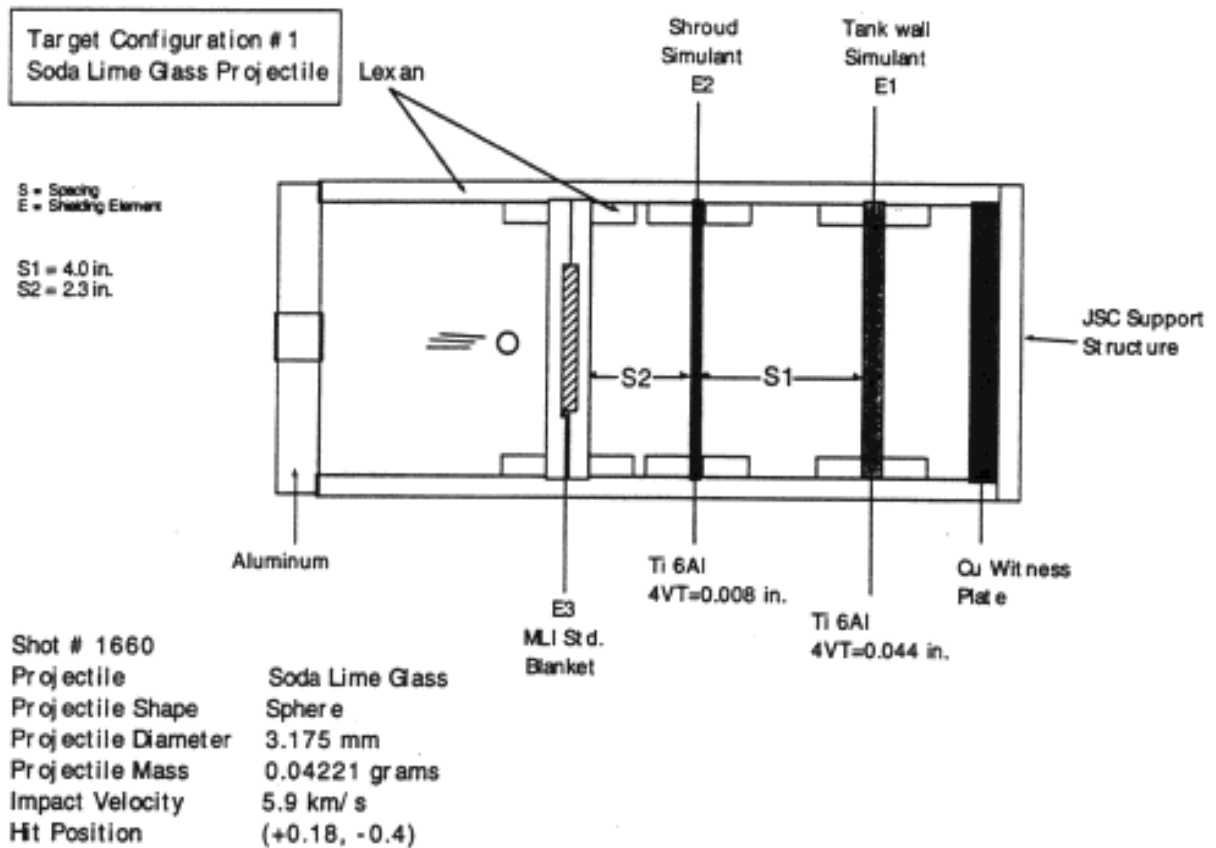
#### 3.2.1.4 Test Setup

Five generic types of target configuration were evaluated:

1. MLI or Beta MLI/space/tank wall
2. 2 plys BMLI/space/MLI or BMLI/space/tank wall
3. 2 plys BMLI/space/nozzle
4. MLI or BMLI/space/aluminum/space/tank wall
5. Unprotected

In a typical configuration with a two component shield plus the critical component, e.g. MLI blanket/Space (S2)/Aluminum plate/Space (S1)/Propellant tank wall, there are eleven principal variables whose relationships must be understood: the materials of each of the three components, the areal densities of each of the three components, the two spacings between the three components, the three angular relationships between the normals to the components and the velocity vector of the threat. The test program focused on the effects of Beta cloth vs. 20 layer MLI, the spacing between shields and tank walls, shielding material and the thickness of the secondary shield. These parameters are summarized in Table 3-2 and discussed in more detail in Reference 3-4. A description of a representative test configuration and the projectiles used are described in Figure 3-3. This figure illustrates a configuration designed to investigate the effects of spacing, shield material and thickness.

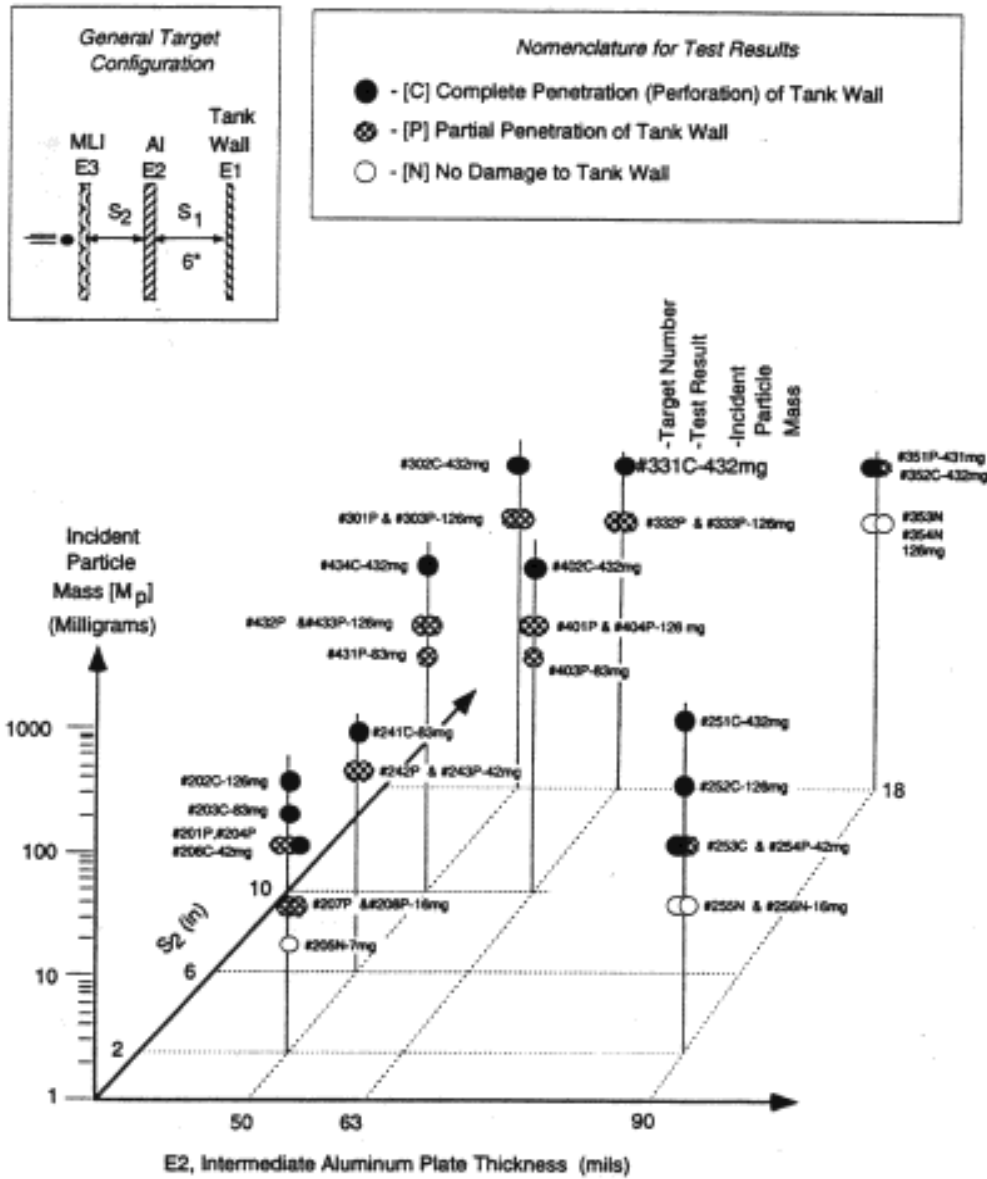
Figure 3 - 3 Representative Test Configuration and Projectile



### 3.2.1.5 Results of Test Program for the Tankage Areas

Test results were plotted in a three dimensional matrix for each protective shielding configuration, Figure 3-4A presents the results of tank wall damage resulting when the spacing (S2 = 2, 6 or 10 inches) between the outer most layer of MLI (E3) and the shielding element (E2 = 50, 63 or 90 mils) is fixed at 6 inches (S1) from the tank wall (E1). See the General Target Configuration box on Figure 3-4A for detail. Figure 3-4B presents results using the same set of variables but replacing the MLI with Beta MLI.

**Figure 3 - 4A. Range Test Results for the S2, E2 Matrix Using Standard MLI (Standard MLI/S2 Spacing/7075 Aluminum Plate /S1 = 6"/Ti6Al4V Tank Wall)**





calculate a temporally incremented description of an impact event. Characterization of the temperature profiles and their history in the debris cloud can provide information concerning the thermodynamic parameters of the impact phenomenon.

In order to estimate critical mass for each configuration the depths, diameters and spatial distribution (clustering tendency) of the ten deepest craters were examined over the range of test particle masses, shielding spacings and target areal densities ( $\text{kg/m}^2$ ).

#### 3.2.1.5.2 Discussion of Test Results

The performance of shielding and critical particle mass estimation is shown in Figure 3-5A for configuration 17. The heavy solid line represents an estimate of the behavior of the 0.5 perforation probability. The dashed line represents an estimate of the behavior of the 0.1 perforation probability. In a similar manner, the light solid line and dotted line represent the 0.5 and 0.9 no damage probabilities, respectively. Figure 3-5A also has data on other configurations. Figure 3-5B shows the relationship between the incident particle *mass* and the resulting distribution of the ten deepest crater depths for the particle masses tested. The two values of the probability of perforation and the two values of the probability of no damage at the 4" spacing coordinate, can be seen in Figure 3-5C. Large particle mass test data was extrapolated to estimate small no damage particle mass in cases where test data was not available. From this analysis probability lines were drawn and critical masses were estimated.

**Figure 3 -5A. Test Results Examining Shield Spacing Bet.  $\beta$  cloth and  $\beta$ \_MLI at 4, 10, and 18 Inches Varying Particle Size at 82.6 mg, 126 mg, and 432 mg \*Critical Mass Estimates**

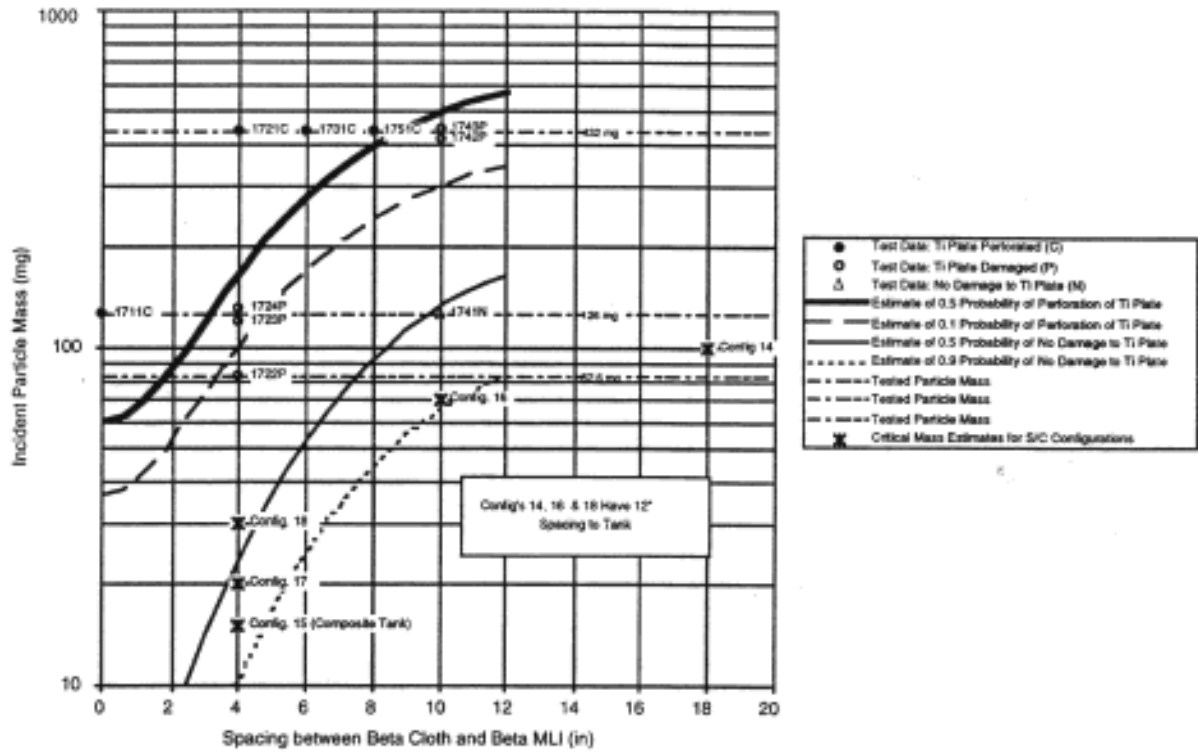


Figure 3- 5B. Crater Depth Distribution as a Function of Incident Particle Mass for Configuration: 2 Layers Beta Cloth/Spacing/Beta ML/Spacing->Ti Plate

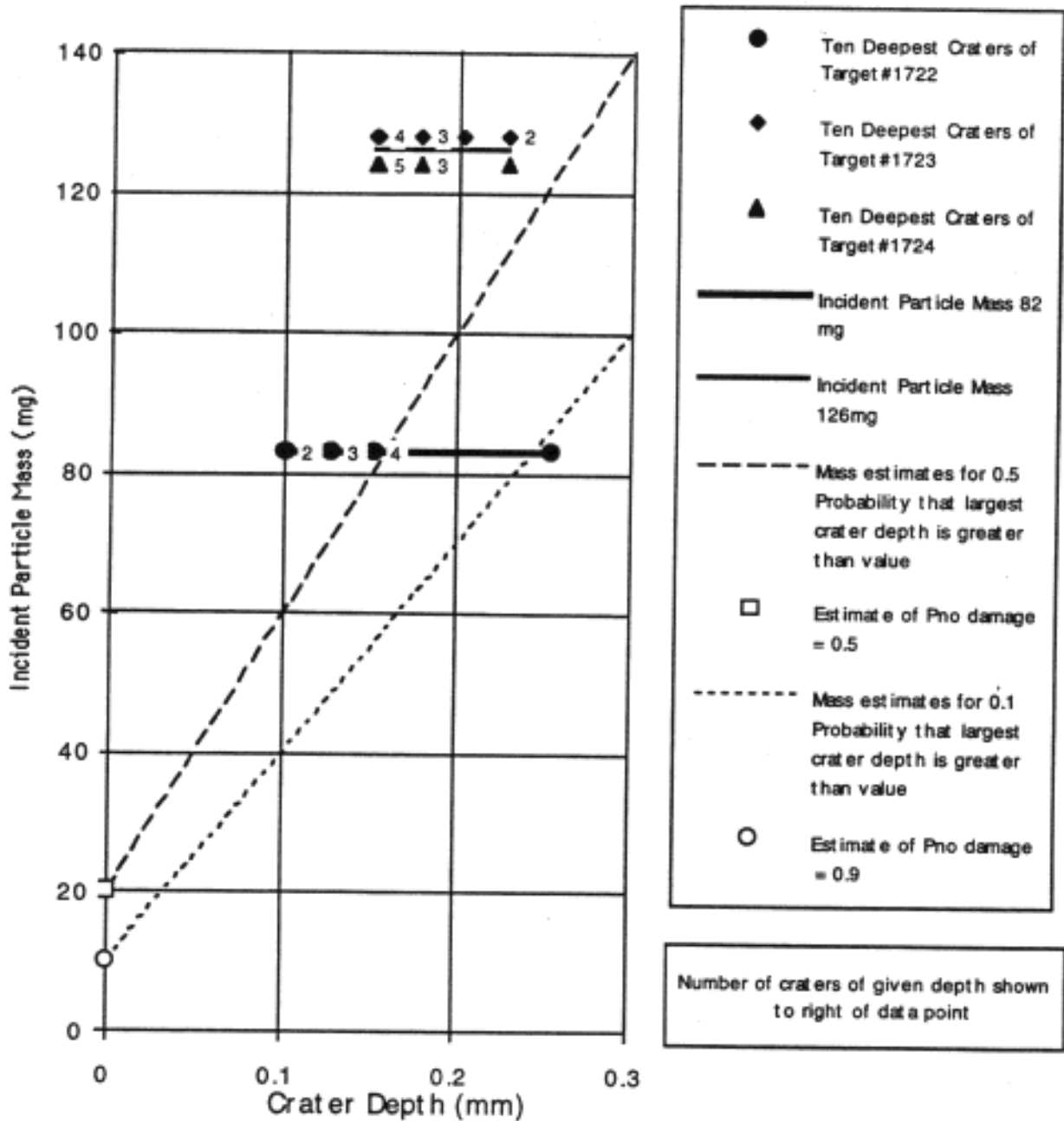
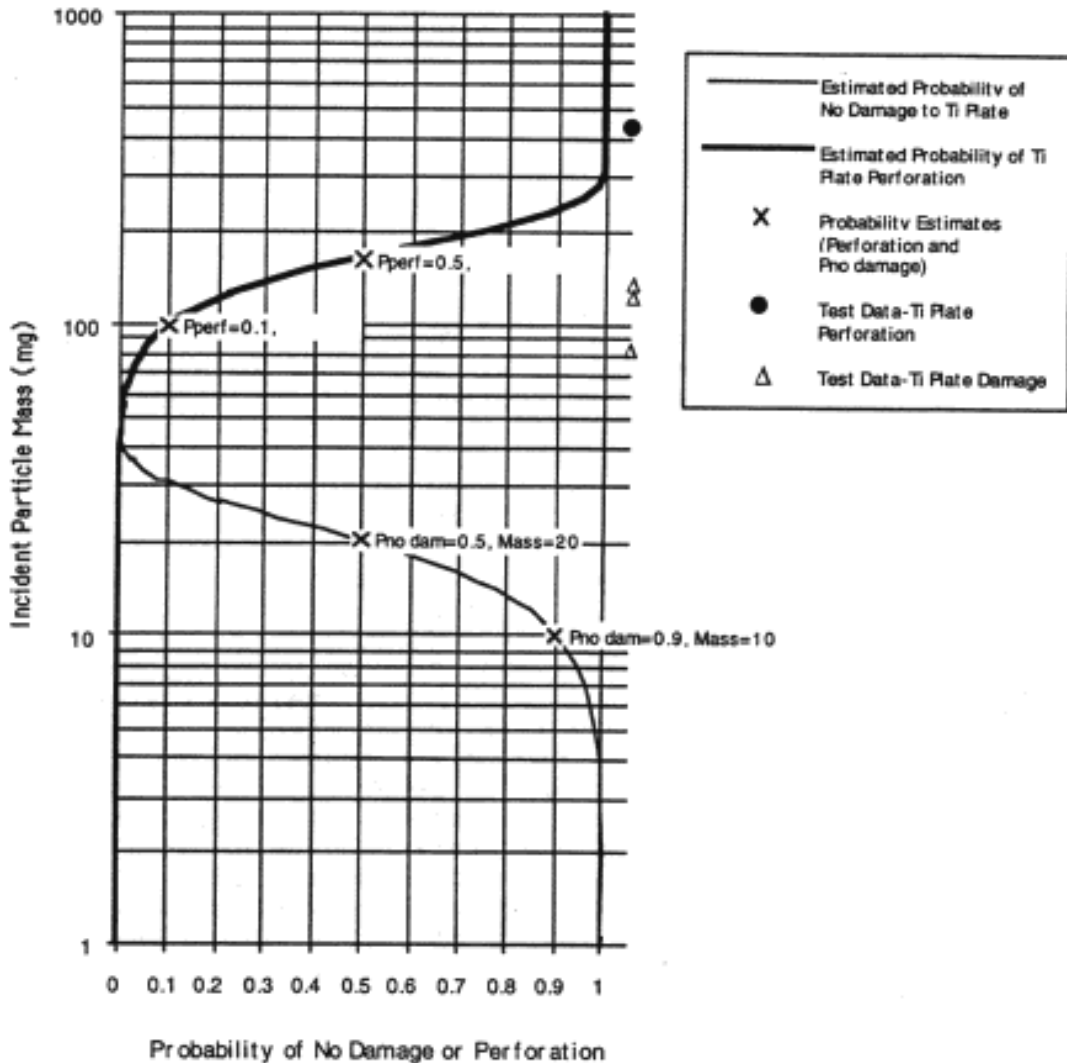


Figure 3-5C. Rough Estimate of the Probability of No Damage to Ti Plate and the Probability of Perforation of Ti Plate for the Target Configuration:  
2 Layers Beta Cloth/4"Spacing/Beta MLI/4" Spacing/Ti Plate



A representative damage distribution analysis for configuration 17 (see Table 3-2) is shown in Figures 3-5A, B & C.

The configuration in Figure 3-5A was impacted by the 126 mg projectile at 5.2 km/s. With zero spacing between the Beta cloth sheet and the Beta MLI shield the titanium plate was perforated. Increasing this spacing to 4" resulted in damage to the titanium plate but it was not perforated. Increasing the spacing to 10" resulted in no damage to the titanium plate.

Similar behavior was demonstrated against the 432 mg projectile. Perforation of the titanium plate occurred at an 8" spacing. Damage occurred in the titanium plate, but no perforation resulted when the spacing was increased to 10 inches.

The increased spacing allows the clustered particles to spread laterally to an extent that the impact of individual debris particles do not interact with each other to cause increased damage or perforation. The momentum deposited on the critical component is dispersed over a greater area. If the tank failure is caused by individual debris particles impacting the critical component increasing the spacing is not expected to have an effect.

Effects of spacing at higher velocities is discussed in Reference 3-6.

Table 3-2 presents the estimates of critical incident particle mass for the final spacecraft configurations. The critical mass estimates for each configuration are given in Column 10. These mass estimates represent the largest particle mass which will not cause damage to the unstressed titanium or filament wound, aluminum composite tank wall when incident at 5-6 km/s with 0° obliquity. Because no damage is allowed in the plates, these mass estimates also apply to pressurized tanks and were therefore input to the Divine Model as the critical masses.

Based on initial test data and engineering judgment the uncertainty in critical mass ( $f_2$ ) was assumed to be represented by a factor which has a distribution with a mean value of 1, and low and high value limits of 0.1 and 1.33, respectively. It is modeled by the concatenation of the half planes of two normal distributions. The left half plane is represented by a normal distribution with a mean of 1 and a standard distribution of 0.7031, which corresponds to a 10% confidence value of 0.1. The distribution is assumed to be truncated below a value of 0.1. The right half plane is represented by a normal distribution with a mean of 1 and a standard distribution of 0.2604, which corresponds to a 90% confidence value of 1.33. The distribution is assumed to be truncated above a value of 1.33.

### 3.2.1.5.3 Prediction of Shield Performance at Velocities Greater than 5 km/s (Hydrocodes)

The test data found that the clustering behavior of mass in the debris cloud that forms after a micrometeoroid passes through a shielding blanket has a major influence on the localized damage done to a critical component. The breakup or melting of the material that contributes to the debris cloud does not sufficiently reduce the threat. The fragments must also be spatially dispersed such that their individual impacts on the critical component do not create interacting damage.

The majority of the particles that impact the Cassini Spacecraft will be at velocities greater than 5-6 km/s. Very little information exists for impacts at velocities greater than 10 km/s. The strategy of the Project was to attempt to use Hydrocode computer models to predict the behavior of the shielding at velocities higher than those which could be tested easily. The concept was to tune the hydrocode to simulate the observed damage at 5-6 km/s and then use it at increased velocities. Attempts were made to simulate the test results in areas such as the amount of fragmentation, depth of penetration, degree of melting or vaporization, dispersion angle and spatial distribution. In cases where close simulation was not achieved, bounding cases were selected and run at higher velocities to determine how critical mass varied with velocity. For the purpose of the analysis it was assumed that critical mass varies inversely with a power of velocity, i.e.  $(1/v)^n$ . The higher the power of  $n$  the larger the effect will be. Based on the hydrocode results and in consultation with micrometeoroid experts at JPL and Johnson SFC it was concluded that the best estimate of  $n$  was 1.0 with a conservative 90% upper bound of 2.0 and a 10% lower bound of 0. No hydrocode runs produced a value of  $n$  over 1.5.

Figure 3-6 shows some typical hydrocode results. For purposes of comparison  $1/v$  and  $1/v^2$  dependencies for 2", 10" and 18" spacing are shown (Reference 3-6).

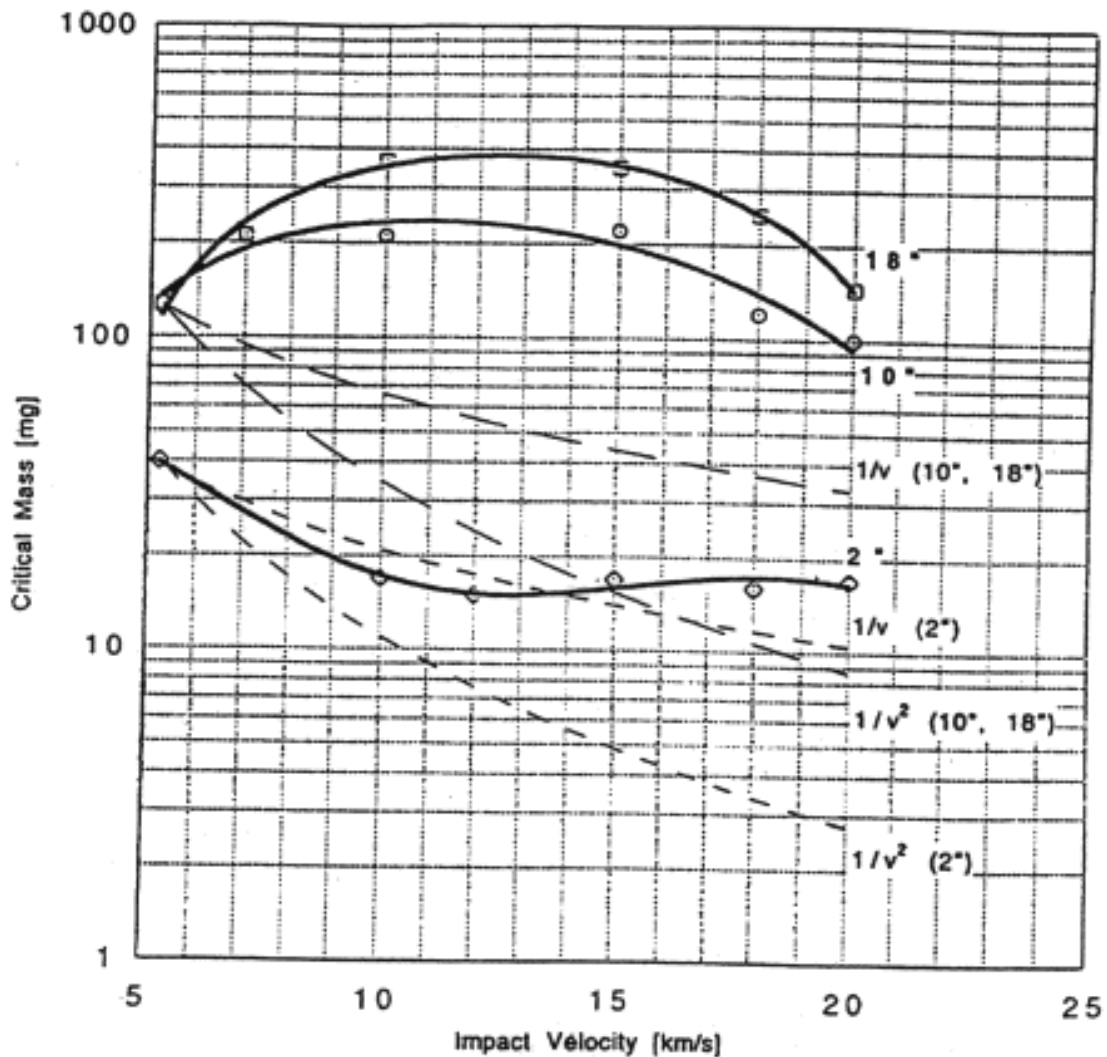
The uncertainty in the effect of failure rate due to the scaling of critical mass with velocity was defined through use of the Divine Model as:

$$f_3 = 0.10346 * e^{(2.2804 * n)}$$

For application of  $f_3$  refer to the failure rate uncertainty factor formula in paragraph 3.1.2. The variable  $f_{3a}$  (the exponent  $n$ ) from the above discussion was represented as a normal distribution, with a mean of 1 and a standard distribution of 0.7813. This corresponds to a 90% confidence value of 2.0 and a 10% confidence value of 0. The distribution was assumed to be truncated below a value of 0 and above a value of 2. For this case, for a 10,000 sample run, the mean value of  $F_{123}$  was found to be 9.19 and the median value was 2.83. Because  $n$  is used as an

exponent in computing  $f_3$ , changing the limits of the variable has a pronounced non-linear influence on the final result (Reference 3-1).

**Figure 3 - 6**  
**Results of Higher Velocity Calculations Which Determine**  
**Critical Mass vs. Velocity at 2, 10 and 18 Inch Spacing**



3.2.1.6 Changes To The Probability of Failure Model Due to Micrometeoroid Induced Tank Failure

In addition to micrometeoroid testing, improvements were made to the failure models. The micrometeoroid environment for the Cassini mission was initially evaluated using the Neil Divine

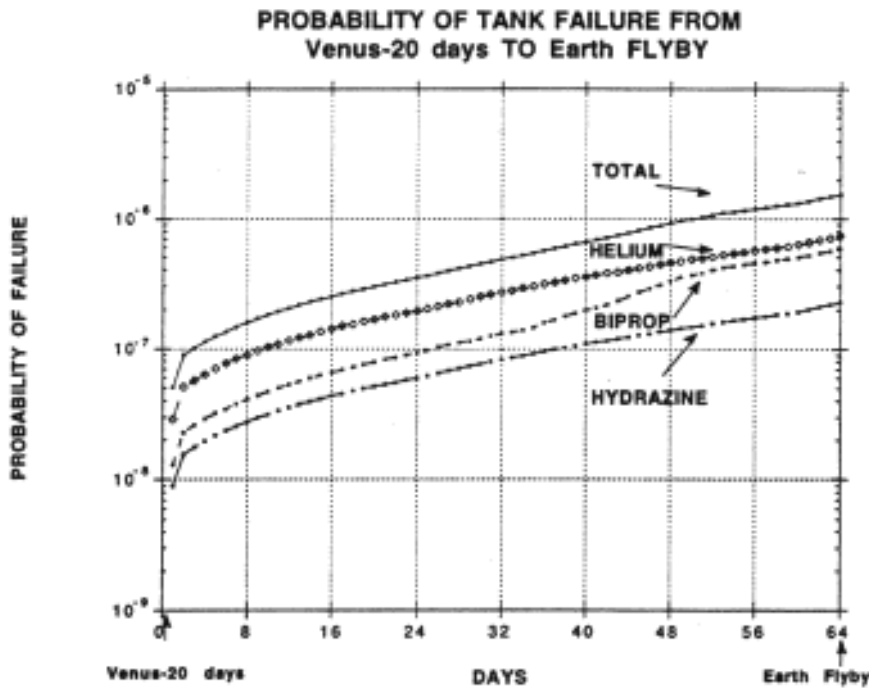
micrometeoroid model. Failures were calculated based on simplified shielding models and fluences averaged around the spacecraft longitudinal axis (Z axis).

The model has subsequently been converted from an omnidirectional model to a uni-directional model to account for the significant decrease in fluence on the non-ram side of the spacecraft and to allow for the probe and the newly added main engine cover shielding on the ram side of the spacecraft. (Ram direction is defined as direction of maximum relative velocity)

The Divine Model incorporates the latest data on the interplanetary micrometeoroid environment and is derived from in-situ data from Pioneer 10 and 11, Helios 1, Galileo, and Ulysses, ground-based radar and zodiacal light measurements, and interplanetary flux measurements near the Earth (spacecraft and lunar craters). It consists of 5 separate populations, each having separable distributions in particle mass and in orbital inclination, eccentricity, and perihelion distance. Using data from this model and best engineering judgment the uncertainty in fluence ( $f_l$ ) was assumed to be represented as a normal distribution, with a mean of 1 and a standard deviation of 3. The distribution was assumed to be truncated below 0 (References 6 and 7).

The resulting fluence above the critical mass was calculated for all solid angles for every tank node and summed. A view factor which represents the fraction of the fluence reaching the target was calculated for each sector and the nodes associated with it. The directional fluences calculated were then multiplied by the geometrical view factor ( $V_i$ ) specified for each of the nodes and configurations and then multiplied by the areas involved to produce the probability of failure for each of the tanks. The probability of failure, for the final spacecraft configuration, calculated as a function of time for the segment from Venus -20 days to Earth is illustrated in Figure 3-7. The total cumulative probability of tank failure from Venus -20 days to Earth Flyby is  $1.55E-6$ , and from Earth -10 days to Earth Flyby is  $4.13E-7$  (Reference 3-7).

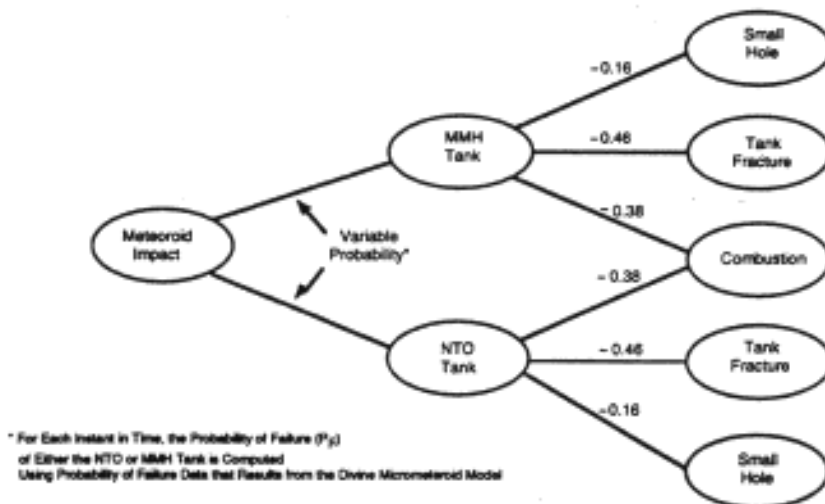
Figure 3-7



### 3.2.1.6.1 Changes in $\Delta V$ Model

A Monte Carlo model simulating the results of five different tank micrometeoroid failure modes was developed. The five modes include a small hole leak or single tank fracture in each of the two bipropellant tanks and one mode where both tanks rupture, propellants mix and combustion ensues. The paths, graphically depicted in Figure 3-8, represent the set of all possible outcomes resulting from a micrometeoroid penetrating a propellant tank.

Figure 3 - 8  
 Calculated Probabilities for Possible Scenario Paths Result  
 from Micrometeoroid Damage to Propellant Tanks



The probability of a given tank being struck and damaged is based on an analysis of the exposed tank area, as well as the location, thickness and spacing of the protective blankets.

The ratio of micrometeoroid induced oxidizer tank failure probability to fuel tank failure probability varies over the mission based on spacecraft orientation and RAM direction. Note that for the primary mission a fuel tank failure tends to push the spacecraft away from the Earth while an oxidizer tank failure tends to push the spacecraft in the general direction of the Earth.

Some small perforations in the tank wall (smaller than approximately 1.0 cm in diameter) will not propagate through the tank. In these cases the fluids and gases contained in the tank will jet out through the pinhole. Penetration of the tank without causing crack propagation can occur only in the thicker cylindrical section of the tank. Taking the ratio of the tank girth area, that is susceptible to puncture, to the total tank area yields a value of 0.16 (Reference 3-8). This small hole probability of occurrence was represented by a Gaussian distribution with a mean value of 0.16 and  $3\sigma$  uncertainty of 0.032 (corresponding to a .20 variation of the mean value). Holes larger than approximately 1.0 cm in diameter will propagate through the tank wall causing disintegration of the tank (Reference 3-9 & 11). If fragments from the ruptured tank impact the other bipropellant tank the second tank may also rupture.

When both bipropellant tanks rupture the MMH and NTO may mix and combust. If this occurs the core structure between the two tanks will rupture and release the combustion products in a lateral direction. The probability of "combustion" was based on a

lateral direction. The probability of "combustion. was based on a simple mechanical model that varied the number, size, and velocity of tank fragments. If a fragment with sufficient impulse impacted the adjacent tank, fracture and consequential combustion was assumed to occur. Selection of the number of fragments allows an estimate of the combustion probability to be made from the model. Examination of experimental data from tank fracture tests indicated that a tank similar to the Cassini design broke into a large number of pieces when ruptured. Based on this experimental evidence it was assumed that the number of tank fragments could be represented by a Gaussian distribution with a mean value of 20 and a  $3\sigma$  uncertainty of 6. The model predicted a .38 probability of combustion with a  $3\sigma$  uncertainty of  $\pm 0.06$  (Reference 3-9).

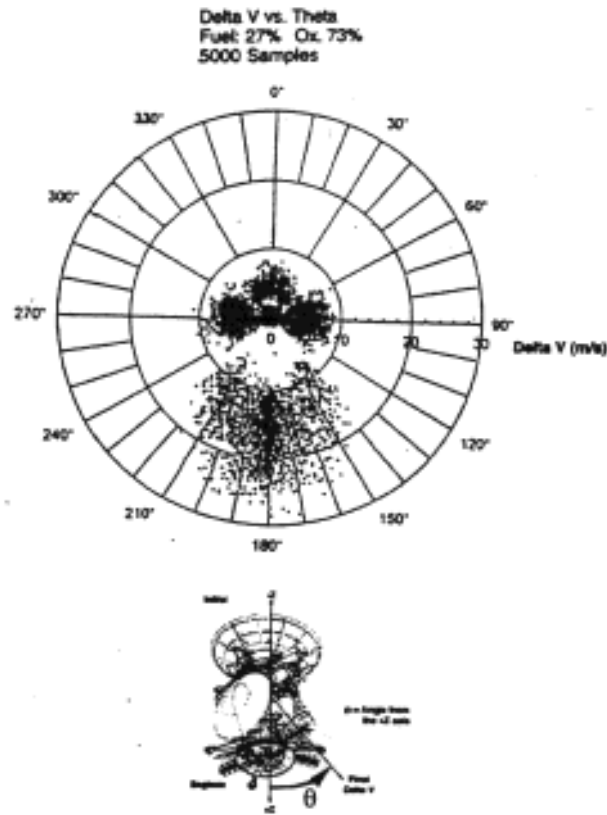
The probability of the remaining scenario, a single tank rupture without combustion, was taken as the difference i. e. 1 minus probability of a small hole (0.16) minus the probability of combustion (0.38), = 0.46 single tank rupture, no combustion.

The models were run independently and concurrently to develop  $\Delta V$  distributions.

#### 3.2.1.6.2 Resultant $\Delta V$ from the Monte Carlo Model

Resultant  $\Delta V$ s depend on the impulse imparted to the spacecraft, spacecraft mass, angular orientation of the impulse vector with respect to the spacecraft +Z axis and time during which the impulse is being applied. For each Monte Carlo case involving a tank failure scenario, the impulse imparted to the spacecraft, the angular orientation of the impulse vector with respect to the spacecraft and the time duration of the event were calculated. Since the flow fields are complex, it was felt that a stochastic representation of the resulting  $\Delta V$  magnitude and direction was most appropriate for this situation. Figure 3-9 represents the  $\Delta V$  magnitude and direction imparted to the spacecraft as a result of micrometeoroid induced tank failure. Fuel tank rupture is depicted as the cluster above the center point on the +Z axis (00) and oxidizer tank rupture is along the -Z axis in the 180° axis. Z is the longitudinal axis of the spacecraft which is typically oriented away from the Sun. The X and Y axis are 90° to the Z axis. Resultant data for the combustion case are the clusters to the right and left of center. The small hole leak is represented by the tight cluster around the center point of the graph. All values are symmetric around the Z axis. Results are representative of the primary mission.

Figure 3-9  
Spacecraft  $\Delta V$  Magnitude and Direction as a Result of  
Micrometeoroid Induced Tank Failure



### 3.2.1.6.3 Small Hole Model

Most micrometeoroids large enough to penetrate a propellant tank will fracture the tank. However, there are holes approximately 1.0 cm in diameter that can be produced in the thickened girth of the tanks. If a micrometeoroid punctures a bipropellant tank the fluids under pressure will jet out through the small hole until the tank is depleted. The helium pressure regulator is isolated throughout most of the mission, so the ejection process will occur in a blowdown mode. Generally a liquid stream will be expelled from the hole, followed by the pressurized gas and vapors as the ullage volume reaches the position of the hole. In cases large enough for the forces to overwhelm the attitude control system, the spacecraft will spin up. These cases are assumed to be unrecoverable but there is significant cancellation of forces and relatively little  $\Delta V$  (Reference 3-8 & 10). The parameters that were stochastically

varied in a Monte Carlo routine was to model the small hole case are detailed in Reference 3-9. Three of these parameters, hole size, tank temperature and angle of escaping fluid are described below. The upper limit of the hole diameter was assumed to be the largest hole size that could be sustained without crack propagation throughout the tank. The lower limit of the hole diameter is based on the minimum size hole that would allow the force of the escaping gas to overwhelm the attitude control system. The tank temperatures were assumed to vary over their expected operational limits, taking into account the cooling that would occur during the extended time that the blowdown process would take. The angle of the escaping fluid from the MMH tank was bounded on one side by the high gain antenna structure. The flow from the NTO tank was assumed to be axial since no corresponding structure exists along the +Z axis. The angular uncertainties were chosen to be indicative of the confidence in the mean values (Reference 3-11).

Below the lower size limit of the small hole (0.14 cm diameter) the force of escaping gas can be countered by the attitude control system (Reference 3-10). Although it may result in a high duty and generate up to 60 m/s in the -z direction, it would require two to six days for this to occur and this provides sufficient time to perform an emergency avoidance maneuver. These recoverable cases are not included in Figure 3-9 but are factored with a probability of no-recovery into the overall analysis. If the spacecraft loses commendability during the recovery period (section 3.5), the hydrazine will eventually be depleted and the spacecraft will spin up and respond as it did for the larger pinhole failure described in the above paragraph.

#### 3.2.1.6.4 Tank Failure Model

The total impulse imparted to the spacecraft as a result of a single bipropellant tank rupture is the sum of the impulse from the pressurant gas, vapor and liquid propellant. Variables include hole location, ullage bubble location, amount of liquid expelled by pressurant gas, rate of liquid propellant vaporization, and mass distribution within the escaping jet. (Reference 3-9)

#### 3.2.1.6.5 Combustion Model

In a percentage of the cases where a tank is destroyed by a micrometeoroid impact the shrapnel generated by the first failure will puncture the second tank. The two propellants will come into contact and combustion will occur within the core structure in the area between the two tanks. Combustion continues and pushes the liquids apart. The noncombusted propellants will be expelled from the ends of the core structure with resulting velocity vectors in the +/-Z direction. Pressures will build up

quickly causing the central core to fail allowing combustion products to be ejected from the spacecraft in approximately the X-Y plane. Once the core is ruptured, the internal pressure is relieved and the reaction ceases because the two liquids are moving apart and not likely to contact each other again (Reference 3-12). The impulse generated from the combustion (0 to 1% of the total propellant energy) was based on test data in the literature (Reference 3-12 & 13).  $\Delta V$  was calculated to be the vector sum of the  $\Delta V$  derived from combustion products expelled in the X-Y direction and that derived from the liquid and vapors being ejected along the +/-Z axis (significant cancellation occurs in the Z axis). Parameters that were varied in the Monte Carlo analysis used to simulate combustion included; percent of propellant combusted, size and number of holes generated in the core structure, angle of expulsion, and time required to expel the uncombusted oxidizers and fuel from the ends of the core structure. The resultant AV vector was assumed to be represented by a Gaussian distribution with a mean value of 5 m/s and a  $3\sigma$  of  $\pm 5$  m/s. The direction of the vector was determined to be a Gaussian distribution with a mean value of  $90^\circ$  (in the X-Y plane) and a  $3\sigma$  values of  $\pm 45^\circ$ .

Five thousand Monte Carlo samples involving all possible tank fracture scenarios were run.

#### 3.2.1.6.6 Other $\Delta V$ Model Changes

Based on additional information from interviews within the industry the probability of helium tank failure causing a propellant tank failure was increased from 5% assumed in Reference 3-3 to a value of 50% (similar to that assumed for the hydrazine tank). Helium and hydrazine tank ruptures were assigned an equal probability of failing either an oxidizer or fuel tank (Reference 3-11).

#### 3.2.2 Additional Failure Mode Analysis

Since the publication of Volume 3: Cassini Earth Swingby Plan, November 18, 1993, eleven additional failure modes were examined in more detail. Most involve failure in the on-board fault protection or are very low probability events. These included a pyro valve failure, a leak in the propellant tank upstream of the isolation valve, a failure in either the main engine valve or thruster valve fault protection and a main engine failure resulting in a ruptured feed line or oxidizer tank that could provide large  $\Delta V$ s. These were input to the final Earth impact analysis as indicated in Table 3-1. The results revealed that only the pyro valve failure can cause any significant effect

on the probability of Earth impact. Even this would only occur if a pyro valve were actuated during the Earth swingby period. This is prohibited by documented project requirements and mission constraints. The other failure modes were characterized by extremely low failure probabilities or required multiple failures with a resulting low probability of occurrence, or were recoverable. These new failure modes are further described below:

Pyro Valve Failure (event driven): This was conservatively modeled as a catastrophic failure that can occur whenever a pyro valve is opened or closed. This failure is characterized by propellant liquid/vapor mixing resulting in combustion, and/or structural failure in the valve, propellant tank or line failure following a pyro valve actuation. Based on review of industry experience and engineering judgment the probability of this failure is conservatively estimated at  $10^{-3}$  failures per pyro event (Table 3-1).

Passive Tank Failure (time driven): This is another unrecoverable but very unlikely failure that might theoretically occur anytime during cruise due to manufacturing defects and long-term exposure to high pressure propellant. Based on fracture analysis the probabilities of failure assigned for this event were: 10%,  $10^{-10}$  per day; 50%,  $10^{-9}$  per day; 90%,  $10^{-3}$  per day. Reference 3-14 demonstrates that the failure rates rarely are even lower.

Critical Feed System Leak is recoverable for short-term Earth avoidance in scenarios modeled both before and after E-5 except in the worst case 10% Model where torque exceeds control authority and/or there is a second failure in AACS, CDS or PPS causing the S/C to spin up. The mission is not recoverable. Based on analysis and engineering judgement the probabilities of failure were: 10%,  $0.125 \times 10^{-6}$  per day; 50%,  $0.25 \times 10^{-6}$  per day; 90%,  $0.5 \times 10^{-6}$  per day (Table 3-1).

Thruster latch valve fault protection failures and main engine latch valve fault protection failures are recoverable failures with probabilities of occurrences of less than  $5 \times 10^{-6}$  per day at the time of the Earth Swingby (Table 3-1).

In evaluating the effects of a main engine failure it was determined that there is not enough energy to rupture the feed lines or tanks and thereby cause any significant change in  $\Delta V$  (Reference 3-15). These new component failure modes plus a summary of the original failure modes documented in Reference 3-3 is included in Table 3-1.

### 3.3 INTERNAL SPACECRAFT FAILURES

#### 3.3.1 Internal Bus Probability of Failure

The probability of spacecraft loss was calculated as a function of time from launch for the primary and secondary missions. The definition of spacecraft loss is the inability to maneuver the spacecraft. This inability may be due to an inability to command, obtain tracking and telemetry, maintain attitude authority, or to actually execute a translational maneuver. Both the bipropellant and the monopropellant propulsion systems are designed to provide adequate maneuvering capability to avoid short or long-term impacts.

The probability is dominated by two classes of failures: (1) spacecraft internal parts failure, common mode failure or design error, and (2) micrometeoroid damage to internal electronics. A model using a Weibull Distribution was developed to simulate hardware reliability, component redundancy, susceptibility to common mode failures and design errors. Vulnerability to micrometeoroid impacts that could destroy single string and/or redundant functionality was also evaluated.

For internal failures, the median reliability as a function of time from launch in increments of 50 days was calculated. These failures were double, or single failures of parts combined with an estimate of design failures and common mode failures not protected by redundancy.

Median internal failure rates were calculated using the Weibull Model but because the model uncertainties appeared to be too low, they were conservatively increased to agree with engineering judgment (Reference 3-16). 10% and 90% curves were calculated for the short-term analysis but, because of the importance of this contributor the entire distribution was used for the long-term predictions.

The results indicate that the mean internal failure probability (one minus the reliability) rises rapidly from zero to 1.5% in the first 50 days, reflecting both early exposure of design failure and early parts failures. The failure rate then decreases reaching about 4.5% total failure probability at two years after launch. From there the failure rate continues at about 0.7% per year.

In addition to these generic internal failure modes, several specialized internal failure rates were available, all having to do with the propulsion system. One of those failures is significant for this calculation, and so was included. The remainder had probabilities low enough to not contribute to overall failure. The significant failure is an event-driven failure of a pyro valve upon firing, and the mean probability is approximately 0.5% loss per firing (median of 0.1%) This combined with the profile of pyro events was included in the calculation.

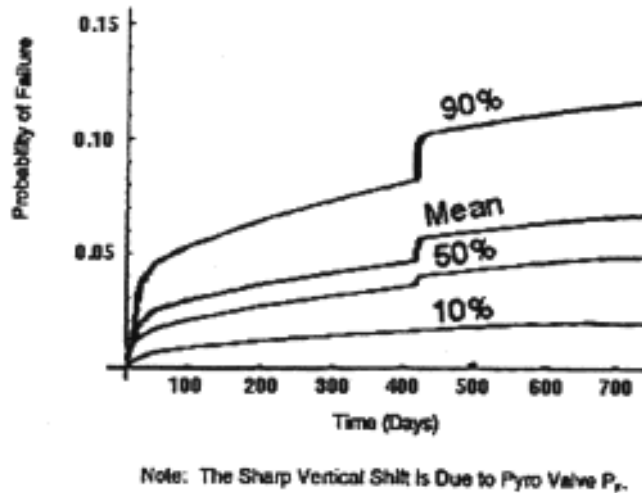
There are four pyro events on the primary and six on the secondary, adding 2% and 3% respectively to the overall failure probabilities.

Vulnerability of the spacecraft functions critical to maneuverability are dominated by the electronic circuit boards, electromechanical devices, interface circuits and cables. If a particle breaches the outer aluminum plate covering these electronics, any parts or boards that are in line of sight to the hole would be damaged. The vulnerable areas of the final spacecraft configuration and the thickness of the shields, subassembly by subassembly were determined. Finally, a Bayesian adjustment on the combined micrometeoroid environment and damage models, was calculated based on the flight experience (Refer to Section 3.3.2). No Bayesian factor was applied to the propellant and pressurant tanks protected by Beta cloth and stand-off shields since there is essentially no flight data upon which to base such a calculation (Reference 3-17 & 18).

These data were then combined to generate a spacecraft loss probability as a function of time for the primary and secondary missions. The resulting probability of failure causing loss of control from micrometeoroid impacts by SOI for the Primary Mission was approximately 2% and for the Secondary Mission the failure probability was 4%.

The internal and micrometeoroid failures were combined to take into account hybrid failures such as a part failure followed by a micrometeoroid hit on the other half of the redundant assembly. This resulted in an additional fraction of a percent failure. In order to assure that Earth swingby requirements were met the estimates included some conservatism. These results are plotted in Figure 3-10 as a function of time for the Primary Mission. It should be noted that failures occurring after Earth swingby will not affect the short-term or long-term impact probabilities. After the spacecraft is past the Earth and targeted for Jupiter, long-term impacts are very unlikely because resultant trajectories will have periapses greater than 1 AU.

**Figure 3-10** Total Probability of Failure vs. Time from Launch  
(Primary Mission)



Since the external micrometeoroid failures were a small contributor, and to simplify calculations, uncertainties were assumed equal to internal failure uncertainty. This only slightly overestimates the overall uncertainty (Reference 3-16).

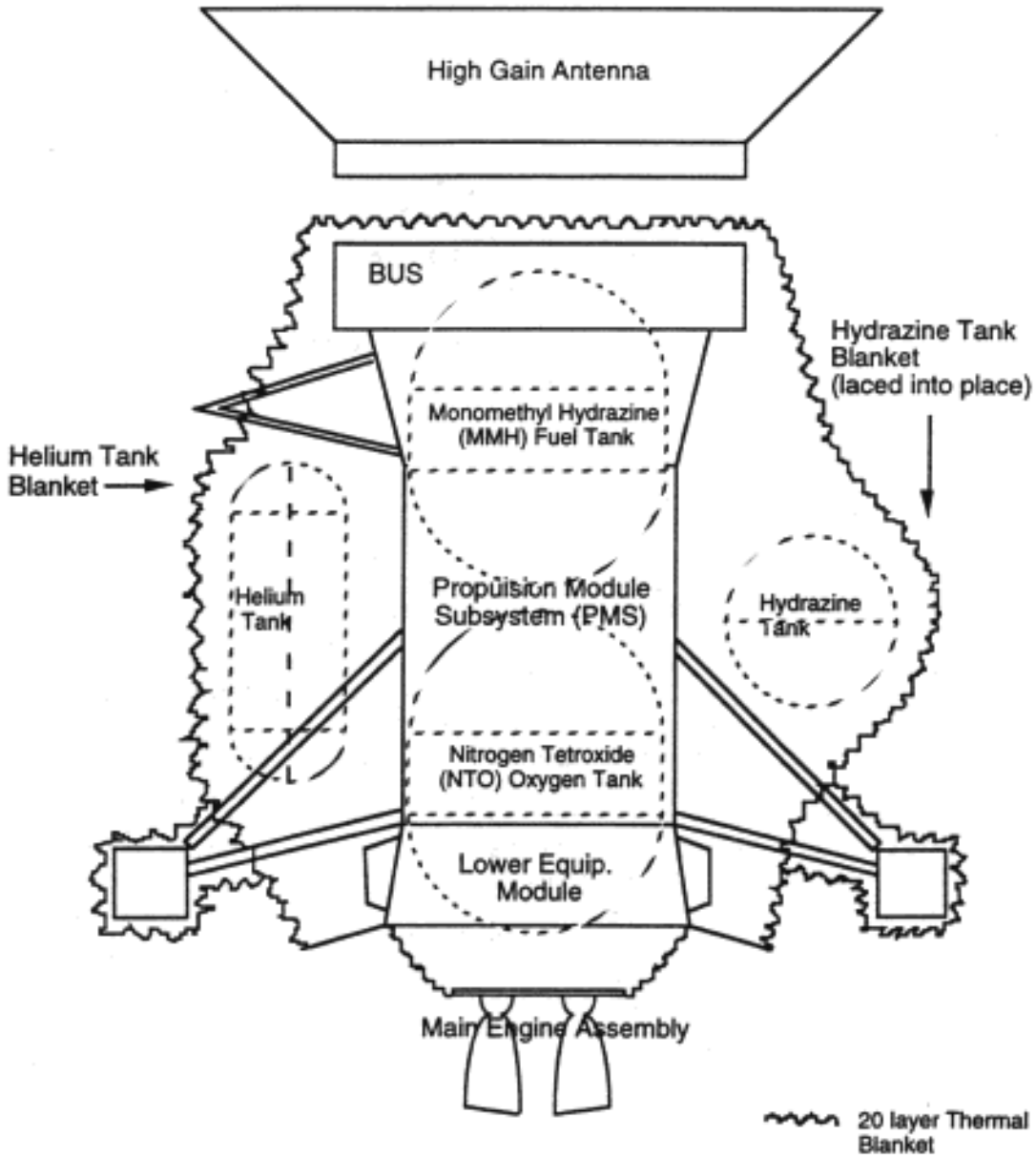
### 3.3.2 Bayesian Correction Factor to Bus Micrometeoroid Failure

A Bayesian analysis was performed in order to reconcile predictions of Bus micrometeoroid failures with previous flight experience. The predicted micrometeoroid failure rates for a Cassini-type mission were described by a probability distribution called the prior probability distribution. This distribution was then updated based on the observed experience of planetary flights. Equivalent Cassini missions with respect to previously flown missions; Galileo, Mars Observer, Voyager 1 and Voyager 2, were calculated using MLI protected areas and relative fluence. The results show that there have been twenty one equivalent Cassini Missions with only one failure (MO). Based on failure analysis it was conservatively assumed that there was a 10% chance that this could have been due to micrometeoroids (Reference 3-17). This results in a corrective factor of 5.1 (Reference 3-18).

3.4 Increased Micrometeoroid Shielding

The original blanket design is given in Figure 3-11. Increased protective shielding was added to the spacecraft design iteratively as preliminary micrometeoroid test results became known.

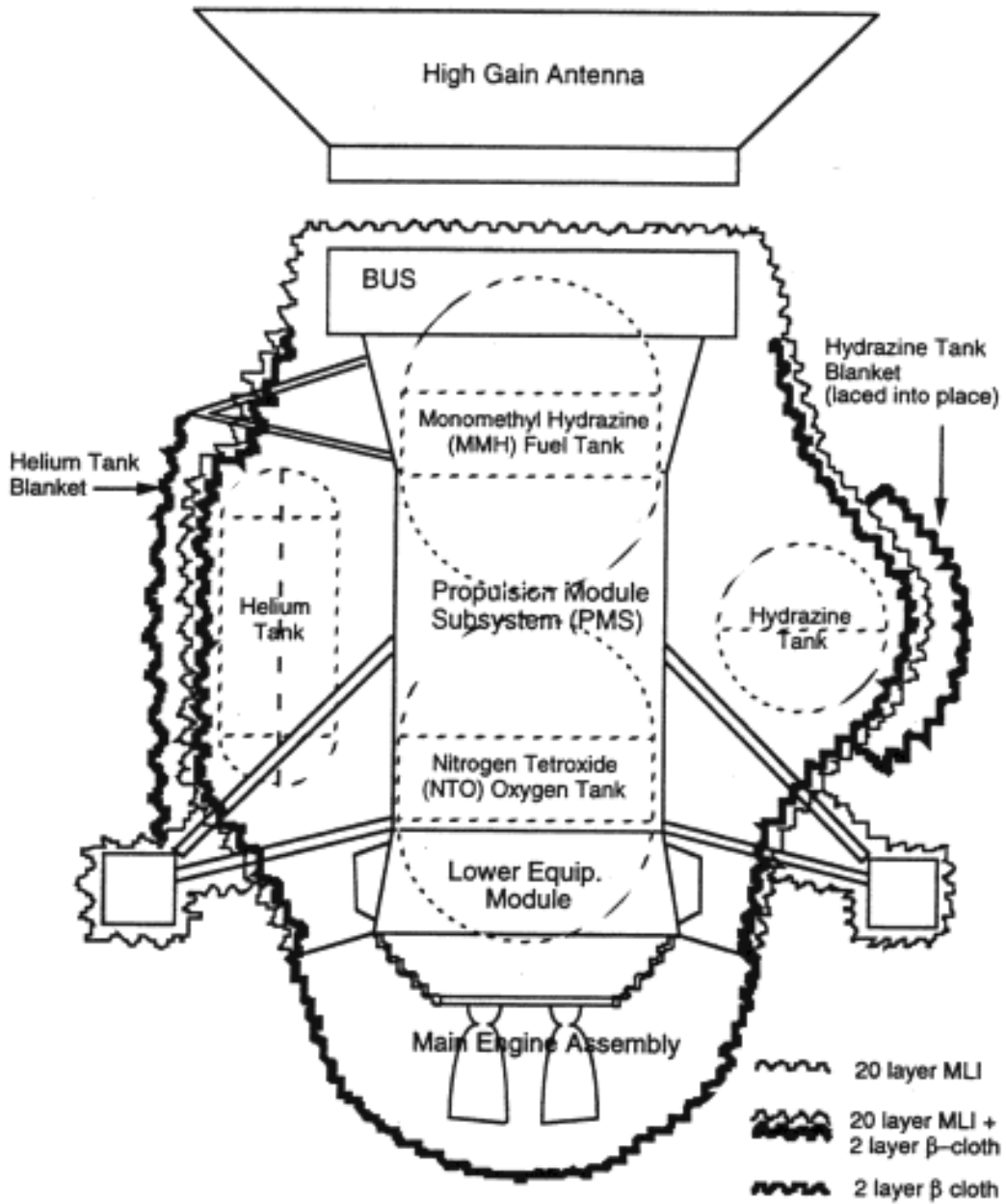
**Figure 3-11 Original S/C Blanket Configuration**



### 3.4.1 Changes in Spacecraft Design to Reduce Failure Probabilities Due to Micrometeoroid Impact

The blanket design was modified as shown in Figure 3-12. The primary modifications were to add two layers of Beta cloth to the Core Propulsion Module, plus two layers of Beta cloth in front of the Helium and Hydrazine tanks. For the Helium tank, this shield looks like a large sail that cocoons the tank. For the Hydrazine tank, the shield is laced into place and held off of the thermal blankets using 4" spacers. A two layer Beta cloth blanket was also added to cover the Main Engine Assembly. Additionally the shear plates covering unshielded electronics bays (including Bay B) were increased from 70 to 350 mils.

**Figure 3 -12 Modified S/C Blanket Configuration for Micrometeoroid Protection**



### 3.5 Probability of No Recovery ( $P_{NR}$ )

All of the failure modes are identified as either recoverable or non-recoverable. The result of a non-recoverable failure is the inability to execute a propulsive trajectory correction maneuver to place the spacecraft on a safe trajectory (Probability of No Recovery = 1). Following a recoverable failure a corrective maneuver will be made. If a second failure causing loss of command or control capability occurs before the corrective maneuver is accomplished the spacecraft's trajectory cannot be altered. The probability of being able to re-establish a safe trajectory ( $1 - P_{NR}$ ) is modeled as a function of the time from the next Earth encounter. The Probability of No-recovery Logic Diagram is depicted in Figure 3-13. This model was based on engineering judgment and flight experience.

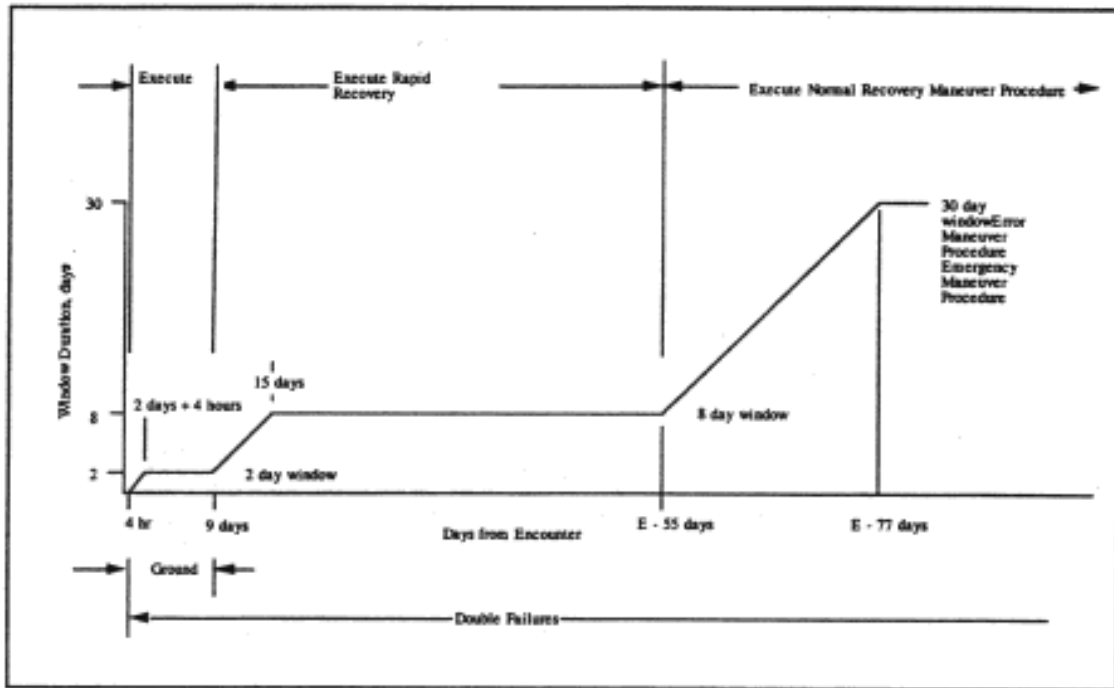


Figure 3-13: Probability of No Recovery Logic

Early in the mission there are large biases in the trajectory and it is extremely unlikely that a failure will result in an Earth impact. When the spacecraft is greater than 77 days from an Earth encounter, the nominal operational procedure is to allow up to 30 days to recover from the failure and return the spacecraft to a safe trajectory. During this time period, the recovery maneuver will be accomplished unless the spacecraft experiences a single catastrophic failure or two failures in redundant half subsystems that preclude further maneuvers. The

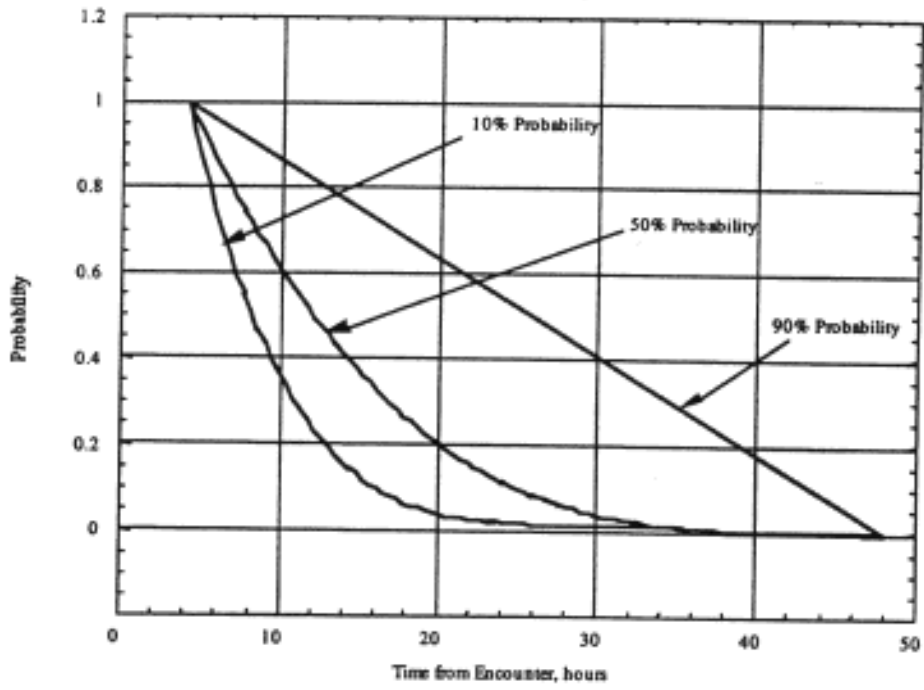
probability of no recovery is, therefore, the probability of the spacecraft losing commendability during the 30 day recovery period. The duration of the recovery period allows for recovery from single non-catastrophic failures.

When the time from encounter is less than 77 days, the time allowed for recovery is decreased linearly such that 55 days, prior to the Earth encounter (the time of the Venus flyby on the primary) the allowable recovery time is 8 days. From 55 days to 15 days prior to the Earth encounter, the nominal operational plan is to allow 8 days from the failure for the execution of the maneuver. The time reduction is obtained by instituting 24 hour per day tracking and requiring that the maneuver only achieves a safe trajectory and not necessarily a trajectory that satisfies the mission objectives. Maneuvers that move the trajectory away from a possible Earth impact will be pre-planned and can be executed, when needed, in less than 24 hours.

From 15 days to 9 days there is a second transition region where the time allowed to execute the maneuver following the failure, decreases linearly from 8 days to 2 days. The operational plan is to execute the rapid recovery maneuver and achieve a safe trajectory within the time limit. Achieving a trajectory that satisfies the mission objectives would require another maneuver after the completion of the recovery maneuver.

After the 9 day point the operational plan is to implement a pre-planned emergency maneuver within 2 days of the failure that placed the spacecraft on the Earth impacting trajectory. The emergency maneuver is designed to achieve a safe trajectory. Due to the limited time available, the emergency maneuver may not be completed due to a second single spacecraft failure. Further, since the time to implement the recovery maneuver is small, a probability that the ground system will not execute properly is introduced at the 9 day point. The ground error component is presented in Figure 3-14 (below). The probability of no recovery is, therefore, equal to the probability of a single spacecraft failure occurring during the 2 day time period before the maneuver is implemented summed with the probability that ground will not implement the maneuver properly in this time period. The mean probability of no recovery from 77 days to 2 days prior to Earth flyby is plotted in Figure 3-15 (Reference 3-19). 10% and 90% curves were based on the relevant spacecraft and ground system contributors.

Figure 3 -14 Probability of No Recovery  
Ground Error Component



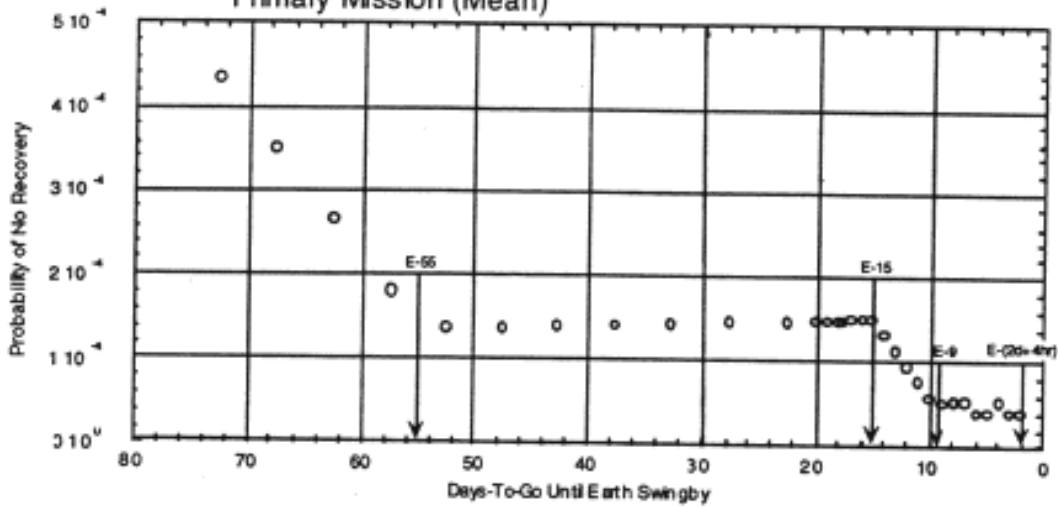
Probability Functions

10%:  $-2.7434e-08 T$

50 %  $-1.7519e-05 T$

90%:  $-0.022727 T + 1.0909$ ;  $1.4e-5$  below 48 hours

Figure 3 - 15 Probability of No Recovery 77 to 2 Days Before Earth Flyby Primary Mission (Mean)



TGG  
2/28/97

Note that in the Table 3-1 that follows there is no direct tie between the 10%, 50% and 90% models in the probability of failure and the delta-V columns.

Table 3-1. Spacecraft Components, Ground Induced Error and Flight Software Failure Probabilities and  $\Delta V$  Effects (Page 1 of 12)

FAILURE MODE	PROBABILITY OF FAILURE	$\Delta V$ (m/sec) and DIRECTION	RECOVERABLE	COMMENTS	TECHNIQUE FOR ESTIMATING FAILURE RATE	REFERENCE MEMO ON FAILURE RATE
1) Stuck Open Thruster Valve (Modified)			Yes for short-term Earth avoidance. Yes for the mission.		Flight Data	Ref 3-2, IOM: 353CAS/PMS-93-177, Rev. A, "Assessment of Cassini Propulsion System Failures, Their Probabilities of Occurrence, and $\Delta V$ s Produced", dated 2/22/95
<b>A. Z Thrusters</b>						
(1) Mechanical Failure	PF $\leq 5.0 \times 10^{-7}$ 10% PF $\leq 5.0 \times 10^{-6}$ 50% PF $\leq 5.0 \times 10^{-5}$ 90% Per thruster/day	$\Delta V_z$ $\Delta V$ Magn. = Gaussian Best Est.: $M = 2.1 \times 10^1$ ; $\sigma = 3 \times 10^1$ $M = -20\%$ , $\sigma = -50\%$ 10% $M = +20\%$ , $\sigma = +50\%$ 90% Direction = -Z	Yes for short-term Earth avoidance. Yes for the mission.		Flight Data	Ref 3-2, IOM: 353CAS/PMS-93-177, Rev. A, "Assessment of Cassini Propulsion System Failures, Their Probabilities of Occurrence, and $\Delta V$ s Produced", dated 2/22/95
(2) Electrical Failure	PF $\leq 2.0 \times 10^{-7}$ 10% PF $\leq 2.0 \times 10^{-6}$ 50% PF $\leq 2.0 \times 10^{-5}$ 90% Per thruster/day	$\Delta V_z$ $\Delta V$ Magn. = Uniform $3 \times 10^1 \rightarrow 6 \times 10^1$ 10% $3 \times 10^1 \rightarrow 6 \times 10^1$ 50% $3 \times 10^1 \rightarrow 6 \times 10^1$ 90% Direction = -Z	Yes for short-term Earth avoidance. Yes for the mission.		Flight Data	Ref 3-2, IOM: 353CAS/PMS-93-177, Rev. A, "Assessment of Cassini Propulsion System Failures, Their Probabilities of Occurrence, and $\Delta V$ s Produced", dated 2/22/95
<b>B. Y Thrusters</b>						
(1) Mechanical Failure	PF $\leq 5.0 \times 10^{-7}$ 10% PF $\leq 5.0 \times 10^{-6}$ 50% PF $\leq 5.0 \times 10^{-5}$ 90% Per thruster/day	$\Delta V_{+y, -y}$ $\Delta V$ Magn. = Gaussian Best Est.: $M = 1.06 \times 10^1$ ; $\sigma = 1.5 \times 10^1$ $M = -20\%$ , $\sigma = -50\%$ 10% $M = +20\%$ , $\sigma = +50\%$ 90% Direction = -y or +y $\Delta V_z$ $\Delta V$ Magn. = Gaussian Best Est.: $M = 3.7 \times 10^1$ ; $\sigma = 5 \times 10^1$ $M = -20\%$ , $\sigma = -50\%$ 10% $M = +20\%$ , $\sigma = +50\%$ 90% Direction = -Z	Yes for short-term Earth avoidance. Yes for the mission.		Flight Data	Ref 3-2, IOM: 353CAS/PMS-93-177, Rev. A, "Assessment of Cassini Propulsion System Failures, Their Probabilities of Occurrence, and $\Delta V$ s Produced", dated 2/22/95
(2) Electrical Failure	PF $\leq 2.0 \times 10^{-7}$ 10% PF $\leq 2.0 \times 10^{-6}$ 50% PF $\leq 2.0 \times 10^{-5}$ 90% Per thruster/day	$\Delta V_{+y, -y}$ $\Delta V$ Magn. = Uniform $3 \times 10^1 \rightarrow 6 \times 10^1$ 10% $3 \times 10^1 \rightarrow 6 \times 10^1$ 50% $3 \times 10^1 \rightarrow 6 \times 10^1$ 90% Direction = +y or -y $\Delta V_z$ $\Delta V$ Magn. = Uniform $7 \times 10^1 \rightarrow 1.4 \times 10^2$ 10% $7 \times 10^1 \rightarrow 1.4 \times 10^2$ 50% $7 \times 10^1 \rightarrow 1.4 \times 10^2$ 90% Direction = -Z	Yes for short-term Earth avoidance. Yes for the mission.		Flight Data	Ref 3-2, IOM: 353CAS/PMS-93-177, Rev. A, "Assessment of Cassini Propulsion System Failures, Their Probabilities of Occurrence, and $\Delta V$ s Produced", dated 2/22/95
2) Stuck-Open Main Engine Valve (Modified)						
<b>A. Mechanical Failure</b>						
(1) Oxidizer Valve Failure	PF $\leq 0.16 \times 10^{-7}$ 10% PF $\leq 0.16 \times 10^{-6}$ 50% PF $\leq 0.16 \times 10^{-5}$ 90% Per Engine Firing	$\Delta V_z$ $\Delta V$ Magn. = Gaussian Best Est.: $M = 4 \times 10^1$ ; $\sigma = 4 \times 10^1$ $M = -20\%$ , $\sigma = -50\%$ 10% $M = +20\%$ , $\sigma = +50\%$ 90% Direction = -Z	Yes for short-term Earth avoidance. Yes for the mission.		Flight Data	Ref 3-2, IOM: 353CAS/PMS-93-177, Rev. A, "Assessment of Cassini Propulsion System Failures, Their Probabilities of Occurrence, and $\Delta V$ s Produced", dated 2/22/95

Table 3-1. Spacecraft Components, Ground Induced Error and Flight Software Failure Probabilities and  $\Delta V$  Effects (Page 2 of 12)

FAILURE MODE	PROBABILITY OF FAILURE	$\Delta V$ (m/sec) and DIRECTION	RECOVERABLE	COMMENTS	TECHNIQUE FOR ESTIMATING FAILURE RATE	REFERENCE MEMO ON FAILURE RATE
(2) Fuel Valve Failure	PF $\leq 0.16 \times 10^{-7}$ 10% PF $\leq 0.16 \times 10^{-6}$ 50% PF $\leq 0.16 \times 10^{-5}$ 90% Per Engine Firing	$\Delta V$ -z $\Delta V$ Magn. = Gaussian Best Est.: M = $2.4 \times 10^3$ ; $\sigma = 2 \times 10^3$ M = -20%, $\sigma = -50\%$ 10% M = +20%, $\sigma = +50\%$ 90% (In -Z direction)	Yes for short-term Earth avoidance.  Yes for the mission.		Flight Data	Ref 3-2, IOM: 353CAS/PMS-93-177, Rev. A, "Assessment of Cassini Propulsion System Failures, Their Probabilities of Occurrence, and $\Delta V$ s Produced", dated 2/22/95
B. Electrical Failure						
(1) Oxidizer and Fuel Valves Remain Open	PF $\leq 0.07 \times 10^{-7}$ 10% PF $\leq 0.07 \times 10^{-6}$ 50% PF $\leq 0.07 \times 10^{-5}$ 90% Per Engine Firing	$\Delta V$ -z $\Delta V$ Magn. = Gaussian Best Est.: M = $1.5 \times 10^3$ ; $\sigma = 1 \times 10^3$ M = -20%, $\sigma = -50\%$ 10% M = +20%, $\sigma = +50\%$ 90% (In -Z direction)	Yes for short-term Earth avoidance.  Yes for the mission.		Flight Data	Ref 3-2, IOM: 353CAS/PMS-93-177, Rev. A, "Assessment of Cassini Propulsion System Failures, Their Probabilities of Occurrence, and $\Delta V$ s Produced", dated 2/22/95
3) Accelerometer Failure (No Change)	PF = $6 \times 10^{-4}$ 10% PF = $1 \times 10^{-3}$ 50% PF = $1.6 \times 10^{-3}$ 90% Per Day Between Maneuvers PLUS PF = $4.8 \times 10^{-3}$ 10% PF = $8 \times 10^{-3}$ 50% PF = $1.3 \times 10^{-2}$ 90% Per Day During Maneuvers	Magn. = Gaussian M = 4%, $\sigma = 1.33\%$ 10% M = 5%, $\sigma = 1.67\%$ 50% M = 6%, $\sigma = 2\%$ 90% Of Planned Mavr. Direction: -Z	Yes for short-term Earth avoidance.  Yes for the mission.		Analysis	Ref 3-2, IOM: 353CAS/PMS-93-177, Rev. A, "Assessment of Cassini Propulsion System Failures, Their Probabilities of Occurrence, and $\Delta V$ s Produced", dated 2/22/95
4) Main Engine Gimbal Actuator Failure (No Change)	PF = $1.02 \times 10^{-4}$ 10% PF = $1.70 \times 10^{-4}$ 50% PF = $2.72 \times 10^{-4}$ 90% Per Maneuver	Magn. = Gaussian M = $4 \times 10^3$ , $\sigma = 8 \times 10^4$ 10% M = $1.3 \times 10^3$ , $\sigma = 2.6 \times 10^3$ 50% M = $2.6 \times 10^3$ , $\sigma = 5.2 \times 10^3$ 90% Meters Per Second Direction: Uniform lateral	Yes for short-term Earth avoidance.  Yes for the mission.		Analysis	Ref 3-3, JPL D-10178-3, "Cassini Program Environmental Impact Statement, Supporting Study, Vol. 3: Cassini Earth Swingby Plan", dated 11/18/93
5) AACCS Flight Software Error (No Change)	PF = $5.0 \times 10^{-4}$ 10% PF = $5.0 \times 10^{-3}$ 50% PF = $1.0 \times 10^{-2}$ 90% Per Day	(50%) RCS $3 \times 10^{-4}$ 10% $1 \times 10^{-3}$ 50% $5 \times 10^{-3}$ 90% Direction: Uniform spherical (50%) Main Engine $2 \times 10^{-3}$ 10% $8 \times 10^{-3}$ 50% $1.7 \times 10^{-2}$ 90% Direction: -Z Meters Per Second	Yes for short-term Earth avoidance.  Yes for the mission.		Analysis	Ref 3-3, JPL D-10178-3, "Cassini Program Environmental Impact Statement, Supporting Study, Vol. 3: Cassini Earth Swingby Plan", dated 11/18/93
6) CDS Flight Software Error (No Change)	PF < $1 \times 10^{-4}$ 10% PF < $1 \times 10^{-3}$ 50% PF < $1 \times 10^{-2}$ 90% Per Day	Magn.: Last commanded $\Delta V$ Direction: -Z	Yes for short-term Earth avoidance.  Yes for the mission.		Analysis	Ref 3-3, JPL D-10178-3, "Cassini Program Environmental Impact Statement, Supporting Study, Vol. 3: Cassini Earth Swingby Plan", dated 11/18/93

Table 3-1. Spacecraft Components, Ground Induced Error and Flight Software Failure Probabilities and  $\Delta V$  Effects (Page 3 of 12)

FAILURE MODE	PROBABILITY OF FAILURE	$\Delta V$ (m/sec) and DIRECTION	RECOVERABLE	COMMENTS	TECHNIQUE FOR ESTIMATING FAILURE RATE	REFERENCE MEMO ON FAILURE RATE
7) Anomalous Sun Search (No Change)	PF = $1 \times 10^7$ 10% PF = $1 \times 10^4$ 50% PF = $2 \times 10^4$ 90%  Per Maneuver	Magn. = Uniform: 0 - $5 \times 10^2$ 10% 0 - $6.3 \times 10^2$ 50% 0 - $7.6 \times 10^2$ 90%  Meters Per Second  Direction: Uniform spherical	Yes for short-term Earth avoidance.  Yes for the mission.		Analysis	Ref 3-3, JPL D-10178-3, "Cassini Program Environmental Impact Statement, Supporting Study, Vol. 3: Cassini Earth Swingby Plan", dated 11/18/93
Ground Induced Errors						
8) Erroneous Ground Initiation of TCM (No Change)	PF = $2 \times 10^{10}$ 10% PF = $2 \times 10^9$ 50% PF = $2 \times 10^8$ 90%  Per Day	Conservatively assumed probability of impact given failure = 1	Yes for short-term Earth avoidance.  Yes for the mission.		Analysis	Ref 3-3, JPL D-10178-3, "Cassini Program Environmental Impact Statement, Supporting Study, Vol. 3: Cassini Earth Swingby Plan", dated 11/18/93
9) Navigation Design Error (No Change)	PF = $6.9 \times 10^9$ 10% PF = $1.1 \times 10^7$ 50% PF = $1.7 \times 10^6$ 90%  Per Maneuver	Error equally likely in any of three components ( $\Delta V$ , roll, yaw) 0 - 1% 10% 0 - 10% 50% 0 - 100% 90%  Command Value	Yes for short-term Earth avoidance.  Yes for the mission.		Analysis	Ref 3-3, JPL D-10178-3, "Cassini Program Environmental Impact Statement, Supporting Study, Vol. 3: Cassini Earth Swingby Plan", dated 11/18/93

Table 3-1. Spacecraft Components, Ground Induced Error and Flight Software Failure Probabilities and  $\Delta V$  Effects (Page 4 of 12)

FAILURE MODE	PROBABILITY OF FAILURE	$\Delta V$ (m/sec) and DIRECTION	RECOVERABLE	COMMENTS	TECHNIQUE FOR ESTIMATING FAILURE RATE	REFERENCE MEMO ON FAILURE RATE
10) Pyro Valve Failure (New)	<p>Combined distribution function splicing 1) and 2). Combined Median = <math>1 \times 10^{-3}</math></p> <p>1) For values below the combined median use: lower half of one normal distribution Median = <math>1 \times 10^{-3}</math> <math>3\sigma</math> low of 0 (truncate below 0)</p> <p>2) For values above the combined median use: upper half of a second normal distribution Median = <math>1 \times 10^{-3}</math> <math>3\sigma</math> high of <math>1 \times 10^{-2}</math> (truncate above <math>1 \times 10^{-3}</math>)</p> <p>Normal Distribution</p> <p>Per pyro valve firing</p>	<p>For <math>\Delta V</math> use the Biprop <math>\Delta V</math> Model.</p> <p>Assume the ratio of fuel tank failures to oxygen tank failures is 1:1.</p>	<p>No for short-term Earth avoidance.</p> <p>No for the mission.</p>	<p>1. Propellant liquid/vapor mixing, combustion or valve structural failure cause propellant tank or line failure following a pyro valve actuation.</p>	Analysis	<p>Ref 3-11, IOM: 311.12/95-142, "Monte Carlo Analysis of Cassini Spacecraft <math>\Delta V</math> Produced by Micrometeoroid Impact", dated 11/30/95 (For description of Biprop <math>\Delta V</math> Model)</p>
11) Passive Tank Failure (New)	<p><math>1 \times 10^{-10}</math> 10% <math>1 \times 10^{-9}</math> 50% <math>1 \times 10^{-8}</math> 90%</p> <p>Per Day</p> <p>Lognormal</p>	<p>For <math>\Delta V</math> use the Biprop Small Hole Model</p>	<p>No for short-term Earth avoidance.</p> <p>No for the mission.</p>	<p>1. Failure probabilities are based on a fracture mechanics. Tanks will have already survived higher pressures and temperatures earlier in the mission. (These holes will be 1 cm or less in diameter. Larger holes will cause the tank to burst but wouldn't occur in this passive failure mode. Leakage through holes smaller than 0.14 cm will be countered by the AACS system. These will produce <math>\Delta V</math>'s similar to the critical feed system leak described in Failure #13 and #14 below and are covered by them.)</p>	Analysis	<p>Ref 3-10, IOM: 311.6/97-063-G1J "Determination of Limiting Small Hole Threshold", dated 4/18/97 (For description of limit of 0.14 cm)</p> <p>Ref 3-11, IOM: 311.12/95-142, "Monte Carlo Analysis of Cassini Spacecraft <math>\Delta V</math> Produced by Micrometeoroid Impact", dated 11/30/95 (For description of Small Hole <math>\Delta V</math> Model)</p>

Table 3-1. Spacecraft Components, Ground Induced Error and Flight Software Failure Probabilities and  $\Delta V$  Effects (Page 5 of 12)

FAILURE MODE	PROBABILITY OF FAILURE	$\Delta V$ (m/sec) and DIRECTION	RECOVERABLE	COMMENTS	TECHNIQUE FOR ESTIMATING FAILURE RATE	REFERENCE MEMO ON FAILURE RATE
12) Main Engine Catastrophic Failure (New)	$1 \times 10^{-6}$ 10% $1 \times 10^{-5}$ 50% $1 \times 10^{-4}$ 90%  Per Firing  Lognormal	Use Main Engine Valve Fail-Open Model  (Use -Z thrust model, use ox valve to fuel valve failure at ratio 50:50.)	Yes for short-term Earth avoidance.  Yes for the mission.	1. Analysis indicates there is not enough energy in the propellant (that could collect in the engine) to fracture the propellant valve bolts, endangering the oxidizer tank that releases significantly more $\Delta V$ . Failure rate is based on review of R4D Engine data and engineering judgement.  2. Main Engine fails explosively during a firing and causes structural damage to the propellant valves	Engineering judgement	Ref 3-15, TOM: 352K-97-008, "Main Engine Valve Impacting Oxidizer Tank", dated 1/31/97

Table 3-1. Spacecraft Components, Ground Induced Error and Flight Software Failure Probabilities and  $\Delta V$  Effects (Page 6 of 12)

FAILURE MODE	PROBABILITY OF FAILURE	$\Delta V$ (m/sec) and DIRECTION	RECOVERABLE	COMMENTS	TECHNIQUE FOR ESTIMATING FAILURE RATE	REFERENCE MEMO ON FAILURE RATE
13) Critical Feed System Leak Occurring Prior to E-5 days (New)	$0.125 \times 10^{-4}$ 10% $0.25 \times 10^{-4}$ 50% $0.5 \times 10^{-4}$ 90%  Per Day  Lognormal	10% Model: (Torque exceeds control authority and/or if there is a second failure preventing recovery it occurs shortly following the 1st failure and occurs in AACs, CDS or PPS causing the SAC to spin up.) For $\Delta V$ use the Biprop Small Hole Model  50% Model: (Condition described above occurs after half of propellant leaks out) $\Delta V$ sum 1) and 2): 1) uniformly around $4\pi$ steradians, median=60 m/s, range 0 (-3 $\sigma$ ) (10%) - 120 (+3 $\sigma$ ) (90%). Normal Distribution 2) The second vector is as described for second vector of the 50% Model in Failure #18.  90% Model: (Control authority not exceeded. If there is a 2nd failure preventing recovery it occurs in RPS or PMS preventing uplinking emergency avoidance maneuver.) $\Delta V$ uniformly around $4\pi$ steradians, median=120 m/s from 0 (-3 $\sigma$ ) (10%) - 240 (+3 $\sigma$ ) (90%). Normal Distribution	No for 10% $\Delta V$ Model for short-term Earth avoidance.  Yes for 50% $\Delta V$ Model for short-term Earth avoidance.  Yes for 90% $\Delta V$ Model for short-term Earth avoidance.  No for the mission.	10% Model: See Failure #11, Reference #11.	Analysis and engr. judgement	Ref 3-10, IOM: 311.6/97-063-GIJ, "Determination of Limiting Small Hole Threshold", dated 4/18/97  Ref 3-11, IOM: 311.12/95-142, "Monte Carlo Analysis of Cassini Spacecraft $\Delta V$ Produced by Micrometeoroid Impact", dated 11/30/95

Table 3-1. Spacecraft Components, Ground Induced Error and Flight Software Failure Probabilities and  $\Delta V$  Effects (Page 7 of 12)

FAILURE MODE	PROBABILITY OF FAILURE	$\Delta V$ (m/sec) and DIRECTION	RECOVERABLE	COMMENTS	TECHNIQUE FOR ESTIMATING FAILURE RATE	REFERENCE MEMO ON FAILURE RATE
14) Critical Feed System Leak Occurring After E-5 days. (New)	Same as Failure #13 above.	<p>10% Model: (Torque exceeds control authority and/or if there is a second failure preventing recovery it occurs shortly following the first failure and occurs in AACS, CDS or PPS causing the S/C to spin up.) For <math>\Delta V</math> use the Biprop Small Hole Model</p> <p>50% Model: (Condition described above occurs approximately half way to Earth from time of leak.) <math>\Delta V</math> sum of vectors 1) and 2): 1) uniformly around <math>4\pi</math> steradians varies 0 - "<math>v</math>", "<math>v</math>" median=0.075 m/s, 10% factor of 10 lower, 90% factor of 10 higher. Lognormal 2) The second vector is as described in the second vector of the 50% Model in Failure #18.</p> <p>90% Model: (Control authority not exceeded. If there is a second failure preventing recovery it occurs in RPS or PMS preventing uplinking emergency avoidance maneuver.) <math>\Delta V</math> uniformly around <math>4\pi</math> steradians varies uniformly 0 - "<math>v</math>", "<math>v</math>" median=0.150 m/s, 10% factor of 10 lower, 90% factor of 10 higher. Lognormal</p>	<p>No for 10% <math>\Delta V</math> Model for short-term Earth avoidance.</p> <p>Yes for 50% <math>\Delta V</math> Model for short-term Earth avoidance.</p> <p>Yes for 90% <math>\Delta V</math> Model for short-term Earth avoidance.</p> <p>No for the mission.</p>	<p>10% Model: See Failure #11, Reference #11.</p> <p>1. Failure rate same as Failure Mode #13 above.</p> <p>2. Assumed effective ISP varied from 25 to 50 sec.</p> <p>3. Effective time of leak (relevant to Earth Swingby) varies from 0 to 5 days.</p> <p>4. Assumed leakage rates as follows: 0.001 x normal RCS 10%; 0.01 x normal RCS 50%; 0.1 x normal RCS 90%. Thruster Flow Rate</p> <p>5. Direction and magnitude of first <math>\Delta V</math> vector depend on location (lever and arm) and direction of leak. The resultant vector is the sum of the vector representing the leak plus the vector representing impulse from the RCS thruster(s) attempting to compensate for the leak.</p> <p>6. See Failure #13, Comment #5.</p>	Analysis	<p>Ref 3-10, IOM: 311.6/97-063-G11, "Determination of Limiting Small Hole Threshold", dated 4/18/97</p> <p>Ref 3-11, IOM: 311.12/95-142, "Monte Carlo Analysis of Cassini Spacecraft <math>\Delta V</math> Produced by Micrometeoroid Impact", dated 11/30/95</p>

Table 3-1. Spacecraft Components, Ground Induced Error and Flight Software Failure Probabilities and ΔV Effects (Page 8 of 12)

FAILURE MODE	PROBABILITY OF FAILURE	ΔV (m/sec) and DIRECTION	RECOVERABLE	COMMENTS	TECHNIQUE FOR ESTIMATING FAILURE RATE	REFERENCE MEMO ON FAILURE RATE
15) RCS Thruster Valve Critical Leak/Fail-open in Combination with Backup Fault Protection Latch Valve Leak Prior to E-5 Days. (New)	$(1/8 \times 10^{-4}) t$ 10% $(1/4 \times 10^{-4}) t$ 50% $(1/2 \times 10^{-4}) t$ 90%  Failures Per Day Lognormal  $t$ = total number of days latch valve is exposed to propellant (approximately equal to number of days since launch+50)	10% Model: (It is assumed that if there is a second failure preventing a recovery maneuver it occurs shortly following the first failure and occurs in AACS, CDS or PPS causing the S/C to spin up) For ΔV use the Biprop Small Hole Model  50% Model: (Condition described above occurs after half the propellant leaks out) ΔV sum 1) and 2): 1) median=30 m/s, 24 m/s (10%) - 36 m/s (90%). Direction: -Z Normal Distribution 2) Second vector is as described in the second vector of the 50% Model in Failure #18.  90% Model: (It is assumed that if there is a second failure preventing a recovery maneuver it occurs in RFS or PMS preventing uplinking emergency avoidance maneuver.) ΔV median=60 m/s, 48 m/s (10%) - 72 m/s (90%). Direction: -Z Normal Distribution	Yes for short-term Earth avoidance.  No for the mission.	10% Model: See Failure #11, Reference #11.  1. The critical leaks defined here are moderate in size in comparison with the excessive leaks experienced in the valve fail-open case. There is little flight data available on these moderate leakage failures (as opposed to valve fail-open failures.) So the thruster valve critical leak failure rate is assumed to be 5 times greater (engineering judgement) than the thruster valve mechanical fail-open rate which was derived from flight data (valve failure rates $5 \times 10^{-4}$ fail/thruster/day). As a sanity check this is roughly equivalent to a 13% probability that one of the four Z-facing or four roll thruster valves will develop a critical (moderate) leak in the 660 days prior to Earth Swingby. Leakage failure rate for four Z-facing thruster valves = $1 \times 10^{-4}$ failures/day. (Don't multiply by 4).  2. Latch valve leakage is more likely than mechanical or electrical latch valve failure. Leakage failure rate assumed equal to that of one thruster valve. Probability is based on total time "T" valve is exposed to propellant. Probability of latch valve critical leak = $(1/4 \times 10^{-4})t$ .  3. Applies to Z-facing thrusters only. Leaks in roll thrusters don't generate V.  4. At this point in mission total ΔV capability of hydrazine RCS thruster system is assumed equal to 60 m/s with a 20% uncertainty due to ISP and propellant load.  5. Probability of both the thruster valve and latch valve failing open would be negligible. Assuming latch valve fail-open rate is same as thrust valve. It would be $2 \times 10^{-11}$ /day.  6. One of four active Z-facing thruster valves on active branch develops a leak in combination with a latch valve that also leaks.  7. Leak rate is large enough to potentially cause an Earth impact.  8. Recovery mode is to perform an emergency avoidance maneuver.	Analysis	Ref 3-10, IOM: 311.6/97-063-GJ, "Determination of Limiting Small Hole Threshold", dated 4/18/97  Ref 3-11, IOM: 311.12/95-142, "Monte Carlo Analysis of Cassini Spacecraft ΔV Produced by Micrometeoroid Impact", dated 11/30/95



Table 3-1. Spacecraft Components, Ground Induced Error and Flight Software Failure Probabilities and  $\Delta V$  Effects (Page 10 of 12)

FAILURE MODE	PROBABILITY OF FAILURE	$\Delta V$ (m/sec) and DIRECTION	RECOVERABLE	COMMENTS	TECHNIQUE FOR ESTIMATING FAILURE RATE	REFERENCE MEMO ON FAILURE RATE
17) RCS Thruster Valve Leaks in Combination with Backup Fault Protection Latch Valve Leak After E-5 Days (New)	Failure rate 5 times higher than failure mode #16.	$\Delta V$ 's are ten times lower than Failure #16.	Yes for short-term Earth avoidance.  No for the mission.		Analysis	Ref 3-10, IOM: 311.697-063-G11, "Determination of Limiting Small Hole Threshold", dated 4/18/97  Ref 3-11, IOM: 311.12/95-142, "Monte Carlo Analysis of Cassini Spacecraft $\Delta V$ Produced by Micrometeoroid Impact", dated 11/30/95
18) Main Engine Valve Critical Leak in Combination with Backup Fault Protection Latch Valve Failure Prior to E-5 days (New)	1/4 X leak failure rates in Failure Mode #15 above.	10% Model: (It is assumed that if there is a second failure preventing a recovery maneuver it occurs shortly following the first failure and occurs in AACs, CDS or PPS causing the S/C to spin up.) For $\Delta V$ use the Biprop Small Hole Model  50% Model: (Condition described above occurs after half of propellant leaks out.) $\Delta V$ sum of two vectors, 1) and 2): 1) Median = 50 m/s 25 m/s (10%)-100 m/s (90%) Uniformly distributed over the unit sphere 2) varies uniformly 0 - "v" "v" Median = 3 m/s 10% factor of 2 lower 90% factor of 2 higher (see Comment #4)  Direction = -Z Lognormal  90% Model: (It is assumed that if there is a second failure preventing a recovery maneuver it occurs in RFS or PMS preventing uplinking emergency avoidance maneuver.) $\Delta V$ median = 100 m/s, 50 m/s (10%) - 200 m/s (90%)  Direction = -Z Normal Distribution	Yes for short-term Earth avoidance.  No for the mission.	1. Recovery maneuver can be done with the thrusters if necessary.  2. Probabilities of thruster leak rates assumed to also apply for these large valves. As seats get larger there are compensating effects. Some tend to increase susceptibility to leakage and some to decrease it. Also, vendors tend to spec valves over this size range at the same allowable leakage levels.  3. Assumed 900 kg (fuel) or 1400 kg (ox) of propellant with effective ISP that varied from 25 to 50 sec.  4. Main engine valve develops leak but latch valve either can't be closed or also leaks. Leak rate is large enough to potentially cause an Earth impact.  5. Recovery mode is to perform an emergency avoidance maneuver.  6. Second Vector in 50% delta-V model is older model that conservatively bounds more accurate Small Hole Model.  7. Statistically includes the RCS thrusters velocity contribution trying to control the S/C in magnitudes of up to 60 m/s or more, depending on original feed system leak location and direction.	Analysis	Ref 3-10, IOM: 311.697-063-G11, "Determination of Limiting Small Hole Threshold", dated 4/18/97  Ref 3-11, IOM: 311.12/95-142, "Monte Carlo Analysis of Cassini Spacecraft $\Delta V$ Produced by Micrometeoroid Impact", dated 11/30/95

Table 3-1. Spacecraft Components, Ground Induced Error and Flight Software Failure Probabilities and  $\Delta V$  Effects (Page 11 of 12)

FAILURE MODE	PROBABILITY OF FAILURE	$\Delta V$ (m/sec) and DIRECTION	RECOVERABLE	COMMENTS	TECHNIQUE FOR ESTIMATING FAILURE RATE	REFERENCE MEMO ON FAILURE RATE
19) Main Engine Valve Critical Leak in Combination with Backup Fault Protection Latch Valve Failure After E-5 Days (New)	Use 10% of failure rates defined in Failure Mode #18 above.	<p>10% Model: (It is assumed that if there is a second failure preventing a recovery maneuver it occurs shortly following the first failure and occurs in AACs, CDS or PPS causing the S/C to spin up) For <math>\Delta V</math> use the Biprop Small Hole Model</p> <p>50% Model: (Condition described above occurs approx. half way to Earth from time of leak.) <math>\Delta V</math> sum vectors 1) and 2): 1) varies uniformly 0 - "v", "v" median = 15 m/s 10% factor of 10 lower, 90% factor of 10 higher. Direction: -Z Lognormal 2) The second vector is as described in the second vector of the 50% Model in Failure #18.</p> <p>90% Model: (It is assumed that if there is a second failure preventing a recovery maneuver it occurs in RFS or PMS preventing uplinking emergency avoidance maneuver.) <math>\Delta V</math> uniformly 0 - "v", "v" median = 30 m/s 10% factor of 5 lower, 90% factor of 5 higher. Direction: -Z Lognormal</p>	<p>Yes for short-term Earth avoidance.</p> <p>No for the mission.</p>	<p>10% Model: See Failure #11, Reference #11.</p> <ol style="list-style-type: none"> <li>1. Assumed 10% of the failure rates defined in Failure Mode #17 because valve is not being activated during this period.</li> <li>2. Maximum <math>\Delta V</math> estimates are based on a nominal main engine flow rate times a factor. The factor is as follows: 1 X 10<sup>3</sup> 10% 1 X 10<sup>2</sup> 50% 1 X 10<sup>1</sup> 90%</li> <li>3. Effective time of leak (relevant to Earth Swingby) varies from 0 to 5 days.</li> <li>4. ISPs vary from 25 to 50 sec.</li> <li>5. Main engine valve develops leak but latch valve either can't be closed or also leaks. Leak rate is large enough to potentially cause an Earth impact.</li> </ol>	Analysis	<p>Ref 3-10, IOM: 311.6/97-063-GII, "Determination of Limiting Small Hole Threshold", dated 4/18/97</p> <p>Ref 3-11, IOM: 311.12/95-142, "Monte Carlo Analysis of Cassini Spacecraft <math>\Delta V</math> Produced by Micrometeoroid Impact", dated 11/30/95</p>

Table 3-1. Spacecraft Components, Ground Induced Error and Flight Software Failure Probabilities and  $\Delta V$  Effects (Page 12 of 12)

FAILURE MODE	PROBABILITY OF FAILURE	$\Delta V$ (m/sec) and DIRECTION	RECOVERABLE	COMMENTS	TECHNIQUE FOR ESTIMATING FAILURE RATE	REFERENCE MEMO ON FAILURE RATE
20) Main Engine Valve Fails-Open in Combination with Backup Fault Protection Latch Valve Failure to Close (New)	$(25 \times 10^{-12})$ @ 10% $(5.0 \times 10^{-12})$ @ 50% $(1.0 \times 10^{-12})$ @ 90%  Failures Per Firing  $t$ = total number of days latch valve is exposed to propellant (approximately equal to number of days since launch +50)	10% Model: (It is assumed that if there is a second failure preventing a recovery maneuver it occurs shortly following the first failure and occurs in AACS, CDS or PPS causing the S/C to spin up.) For $\Delta V$ use the Biprop Small Hole Model  50% Model: (Condition described above occurs after half of propellant leaks out.) $\Delta V$ sum vectors 1) and 2): 1) median = 50 m/s, 25 m/s (10%) - 100 m/s (90%). Direction: -Z Lognormal 2) The second vector is as described in the second vector of the 50% Model in #18.  90% Model: (It is assumed that if there is a second failure preventing a recovery maneuver it occurs in RFS or PMS preventing uplinking emergency avoidance maneuver.) $\Delta V$ median = 100 m/s, 50 m/s (10%) - 200 m/s (90%). Direction: -Z Normal Distribution	Yes for short-term Earth avoidance.  No for the mission.	10 % Model: See Failure #11, Reference #11.  1. Recovery maneuver can be done with the thrusters if necessary.  2. Main engine failure rate derived from flight data and documented in the Cassini Earth Swingby Plan. Rate = $2. \times 10^{-7}$ failures per firing.  3. Latch valve leakage failure rate assumed same as for latch valve in RCS thruster branch described in #16 above.  4. $\Delta V$ based on effective ISP that varies between 25 and 50 sec, and loss of one bipropellant with a mass of 900 kg fuel and 1400 kg oxidizer.  5. Main engine valve fails-open, developing a leak, but latch valve either can't be closed or also leaks. Leak rate is large enough to potentially cause an Earth impact  6. Recovery mode is to perform an emergency avoidance maneuver.  7. Statistically includes the RCS thrusters velocity contribution trying to control the S/C in magnitudes of up to 60 m/s or more, depending on original feed system leak location and direction.	Analysis	Ref 3-10, IOM: 311 6/97-063-GJJ, "Determination of Limiting Small Hole Threshold", dated 4/18/97  Ref 3-11, IOM: 311 12/95-142, "Monte Carlo Analysis of Cassini Spacecraft $\Delta V$ Produced by Micrometeoroid Impact", dated 11/30/95

**Table 3-2 Estimates of Critical Incident Particle Mass  
for Configurations Defined by the Cassini Project**

**CRITICAL PARTICLE MASS**  
Estimated Maximum Incident  
Particle Mass which produces

Config #	Configurations and Nodal Analysis Defined								NO DAMAGE to the Unpressurized Ti Tank Wall at 5 km/s (mg)	Area (m2)	
	Critical Tank	Area Name	Component E3 (Material)	S2 (in)	Component E2 (Material)	E2 Thickness (mils)	S1 (in)	Critical Component E1		Nodes	Area (m2)
1	Fuel	Bus C/O	MLJ	2.5	Ti	8	3	Tank	1.5	1,3,5,7,9,11,13,15	0.152
2	Fuel	Bus C/O	MLJ	2.5	Ti	8	15	Tank	2	2,4,6,8,10,12,14,16	0.152
3	Fuel	UBM	BetaMLI	10	Al	50	16	Tank	70	1,3,5,7,9,11,13,15	0.152
4	Fuel	UBM	BetaMLI	10	Al	50	8	Tank	70	2,4,6,8,10,12,14,16	0.152
5	Fuel	UBM	BetaMLI	12	Al	50	4	Tank	50	17-24	0.152
6	Fuel	PMS	BetaMLI	20	Al	63	2	Tank	40	25,27,29,31,33,35,37,39	0.152
7	Fuel	PMS	BetaMLI	20	Al	63	4	Tank	75	26,28,30,32,34,36,38,40	0.152
8	Oxidizer	PMS	BetaMLI	20	Al	63	4	Tank	75	51,53,55,57,59,61,63,65	0.152
9	Oxidizer	PMS	BetaMLI	20	Al	63	2	Tank	40	52,54,56,58,60,62,64,66,67-74	0.152
10	Oxidizer	LEM	BetaMLI	7	Al	90	2	Tank	25	75,77,85,89	0.152
11	Oxidizer	LEM	BetaMLI	7	Al	90	4	Tank	40	76,78,86,90	0.152
12	Oxidizer	LEM	BetaMLI	16	Al	90	2	Tank	30	79,81,83,87	0.152
13	Oxidizer	LEM	BetaMLI	16	Al	90	4	Tank	60	80,82,84,88	0.152
14	Oxidizer	MEA Cover	2BetaCloth	18	BetaMLI	-	12	Tank	100	75-90	0.152
15	Comp.Helium	Beta Shield	2BetaCloth	4	BetaMLI	-	4	C. Tank	15	210,220,200,201	0.226
16	Comp.Helium	Beta Shield	2BetaCloth	10	BetaMLI	-	12	C. Tank	70	211,221,202,203	0.369
17	Hydrazine	BMJ	2BetaCloth	4	BetaMLI	-	4	Tank	20	304,305,306,307	0.199
18	Hydrazine	BMJ	2BetaCloth	4	BetaMLI	-	12	Tank	30	300,301,302,303	0.199

Note:

*These estimates of critical mass are for a 0.5 probability of critical damage occurrence*

## Reference List

- 3-1. "Computation of Failure Rate Uncertainty Factor F123", JPL IOM 311-9/96-1X (Revision 2), September 4, 1996.
- 3-2. "Assessment of Cassini Propulsion System Failures, Their Probabilities of Occurrence, and  $\Delta$ Vs Produced", JPL IOM 353CAS/PMS-93-17, August 18, 1993, Revision A, February 22, 1995.
- 3-3. "Cassini Program Environmental Impact Statement, Supporting Study, Volume 3: Cassini Earth Swingby Plan", JPL D-10178-3, 699-70-3, November 18, 1993.
- 3-4. "A Hypervelocity Ballistic Test Program Conducted to Evaluate the Particle Shielding on the Cassini Spacecraft", JPL Impact Physics Group, April 18, 1997.
- 3-5. "Summary of Micrometeoroid Protection for the Cassini Propulsion Module", JPL IOM 352K-96-O54, September 21, 1996.
- 3-6. "Evaluation of Meteoroid Shielding on the UEM\* Configurations of the Cassini Spacecraft Using the MAGI High Velocity Impact Code", JPL IOM 5052-96-327, December 26, 1996, Rev. A. April 24, 1997. \*Upper Equipment Module
- 3-7. "Probability of Tank Failure During Cassini Earth Flyby", JPL IOM 5052-96-232, Revision 1, October 1, 1996.
- 3-8. "Small Hole Model for MMH", JPL IOM 354S/TFSE:PS/O52-95:TEC, May 19, 1995.
- 3-9. "Uncertainty in Energy Release", JPL IOM 3535/008-97.TEC, April 30, 1997 (to be made later, in signature cycle).
- 3-10. "Determination of Limiting Small Hole Threshold", JPL IOM 311.6/97063-GIJ, April 18, 1997.
- 3-11. "Monte Carlo Analysis of Cassini Spacecraft AV Produced by Micrometeoroid Impact", JPL IOM 311.12/95-142, November 30, 1995.
- 3-12. "Combustion Models", JPL IOM 3535/.TSFE:l50-95:TEC, November 27, 1995.
- 3-13. "Liquid Propellant Explosive Hazards, Final Report, Volume 1 - Technical Documentary Report", URS Systems Corporation for Air Force Rocket Propulsion Laboratory, Air Force Systems Command, United States Air Force, December 1968.
- 3-14. "Non-environmentally Induced PMS Propellant Tank Failure Risk Assessment JPL, January 31, 1997, IOM 354-NRM-97-109.
- 3-15. "Main Engine Valve Impacting Oxidizer Tank", JPL IOM 352K-97 008, January 31, 1997.

- 3-16. "Spacecraft Loss Calculations", JPL IOM 311.3/97-27, February 21, 1997, Ammended by same author in E:mail 3/4/97 5:04 PM 4800, Re: Loss memo and Various Electronic mail messages, JPL, September 1996 through February 1997.
- 3-17. "Cassini Equivalent Missions Based on MLI Protected Areas and Relative Fluences", JPL IOM 50S1-97-052, February 14, 1997.
- 3- 18. "Bayesian Correction for Cassini Meteoroid Model", JPL IOM 5051 -97-053, February 13, 1997.
- 3-19. 3/5/97 8:55 AM Working Papers -- Probability of No-recovery, JPL IOM not yet published, February, 1997.

## SECTION 4

### SHORT-TERM EARTH IMPACT PROBABILITY

#### 4.1 INTRODUCTION

This section presents the navigation strategy for design and controlling the spacecraft trajectory between injection from Earth orbit and the final Earth swingby for the Cassini mission. It also provides estimates of the probability of impact on the targeted Earth swingbys for the primary and secondary launch opportunities.

The navigation strategy is driven by the project requirement to control the trajectory so that the spacecraft can satisfy the mission objectives while maintaining a low probability of inadvertent Earth reentry.

The details of the effect of failures on the spacecraft trajectory and the techniques used to compute the short-term Earth impact probabilities were presented in reference [4-1] and will not be repeated here.

Only the Earth encounters contained in the reference trajectories are analyzed in this section. The possibility that the spacecraft might become disabled and have a later accidental encounter with the Earth is analyzed in the next section.

#### 4.2 MANEUVER STRATEGY

The primary and secondary launch opportunities include either one or two Earth swingbys. Three Earth swingby trajectory segments have been studied in detail for this report: the Venus 2 to Earth segment on the Cassini primary 1997 VVEJGA launch opportunity, and both the Venus Earth 1 (VET) and the Earth 1-Earth 2 (E1E2) segment from the Cassini secondary 1997 VEEGA launch opportunity. For both primary and secondary launch opportunities, a launch date was chosen that resulted in the minimum altitude for the Earth swingbys. This ensures that the requirement can be met over the launch period for each trajectory.

Analysis for each trajectory segment begins with the last maneuver before the planetary encounter preceding the Earth swingby. This maneuver achieves a flyby at the preceding body which places the spacecraft on a trajectory that flies by the Earth. The preceding body's aimpoint is chosen such that the Earth avoidance criteria will be satisfied. Earlier maneuvers may be targeted to the same aimpoint; however, due to the larger delivery dispersions and the dispersive effects of the swingby, failures during these earlier segments have been found to contribute a negligible amount to the total short-term Earth impact probability. For the VVEJGA trajectory, analysis begins with the maneuver 20 days prior to the second Venus swingby, and for the VEEGA trajectory it begins with the maneuver 20 days before the Venus swingby

(for the VE1 segment) and 7 days before the Earth 1 swingby (for the E1E2 segment).

Mission design for minimal total  $\Delta V$  usage to Saturn requires at least one deterministic Deep Space Maneuver (DSM) for the most effective use of the encounter gravity assists. If a DSM is included in the trajectory segment leading to the Earth swingby, it provides a built-in Earth bias offset, usually large enough so that no additional trajectory bias is needed until after the DSM. The primary 1997 VVEJGA trajectory does not have a DSM in its Venus 2 to Earth segment. Therefore, the Venus 2 encounter must be biased, to provide an adequate bias for the following Earth swingby. The 1997 VEEGA trajectory has a DSM in its E1E2 segment, but this DSM is not large enough to protect the Earth 2 swingby, so additional bias has been added.

In either case, following the swingby or DSM, the bias is gradually removed by a series of maneuvers targeted to biased aimpoints. The desired Earth swingby conditions are only achieved by the final maneuver prior to Earth swingby.

After the final Earth swingby, the trajectories for each mission proceed to destinations well away from Earth. The focus of the short-term Earth avoidance navigation strategy is thus the control of each mission's trajectory prior to the Earth swingbys.

Table 4-1 presents the maneuver profile as well as the impact radii and other swingby parameters for the VVEJGA Earth encounter segment. The series of biased aimpoints is illustrated in the B-plane by Figure 4-1.

Table 4-2 and Figure 4-2 present similar information for the VEEGA Venus to Earth 1 segment, while Table 4-3 and Figure 4-3 present the Earth 1 to Earth 2 segment information. As can be seen, the biased aimpoints all approach the final Earth swingby point from within  $\pm 90^\circ$  of its radial direction, thus satisfying Ground Rule #2 (see Ref. [4-1]). The VEEGA VE1 and E1E2 cases were biased in the manner shown due to considerations that will be discussed in Section 5: Long-Term Earth Impact Probability.

Table 4-1. Primary Mission - Venus to Earth Maneuver/Event Profile

Event	Epoch	Description	Earth Aimpoints	
			B•R (km <sup>2</sup> )	B•T (km)
V-20 day TCM	02-Jun-1999	Achieve desired Venus swingby conditions	150,000	57,510
Venus 2 swingby	22-Jun-1999	Altitude <sup>†</sup> = 1,531 km V <sub>∞</sub> = 8.899 km/s  b  = 10,729 km B <sub>IR</sub> <sup>†</sup> = 9,097 km		
V+10 day TCM	02-Jul-1999	Correct Venus dispersion and partially remove bias	14,400	57,510
E-30 day TCM	18-Jul-1999	Correct dispersion and partially remove bias	2,400	57,510
E-15 day TCM	02-Aug-1999	Correct dispersion and partially remove bias	6,960	10,390
E-6.5 day TCM	10-Aug-1999	Correct dispersion and remove bias	322	8,620
Earth swingby	17-Aug-1999	Altitude = 807 km V <sub>∞</sub> = 15.85 km/s  b  = 8,627 km B <sub>IR</sub> <sup>†</sup> = 7,870 km V <sub>interface</sub> <sup>‡</sup> = 19.34 km/s		

\* 1 km = 0.62 mi 1 km/s = 0.62 mi/s

† Impact radius is reported relative to a minimum safe altitude at closest approach. For Venus, a safe altitude of 100 km was assumed. For Earth, Eq. 5-3 of reference 14-1] was used, yielding a safe altitude of 63 km.

‡ Computed for a 122km altitude: If spacecraft re-enters, this will be the velocity at the interface with the atmosphere

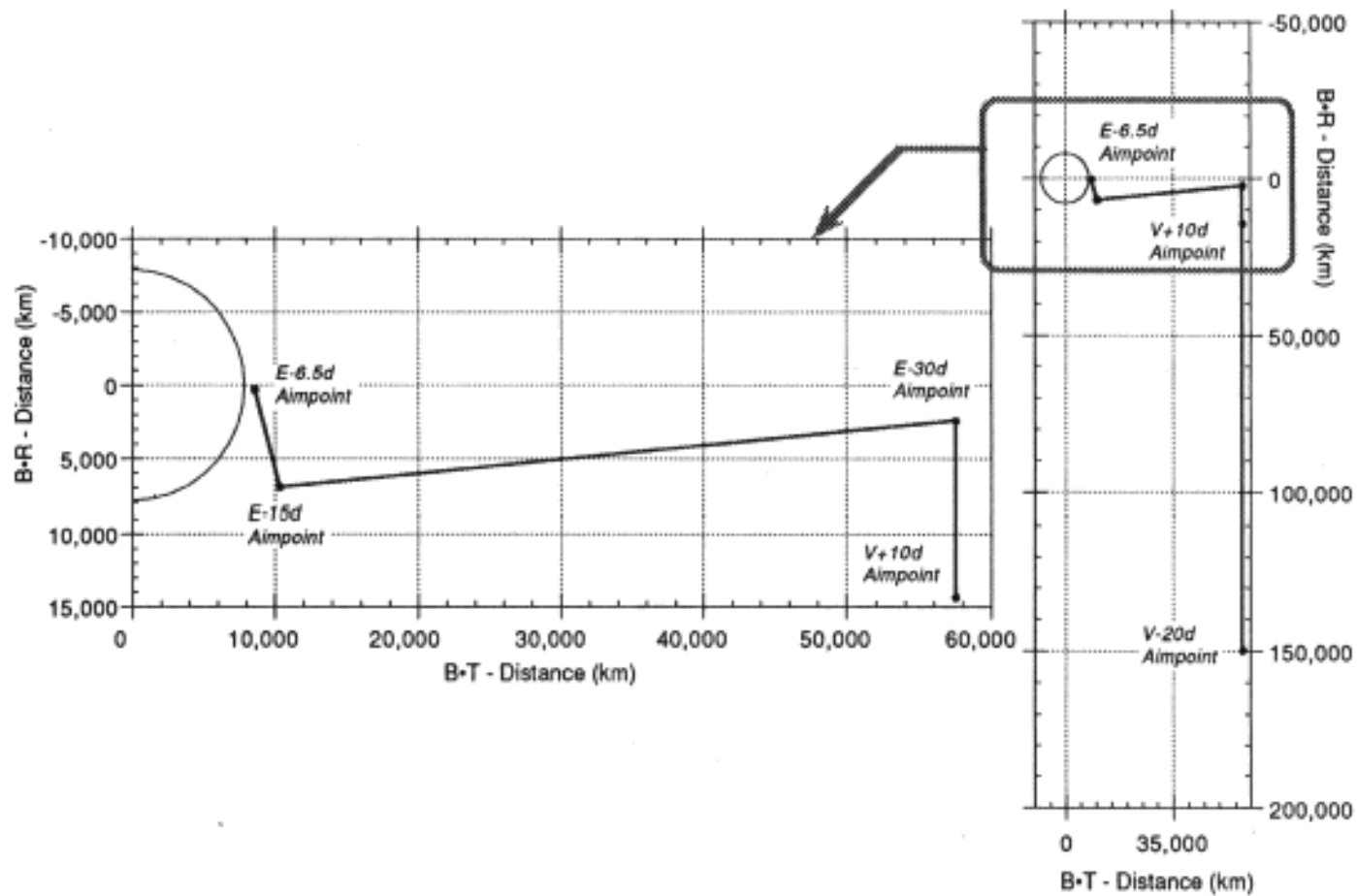


Figure 4-1. Cassini Primary Mission VVEJGA Trajectory - Earth B-Plane

Table 4-2. Secondary Mission - Venus to Earth 1 Maneuver/Event Profile

Event	Epoch	Description	Earth Aimpoints	
			B•R (km)	B•T (km)
V-10 day TCM	30-May-1998	Achieve desired Venus swingby conditions	617,141	2,831,189
Venus swingby	09-Jun-1998	Altitude=2,722 km $V_{\infty}$ = 8.665 km/s $ b $ = 12,360 km $B_{IR}$ = 9,434 km		
V+4 day TCM	13-Jun-1998	Correct Venus dispersion	617,141	2,831,189
E1-100 day TCM	04-Aug-1999	Correct dispersion and partially remove bias	-46,947	88,295
E1-60 day TCM	13-Sep-1999	Correct dispersion and partially remove bias	-44,995	53,623
E1-25 day TCM	18-Oct-1999	Correct dispersion and partially remove bias	0	19,364
E1-7 day TCM	05-Nov-1999	Correct dispersion and remove bias	-2,979	10,515
Earth 1 swingby	12-Nov-1999	Altitude=2,443 km $V_{\infty}$ = 12.87 km/s $ b $ = 10,930 km $B_{IR}$ = 8,511 km $V_{interface}$ = 16.98 km/s		

\* 1 km = 0.62 mi; 1 km/s = 0.62 mi/s

• Impact radius is reported relative to a minimum safe altitude at closest approach. For Venus, a safe altitude of 100 km was assumed. For Earth, Eq. 5-3 of reference [4-1] was used, yielding a safe altitude of 63 km.

≠ Computed for a 122km altitude; If spacecraft re-enters, this will be the velocity at the interface with the atmosphere

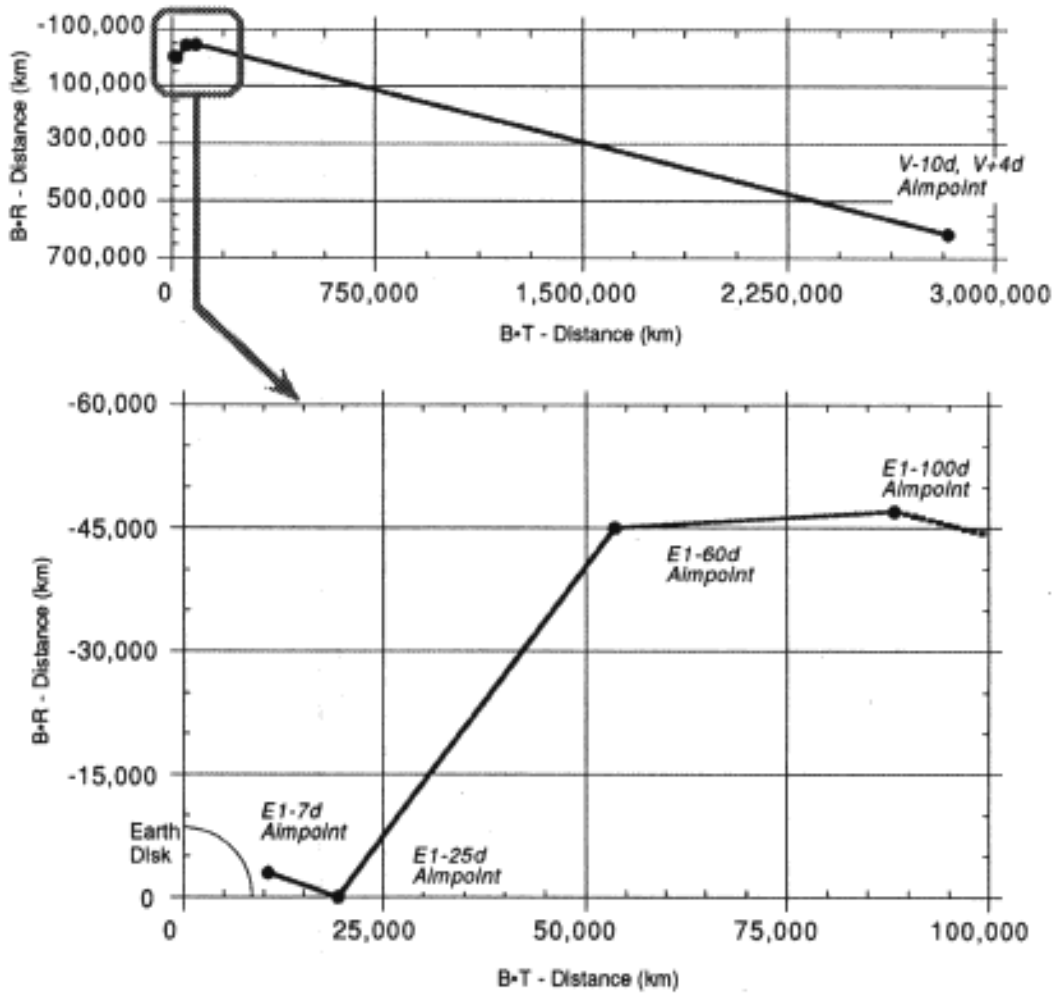


Figure 4-2. Cassini Secondary Mission - Earth 1 B-Plane

Table 4-3. Secondary Mission - Earth 1 to Earth 2 Maneuver/Event Profile

Event	Epoch	Description	Earth Aimpoints	
			B•R (km <sup>†</sup> )	B•T (km)
E1 - 7 day TCM	05-Nov-1999	Achieve desired Earth 1 swingby conditions	512,161	-401,451
Earth 1 swingby	12-Nov-1999	Altitude=2,443 km $V_{\infty}$ = 12.87 km/s $ \mathbf{b} $ = 10,930 km $B_{IR}^{\dagger}$ = 8,511 km $V_{interface}^{\ddagger}$ = 16.98 km/s		
E1+4 day TCM	16-Nov-1999	Correct Venus dispersion	512,161	-401,451
E2-593 day TCM	11-Dec-2000	Correct dispersion and partially remove bias	509,541	-316,808
E2-100 day TCM	18-Apr-2002	Correct dispersion and partially remove bias	303,109	-175,000
E2-50 day TCM	07-Jun-2002	Correct dispersion and partially remove bias	79,224	-76,312
E2-20 day TCM	07-Jul-2002	Correct dispersion and partially remove bias	1,234	-19,962
E2-7 day TCM	20-Jul-2002	Correct dispersion and remove bias	-4,112	-8,718
Earth 2 swingby	27-Jul-1999	Altitude=1,151 km $V_{\infty}$ = 12.74 km/s $ \mathbf{b} $ = 9,639 km $B_{IR}^{\dagger}$ = 8,547 km $V_{interface}^{\ddagger}$ = 16.88 km/s		

\* 1 km - 0.62 mi 1 km/s - 0.62 mi/s

† Impact radius is reported relative to a minimum safe altitude at closest approach. For Venus, a safe altitude of 100 km was assumed. For Earth, Eq. 5-3 of reference [4-1] was used, yielding a safe altitude of 63 km.

‡ computed for a 122km altitude If spacecraft recenters, this will be the velocity at the interface with the atmosphere

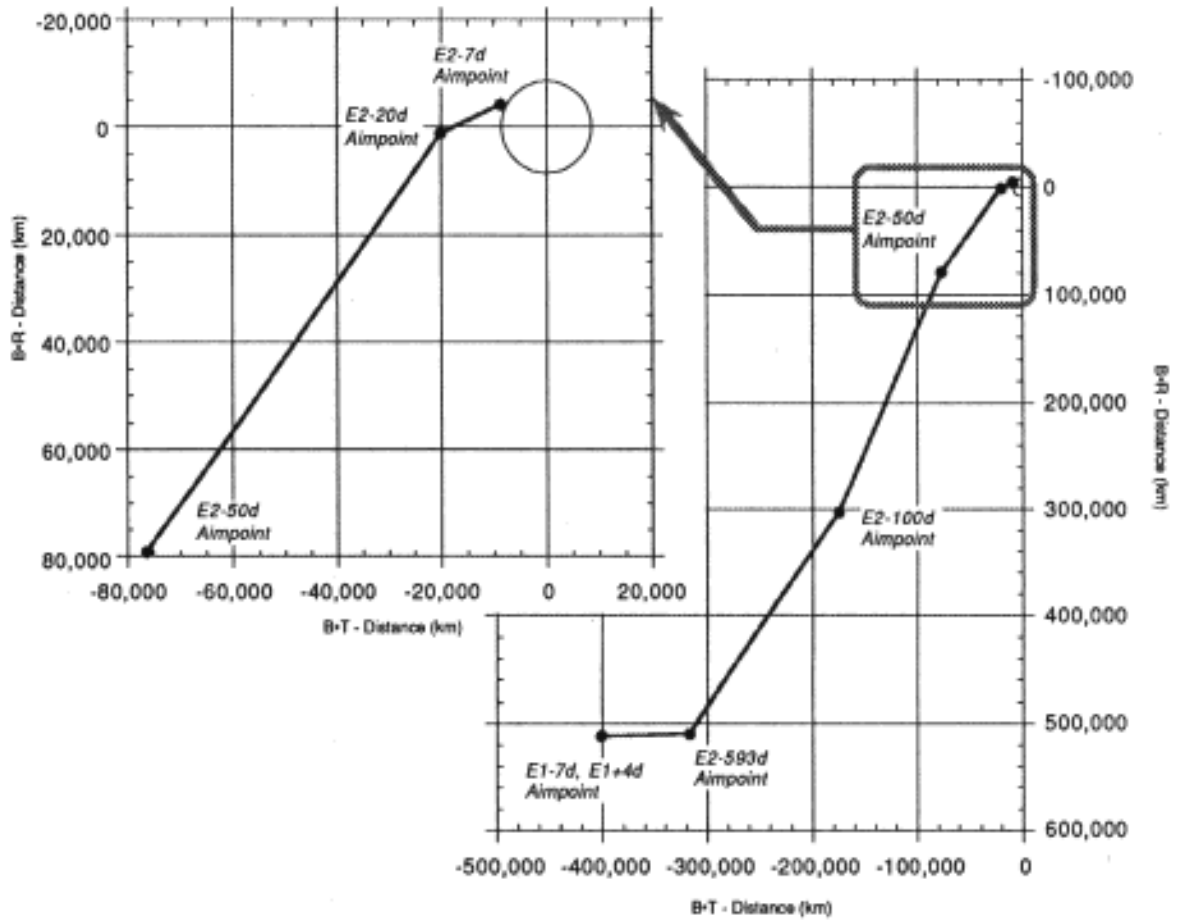


Figure 4-3 Cassini Secondary Mission - Earth 2 B-Plane

### 4.3 NAVIGATION MODELS

The three variables which influence the navigation B-plane dispersions are the influence matrices (K-matrices), the TCM execution uncertainties, and the orbit determination uncertainties. K-matrices model the linearized influence of a perturbation on the trajectory. In practice some degree of error creeps into the calculation of K-matrices. However this variation is small compared to the variation due to the orbit determination uncertainties and TCM execution uncertainties and is not modeled in the software.

B-plane delivery dispersions are estimated at the 10%, 50%, and 90% probability levels using detailed study results. The best estimates of the orbit determination and maneuver execution are used for the 50% model. The uncertainties are multiplied by 1/2 to obtain the 10% model and by 2 to obtain the 90% model.

TCM execution uncertainties, at the  $3\sigma$  requirement level, are given in Table 4-4.

Table 4-4. TCM Execution Errors ( $3\sigma$ )

Error Type	Main Engine	RCS System
Proportional Magnitude	1.0%	6.0%
Proportional Pointing	21.0 millirad	25.0 millirad
Fixed Magnitude	30.0 mm/s	10.0 mm/s
Fixed Pointing	52.5 mm/s	10.0 mm/s

The dominant term in the orbit determination covariance matrix is the B-plane uncertainty. The approximate orbit determination uncertainties are given in Table 4-5 below, for each TCM leading to an Earth encounter.

### 4.4 SHORT-TERM IMPACT PROBABILITY COMPUTATIONS

The details of the technique for computing the short-term Earth impact probability are given in reference [4-1].

### 4.5 ENTRY ANGLE AND ENTRY LATITUDE COMPUTATIONS

Calculations were also performed to estimate the distribution of spacecraft entry angles and latitudes, given impact. The details of the computations are given in reference [4-2]

Table 4-5. 1σ Orbit Determination Uncertainty in B-Plane Position

TCM (days from Enc.)	Primary			Secondary Venus to Earth 1			Secondary Earth 1 to Earth 2		
	10%	50%	90%	10%	50%	90%	10%	50%	90%
V-20d	15	30	60						
V-10, E1-7				11	22	44	13	26	52
<i>Previous Encounter</i>									
E1+4 (E2-984)							1.5×10 <sup>6</sup>	3×10 <sup>6</sup>	6×10 <sup>6</sup>
E2-593							2195	4390	8780
V+4 (E1-517)				209	418	836			
E1, E2-100				30	60	120	73	146	292
E1-60, E2-50				20	40	80	21	42	84
V2+10	31	62	124						
E-30, E1-25d	8	16	32	13	26	52			
E-15, E2-20d	5	10	20				18	37	74
E-6.5; E1, E2-7	12	25	50	12	25	50	12	25	50
<i>Earth Encounter</i>									

#### 4.6 EARTH IMPACT PROBABILITIES

The total short-term probability of Earth impact resulting from in-flight spacecraft and operational failures is the sum of the contributions from each failure. This subsection presents the results of the impact computations for each of the failure modes defined in Section 3. The failure rates and AV distributions are given in Table 3-1.

The impact probability for each continuous failure mode has been computed at 5-day intervals (except for 1-day intervals for the last 20 days and 1-hour intervals for the last day before encounter) and summed over the entire trajectory segment. For Type II failures occurring during discrete maneuver events, the impact probability is a sum over all such events in the segment. The segment totals for each failure mode are presented below.

For Type II failures that occur during maneuvers, the failure is assumed to occur at the end of the maneuver. If the failure occurs after the desired AV has been achieved, the resulting aimpoint will be closer to the Earth leading to higher impact probabilities. Most of these failures can occur at any time during the execution of the maneuver, hence this is a conservative assumption.

A final summary of the short-term mean impact probabilities is given in Table 4-6. In many cases the impact probability computations lead to very small values, which over represent the accuracy of the analysis. Rather than listing these small values, they are denoted by "Nil". whenever the calculated value is  $< 10^{-12}$ .

The total mean probability of short-term Earth impact is  $0.62 \times 10^{-6}$  for the primary trajectory and  $0.48 \times 10^{-6}$  for the secondary trajectory ( $0.40 \times 10^{-6}$  for the E1 swingby and  $0.084 \times 10^{-6}$  for the E2 swingby). These probabilities are very much dominated by the contribution due to micrometeoroid-induced failures.

Variation in the models permits collection of other statistics in addition to the mean values. Figure 4-4 shows the complementary cumulative probability curve for the probability of impact on the primary trajectory, and Figure 4-5 shows the corresponding frequency distribution. Figures 4-9, 4-10, 4-14, 4-15 show the same information for the secondary trajectory.

One other numerical study performed was to calculate the distribution of entry angles, assuming that an Earth-reentry trajectory, piercing the 63 km safe altitude boundary, does occur. Entry angles less than  $7^\circ$  were assumed to lead to skipping back out of the atmosphere and were not included in the results. Figures 4-6, 4-11, and 4-16 give the frequency distributions of entry angle for the primary trajectory Earth swingby and the secondary trajectory E1 and E2 swingbys, respectively. Figures 4-7, 4-12, and 4-17 show the corresponding cumulative probability distributions. The figures show a fall-off of probability near  $90^\circ$  because the area in the middle annulus is small. They also show a fall-off near  $7^\circ$  because the transformation from entry angle to equivalent radius gives a very narrow annulus. The frequency distributions for VVEJGA and for VEEGA E2 tend to be largest near the low entry angles, because the impacts are concentrated toward the point below the final Earth swingby aimpoint.

The nominal velocity of reentry, or velocity at the interface with Earth's atmosphere, was computed at the reference altitude of 122 km (76 mi.), and is 19.34 km/s (11.60 mi/s) for the primary trajectory, 16.98 km/s (10.19 mi/s) for the E1 encounter, and 16.88 km/s (10.13 mi/s) for the E2 encounter on the secondary trajectory. Some variation in these nominal values can occur if the failure mode includes a  $\Delta V$  and/or if the failure occurs early in the trajectory segment.

Finally, the results of the study of latitude distribution given impact are shown in Figures 4-8, 4-13, and 4-18. As expected, the distribution spread is relatively small for the primary and VEEGA E2 swingbys with their 800 km and 1,000 km altitude swingbys and maximum biasing of the trajectory. The VEEGA-E1 swingby has the greatest spread since it is a relatively high swingby. Each distribution is centered over the latitude underneath the final swingby aimpoint.

All longitudes should be considered equally likely for these studies, since the Earth swingby date varies as a function of the launch date. Over the primary VVEJGA launch period the nominal Earth swingby time changes by 1.4 days. Over the secondary VEEGA launch period the nominal Earth swingby time changes by 1.3 days. Thus any longitude could become the most likely one. Even after launch, a micrometeoroid

induced failure could result in a substantial change in the swingby time. As an upper bound, a bipropellant tank failure right after the Venus swingby on the secondary VEEGA trajectory could cause up to a one day change in the E1 swingby time.

#### REFERENCES

[4-1] Cassini Program Environmental Impact Statement Supporting Study, Volume 3: Cassini Earth Swingby Plan, Cassini Project document 699-70-3, 18 November 1993

[4-2] "Estimation of the B-Plane Aimpoint Scatter from Impact Trajectories", IOM 312.B-96-008, 4 March 1996

Table 4-6. Short-Term Mean Earth Impact Probabilities

Failure Mode	Primary (VVEJGA)	Secondary (VEEGA)	
		Earth 1	Earth 2
<b>I. Micrometeoroid-Induced Failure</b>			
Fuel (MMH) Tank	$2.02 \times 10^{-8}$	$5.89 \times 10^{-9}$	$1.35 \times 10^{-9}$
Oxidizer (NTO) Tank	$2.94 \times 10^{-7}$	$2.77 \times 10^{-7}$	$8.38 \times 10^{-9}$
Hydrazine Tank	$4.72 \times 10^{-8}$	$2.37 \times 10^{-8}$	$1.11 \times 10^{-9}$
Helium Tank	$1.51 \times 10^{-7}$	$7.73 \times 10^{-8}$	$3.56 \times 10^{-9}$
<b>II. Major Spacecraft Failures</b>			
<i>Stuck-Open Thruster Valve</i>			
<i>Z-Thruster</i>			
Mechanical Failure	$4.99 \times 10^{-11}$	Nil	Nil
Electrical Failure	$7.69 \times 10^{-11}$	Nil	Nil
<i>Y-Thruster</i>			
Mechanical Failure	$2.13 \times 10^{-10}$	Nil	Nil
Electrical Failure	$1.35 \times 10^{-10}$	Nil	Nil
<i>Stuck-Open Main Engine Valve</i>			
<i>Mechanical Failure</i>			
Oxidizer Valve	Nil	Nil	Nil
Fuel Valve	Nil	Nil	Nil
Electrical Failure	Nil	Nil	Nil
Accelerometer	$7.34 \times 10^{-12}$	Nil	$4.92 \times 10^{-12}$
Main Engine Gimbal	$1.01 \times 10^{-10}$	Nil	Nil
AACS Flight	$7.50 \times 10^{-11}$	Nil	Nil
CDS Flight	$3.25 \times 10^{-12}$	Nil	$4.51 \times 10^{-10}$
Anomalous Sun Search	$2.95 \times 10^{-11}$	Nil	Nil
Spacecraft System*	$8.68 \times 10^{-8}$	Nil	$1.21 \times 10^{-10}$
Pyro-valve	Nil	Nil	Nil
Passive Tank	$1.76 \times 10^{-10}$	Nil	$3.25 \times 10^{-11}$
Main Engine Catastrophic	$8.33 \times 10^{-12}$	Nil	Nil
Critical Feed Sys. Leak (prior to E-5d)	$3.09 \times 10^{-9}$	$8.32 \times 10^{-10}$	$4.00 \times 10^{-10}$
Critical Feed Sys. Leak (after E-5d)	$1.41 \times 10^{-9}$	$2.52 \times 10^{-10}$	$8.00 \times 10^{-10}$
RCS Thruster Leak/Open (prior to E-5d)	$1.05 \times 10^{-9}$	$1.05 \times 10^{-9}$	$1.93 \times 10^{-12}$
RCS Thruster Fail Open (after E-5d)	$1.18 \times 10^{-9}$	Nil	$1.79 \times 10^{-11}$
RCS Thruster Leak (after E-5d)	$1.35 \times 10^{-9}$	$4.77 \times 10^{-11}$	$5.10 \times 10^{-10}$
Main Engine Leak (prior to E-5d)	$1.23 \times 10^{-10}$	$1.02 \times 10^{-10}$	Nil
Main Engine Leak (after E-5d)	$1.51 \times 10^{-9}$	Nil	$1.67 \times 10^{-11}$
Main Engine Fail Open & Valve Failure	Nil	Nil	Nil
<b>III. Ground-Induced Errors</b>			
Erroneous Ground Command**	$1.10 \times 10^{-8}$	$1.50 \times 10^{-8}$	$1.24 \times 10^{-8}$
Navigation Design***	$4.00 \times 10^{-11}$	$2.33 \times 10^{-11}$	$2.80 \times 10^{-11}$
<b>TOTAL</b>	$6.21 \times 10^{-7}$	$4.01 \times 10^{-7}$	$8.35 \times 10^{-8}$

\* Includes Engineering Bus Failure

\*\* Computed as a bound by setting  $P_{1/F} = 1.0$ .\*\*\* Computed as a bound by setting  $\Delta V$  toward the Earth.Notes: Nil indicates mean fractional Earth impact probability  $< 10^{-12}$ ; Three-digit precision is retained to facilitate adding.

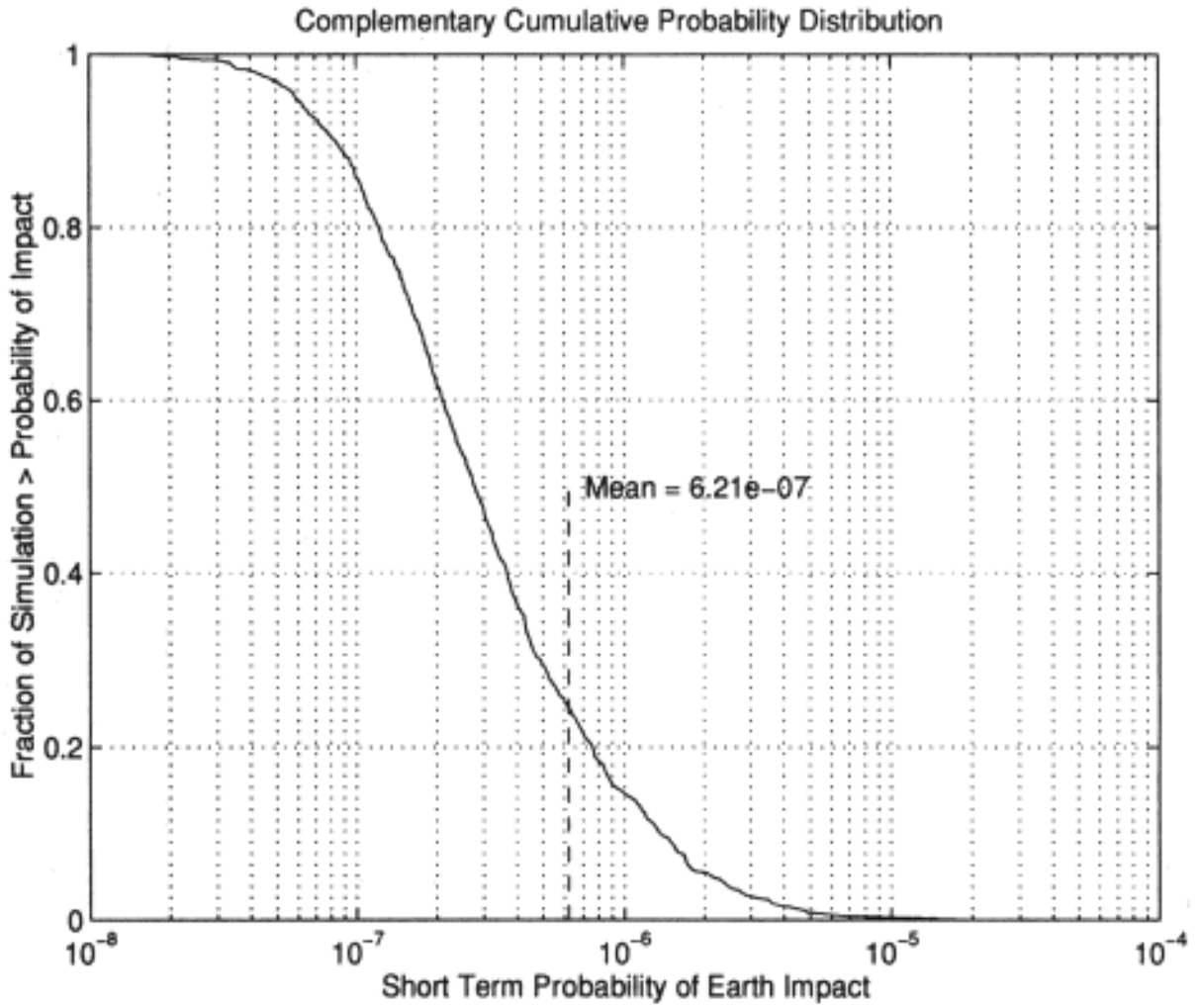


Figure 4-4. Primary Mission: Complementary Cumulative Probability

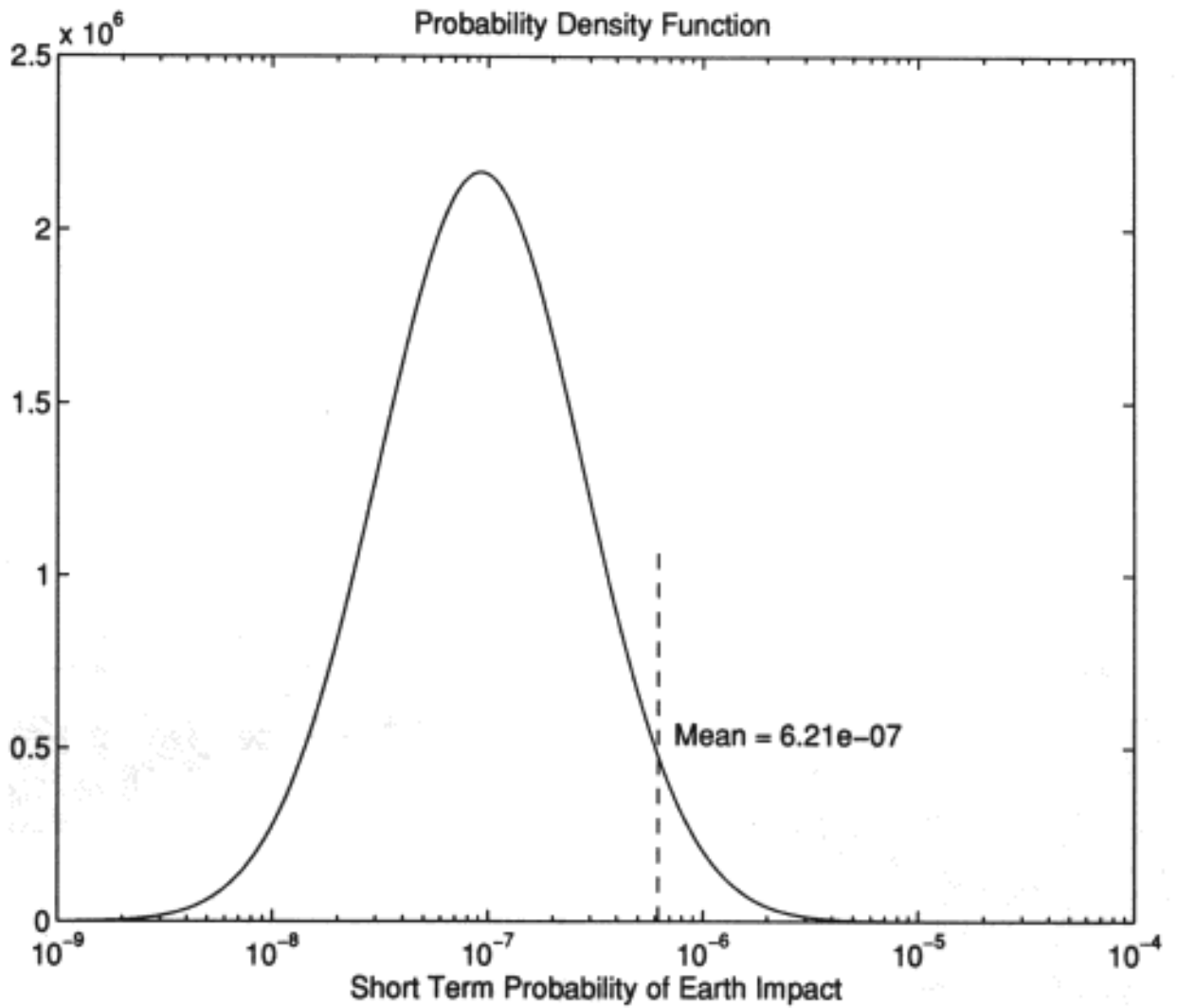


Figure 4-5-Rev.1. Primary Mission: Probability Density Function

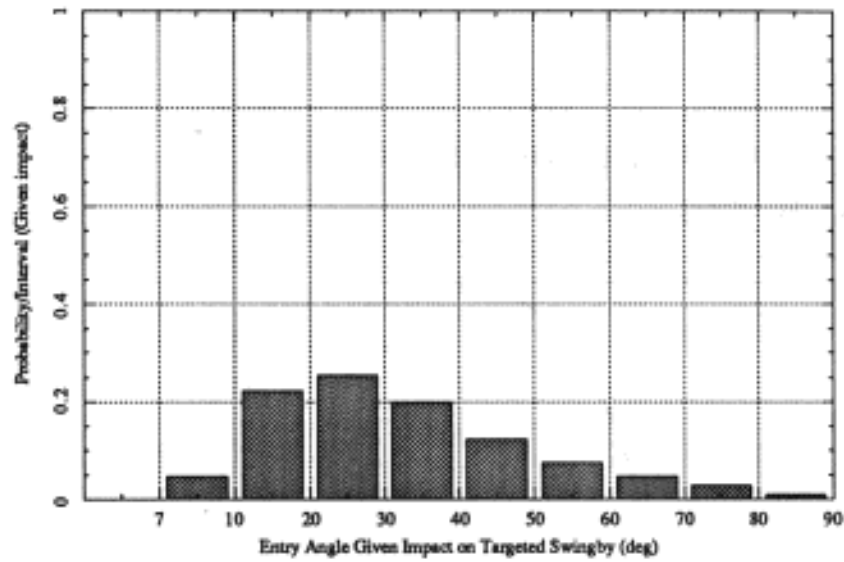


Figure 4-6. Primary: Probability vs. Entry Angle

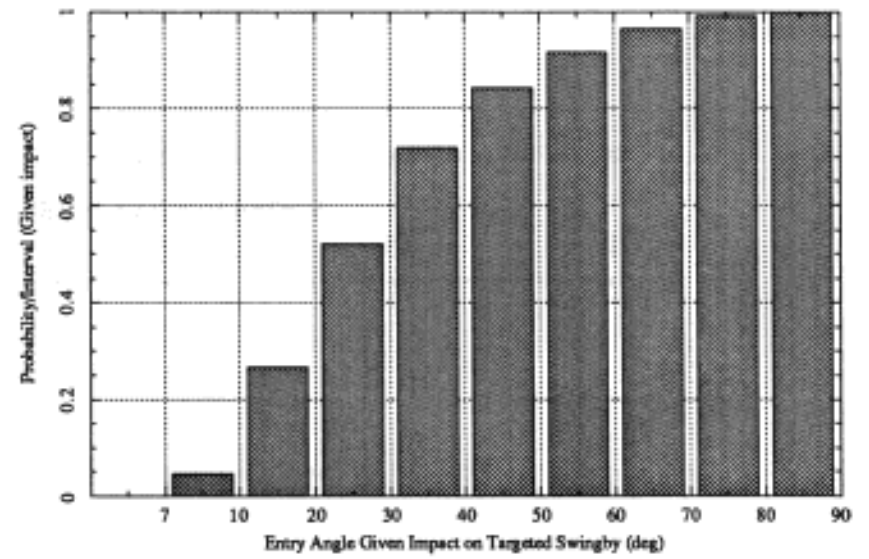


Figure 4-7. Primary: Entry Angle Cumulative Probability

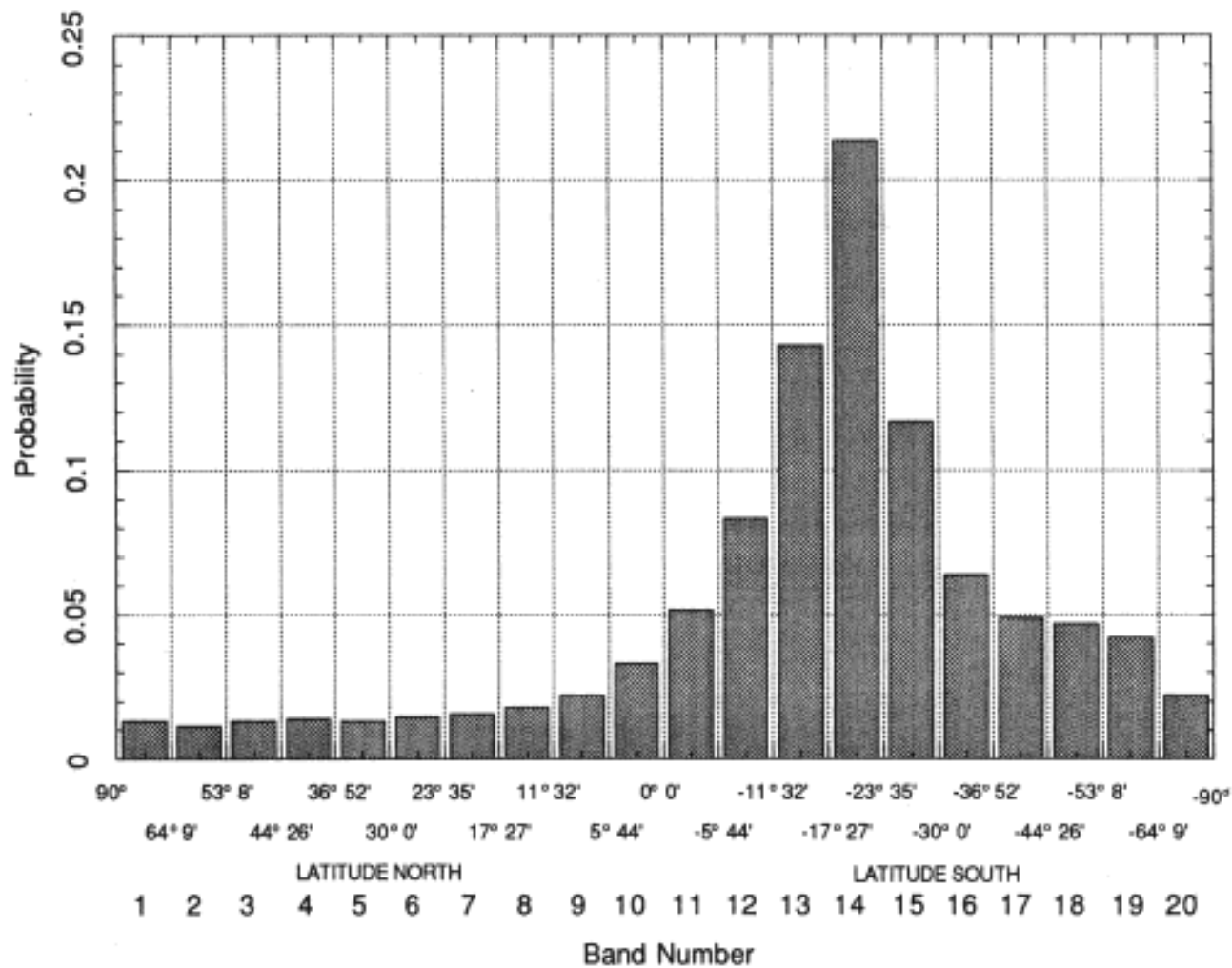


Figure 4-8. Primary Mission: Entry Latitude Probability Distribution

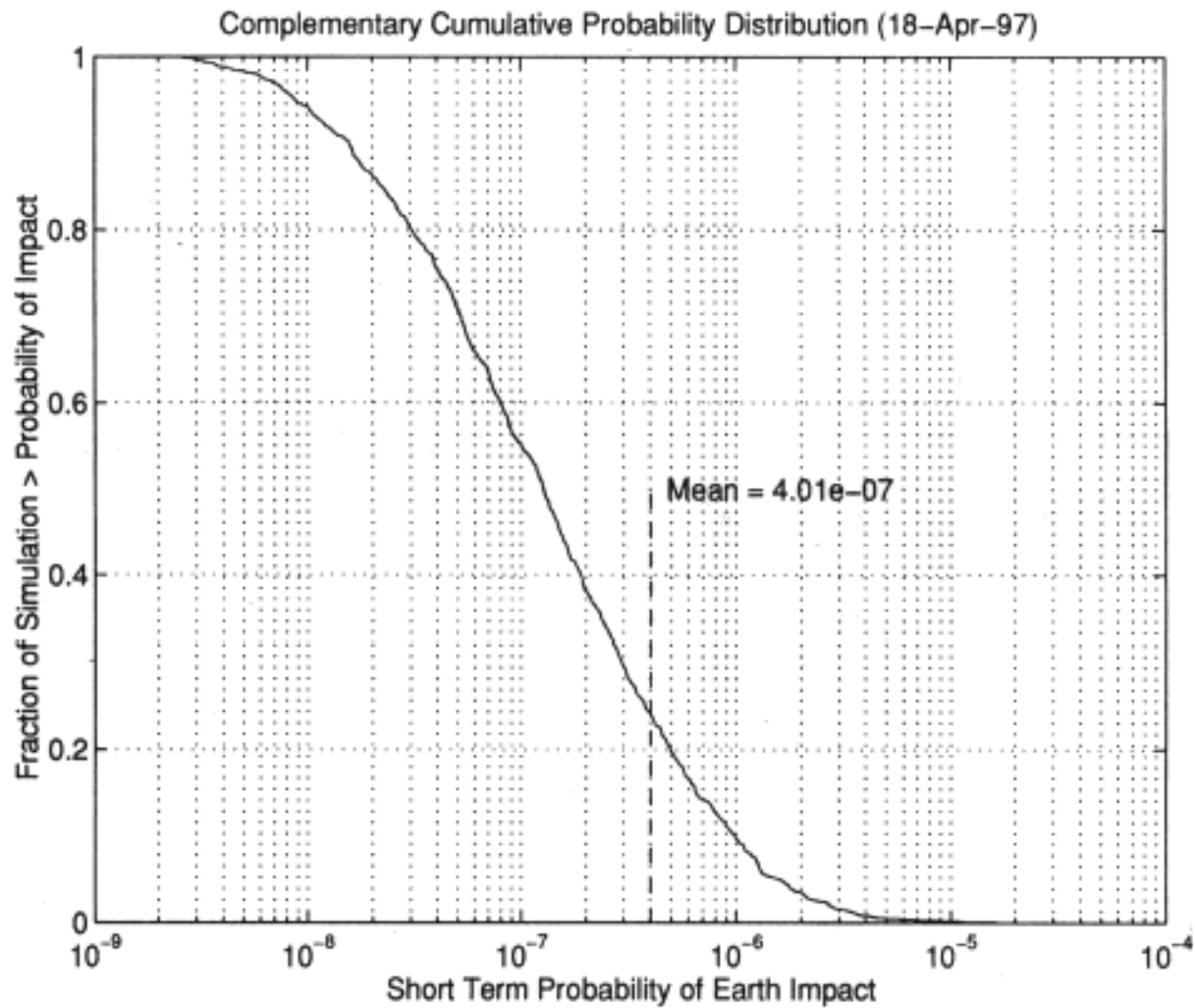


Figure 4-9. Secondary-E1: Complementary Cumulative Probability

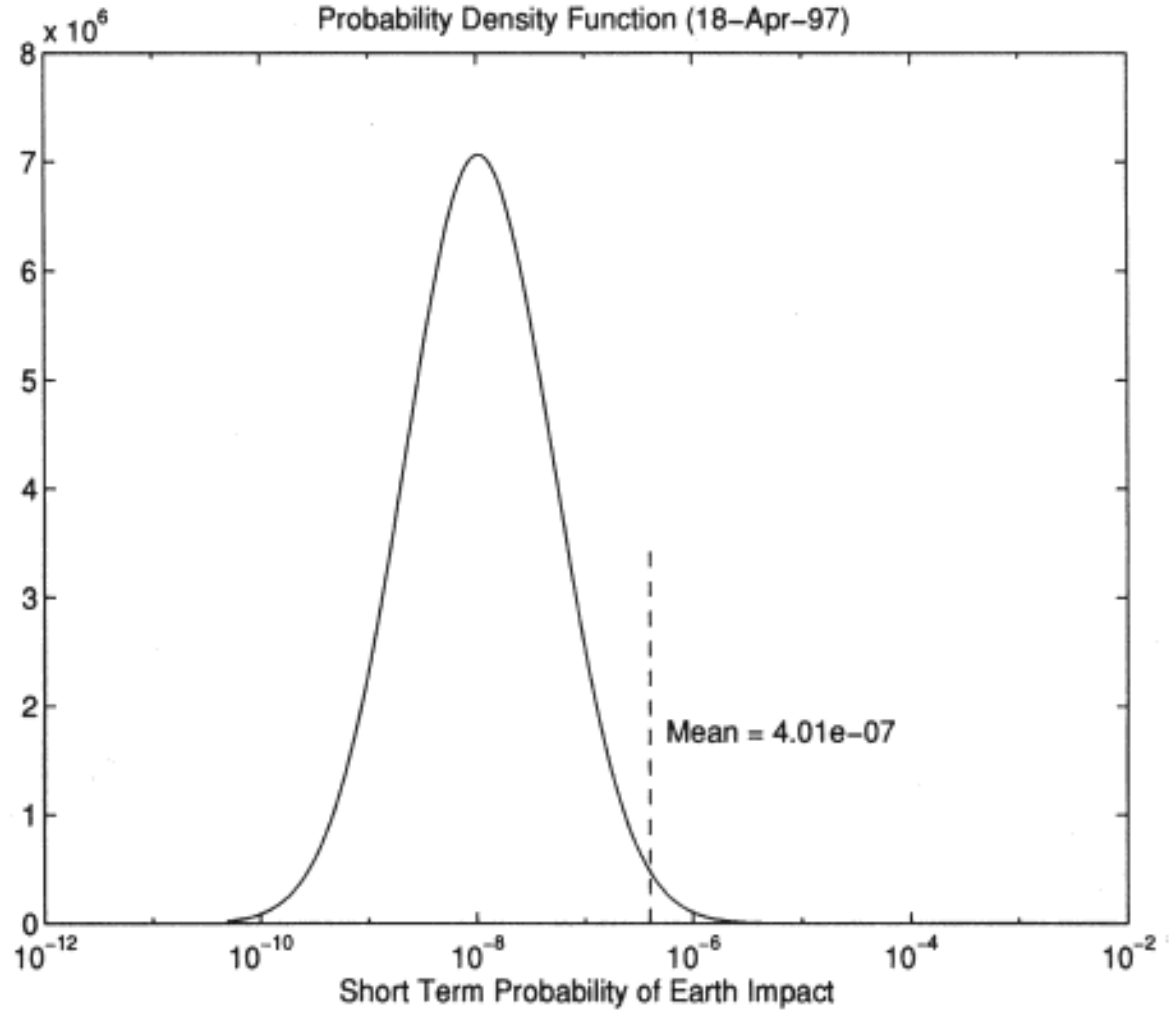


Figure 4-10. Secondary-E1: Probability Density Function

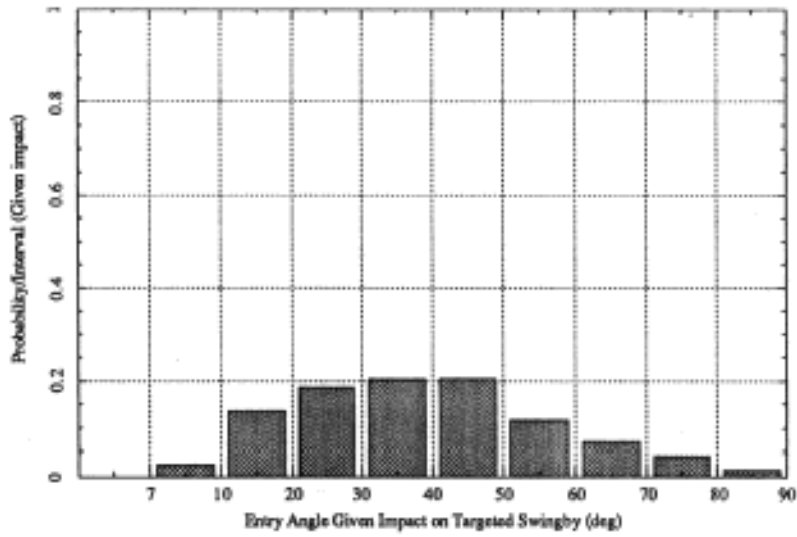


Figure 4-11. Secondary-E1: Probability vs. Entry Angle

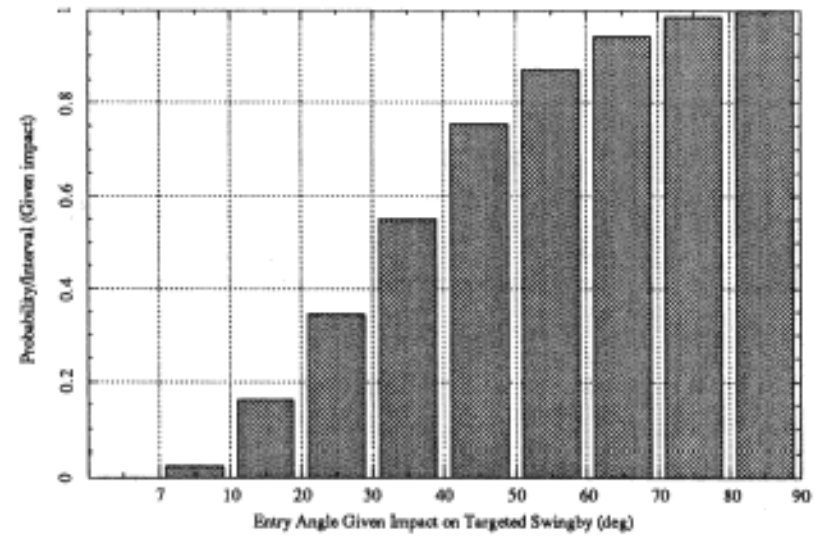


Figure 4-12. Secondary-E1: Entry Angle Cumulative Distribution

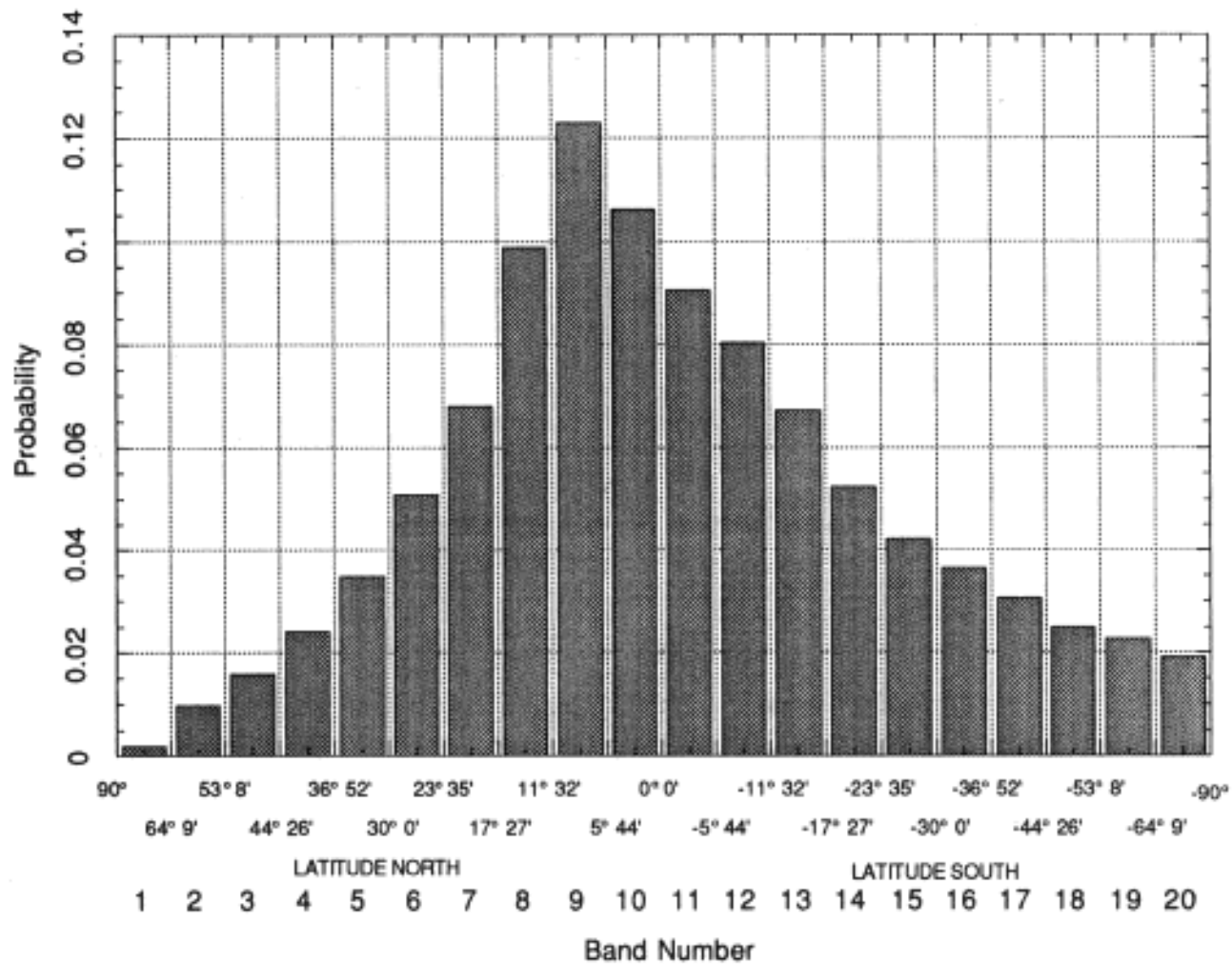


Figure 4-13. Secondary-El: Entry Latitude Probability Distribution

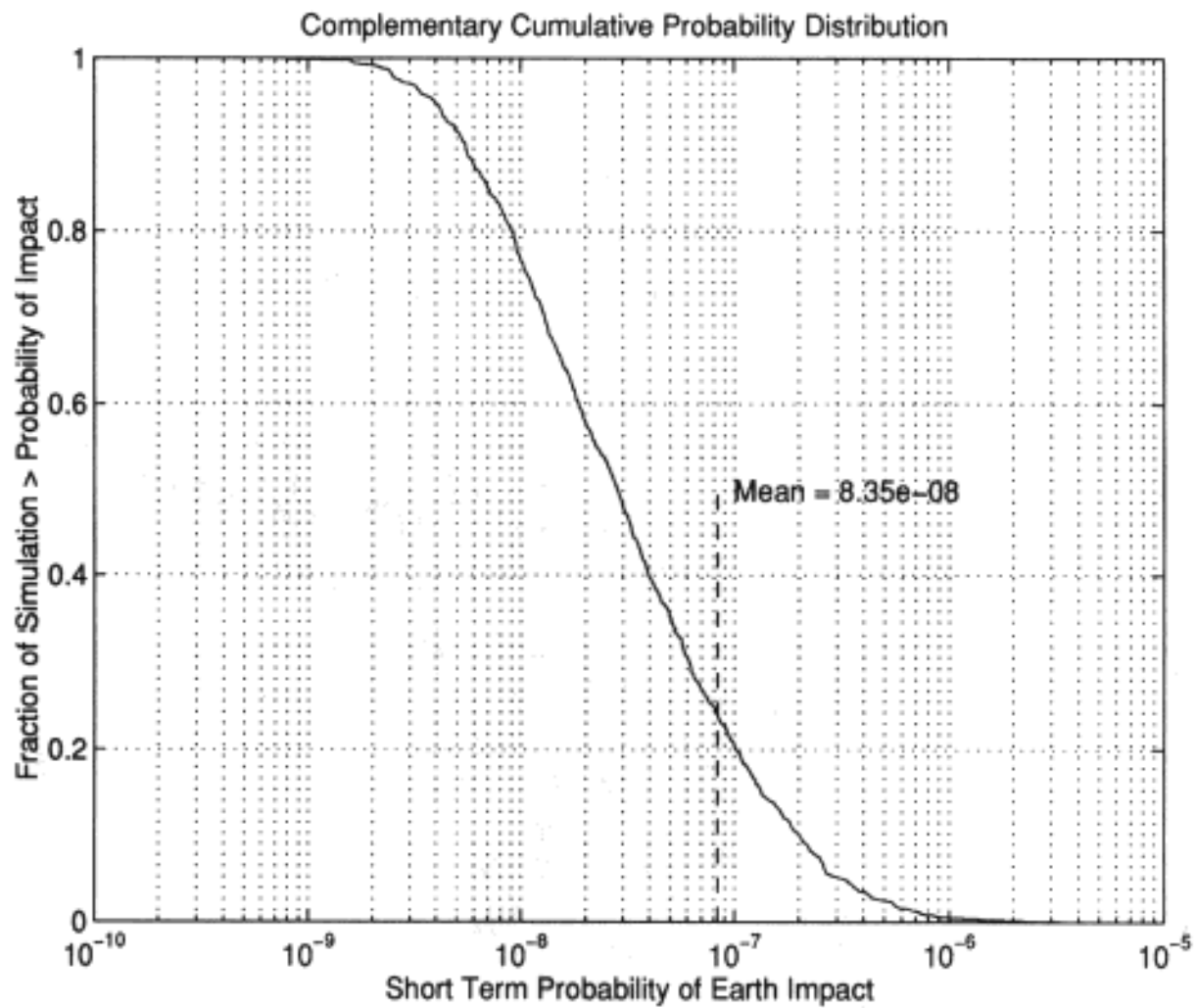


Figure 4-14. Secondary-E2: Complementary Cumulative Probability

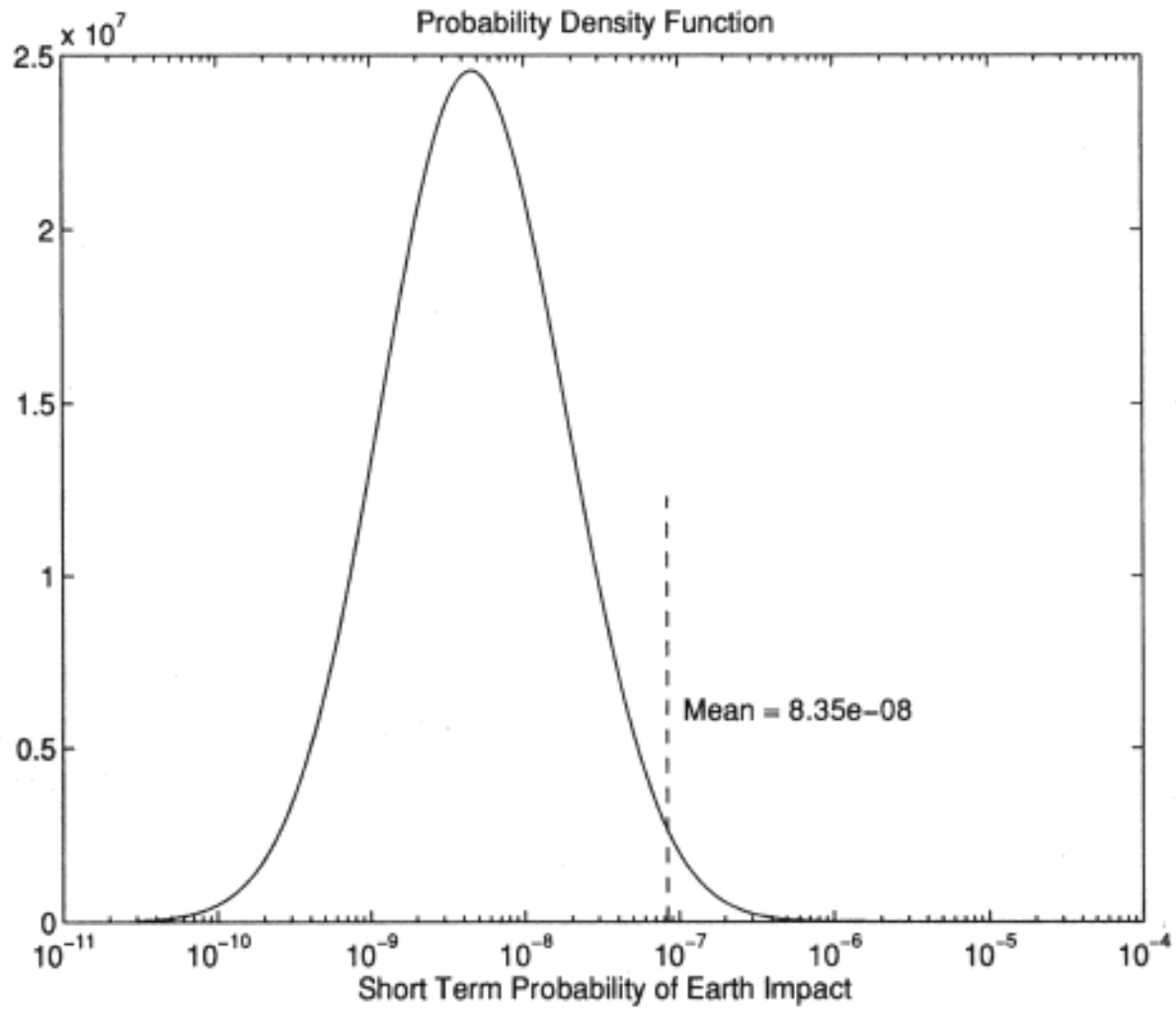


Figure 4-15. Secondary-E2: Probability Density Function

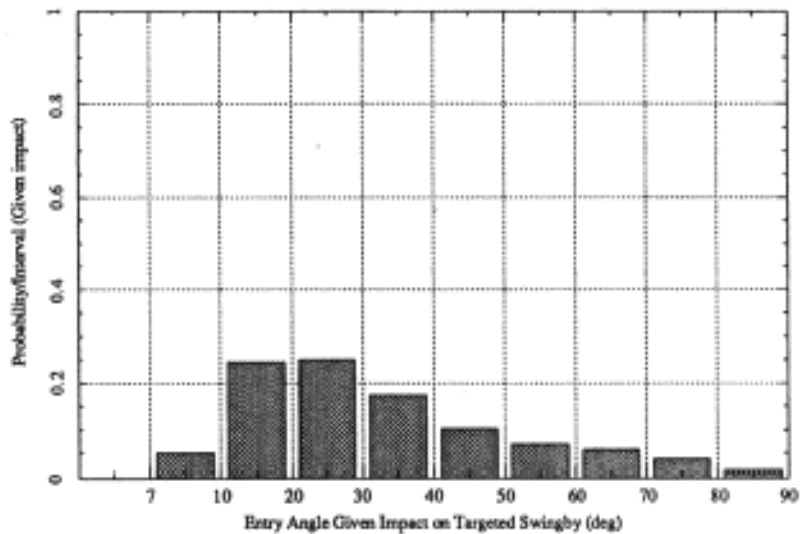


Figure 4-16. Secondary-E2: Probability vs. Entry Angle

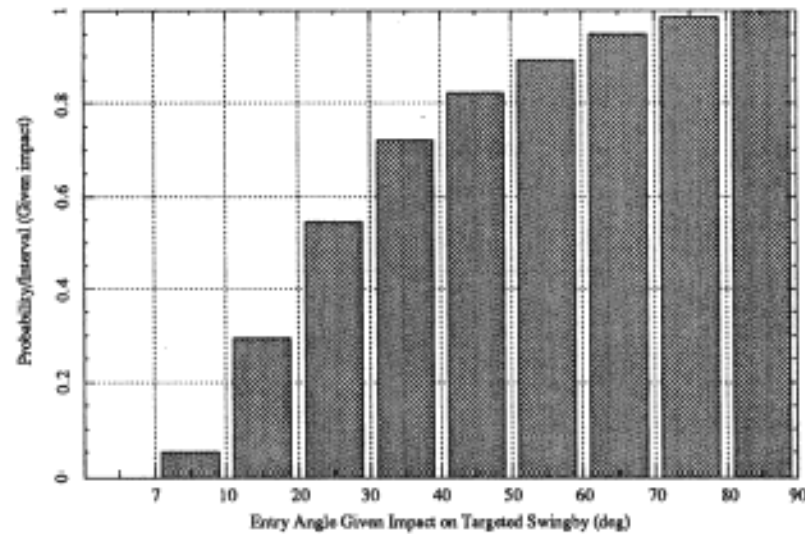


Figure 4-17. Secondary-E2: Entry Angle Cumulative Distribution

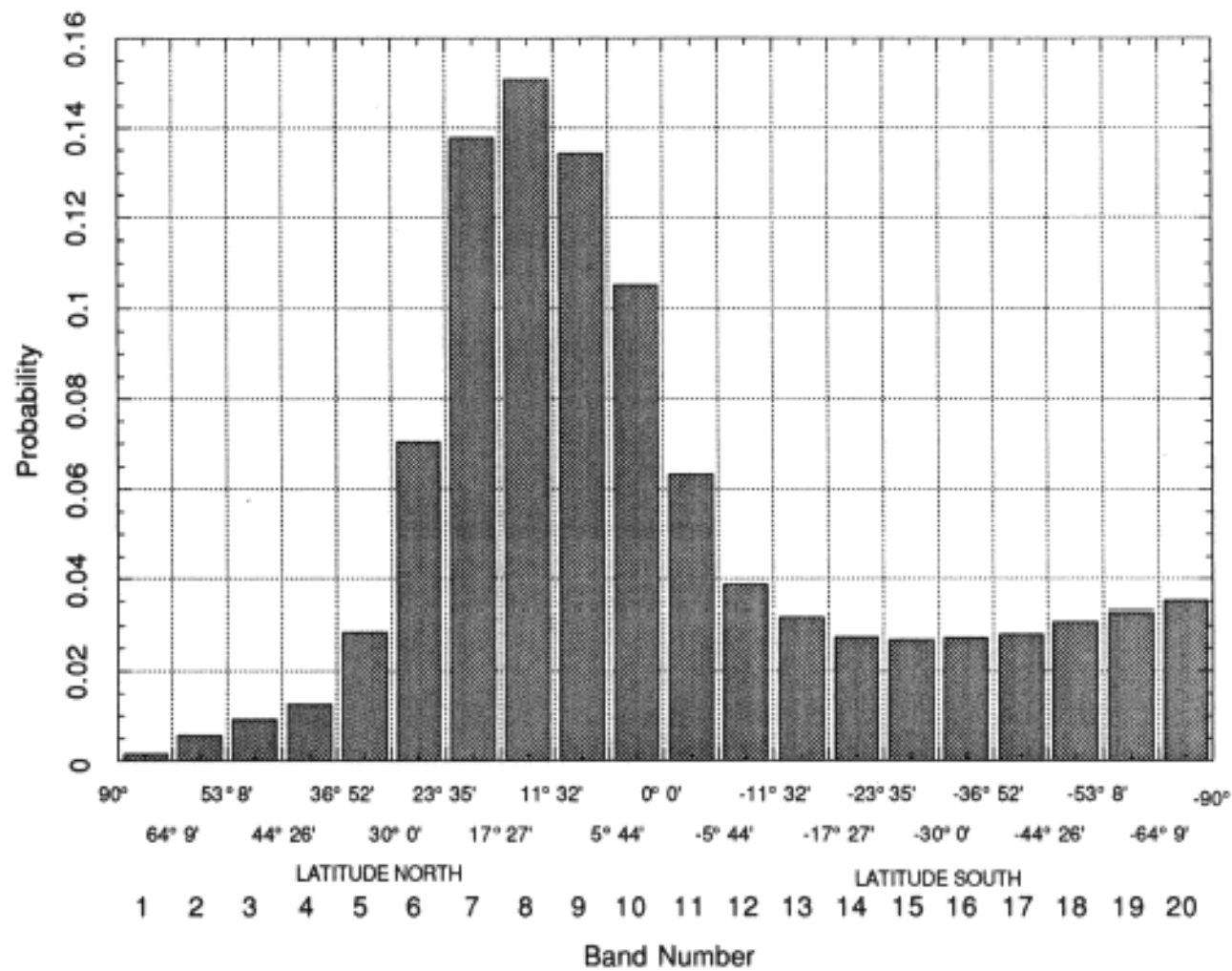


Figure 4-18. Secondary-E2: Entry Latitude Probability Distribution

## SECTION 5

### LONG-TERM EARTH IMPACT PROBABILITY

#### 5.1 INTRODUCTION

During the Cassini mission, there exists the possibility that the spacecraft might become unmaneuverable after successful insertion into its interplanetary cruise trajectory. The short-term impact analysis presented in Section 4 establishes that the probability of Earth impact during a targeted Earth swingby is extremely small. However, if the spacecraft becomes unmaneuverable during interplanetary cruise and does not impact the Earth during a targeted swingby, there is still a remote possibility that long-term perturbations to the orbit could cause the spacecraft to eventually reencounter the Earth. The long-term analysis described in this section computes the probability of Earth impact by a non-targeted swingby for a period of 100 years commencing at the time of spacecraft failure.

To compute the probability of Earth impact, a knowledge of the spacecraft failure probabilities, the uncertainties in the navigation process, and the long-term motion of the spacecraft is required. Use was made of a large body of work refined over the past forty years to estimate the probability of impact by Earth-crossing asteroids. Existing theory which was applicable to lifetime analysis of asteroids and comets was modified to apply to this spacecraft impact analysis.

The purpose of this section is to document the computation of a p.d.f. of the long-term component of the Earth impact probability for the primary VVEJGA and secondary VEEGA Cassini missions. The short and long-term p.d.f.s are then combined into a single p.d.f., as described in Section 6.

#### 5.2 METHOD

The following method is used to compute the long-term Earth impact probability for both the primary and secondary trajectories. An important defining equation for Earth impact probability, which was presented in Subsection 2.1, is as follows:

$$P_I = \Sigma_{FAIL} \Sigma_{TIME} P_F(i) P_{I/F}(i) P_{NR}(i) \quad (5-1)$$

where

- $P_I$  = probability of Earth impact
- $\Sigma_{FAIL}$  = summation over all i failure modes
- $\Sigma_{TIME}$  = summation over long-term time period  
(100 years)
- $P_F(i)$  = probability of failure for ith failure mode
- $P_{I/F}(i)$  = probability of a resultant Earth impact given an ith failure mode
- $P_{NR}(i)$  = probability of no recovery for the ith failure mode given the time to impact

Only those failures which would cause the spacecraft to become unmaneuverable with no chance of recovery are appropriate for the long-term analysis. If the spacecraft could recover, it would permanently enter Saturn orbit at SOI at the end of interplanetary cruise precluding any chance of Earth impact. The PNR term is therefore always equal to 1 for the long-term analysis.

In order for an Earth impact to occur, the spacecraft must fail during cruise ( $P_F(i)$  term) and the spacecraft's orbital geometry must be such that an Earth impact ( $P_{I/F}(i)$  term) occurs in the next 100 years. The significant failure modes for the long-term analysis are spacecraft system internal failure and micrometeoroid impact. Micrometeoroid impact can result in a  $\Delta V$  if a propellant tank is ruptured, although this occurs for only a small subset of the micrometeoroid failure cases. The long-term impact probability has been found to be insensitive to this small subset of cases which impart a  $\Delta V$  to the spacecraft.

Since a single spacecraft trajectory propagation would not be representative of the range of possible trajectories that could result given a failure any time during interplanetary cruise, a Monte Carlo analysis was performed using thousands of trajectories considering a wide range of failure times. The primary and secondary Cassini trajectories were each evaluated using more than 6000 failure cases. Most of the failures are due to spacecraft system internal failure. About two-tenths are from micrometeoroid hits. Associated with each case is an initial spacecraft orbital state, which is perturbed by navigation uncertainty. Since  $\Delta V$ s are only associated with

initial spacecraft orbital state, which is perturbed by navigation uncertainty. Since  $\Delta V$ s are only associated with a fraction of the micrometeoroid failure cases and past analysis has shown their effect to be negligible for the long-term impact probability, the effects of micrometeoroid induced  $\Delta V$ s were ignored in the calculations of initial spacecraft orbital states. Each initial spacecraft state is then propagated for 100 years in the analysis.

For the long-term analysis, probability distributions for the  $P_F(i)$  and  $P_{I/F}(i)$  terms, which are representative of the entire interplanetary cruise, are computed separately and are then combined to yield the Earth impact,  $P_I$ , probability distribution. Spacecraft failure probabilities documented in Section 3 were used to compute a probability distribution for the  $P_F(i)$  term representative of the entire interplanetary cruise for each mission. The failure probability distribution was obtained by randomly sampling the cumulative failure probability distributions as many times as required until ~6000 failure times during cruise were obtained (see Subsection 5.2.2). Only failures during cruise need to be considered since at the end of nominal cruise, the spacecraft enters Saturn orbit.

If the spacecraft becomes unmaneuverable, the orbital geometry of the spacecraft must be such that an Earth impact occurs in the next 100 years. To determine the probability of Earth impact given a failure,  $P_{I/F}(i)$ , use was made of existing theory used to estimate the probability of impact by Earth-crossing asteroids. In this method, the number of passages of the spacecraft through the torus swept out by the Earth as it orbits the Sun is used to compute the probability of Earth impact. In order for an impact to occur, the spacecraft must cross through the Earth torus, and at the time of the crossing, the Earth must be at a position within the torus to cause impact. This intersection geometry is illustrated in Figure 5-1. The term  $P_{I/F}(i)$  is computed as the product of two terms as follows:

$$P_{I/F}(i) = \sum_{\text{TIME}} (N_{\text{CRX}} / N_{\text{CASE}}) P_{I/\text{CRX}} \quad (5-2)$$

where

$P_{I/F}(i)$  = probability of a resultant Earth impact given an occurrence of the  $i$ th failure mode

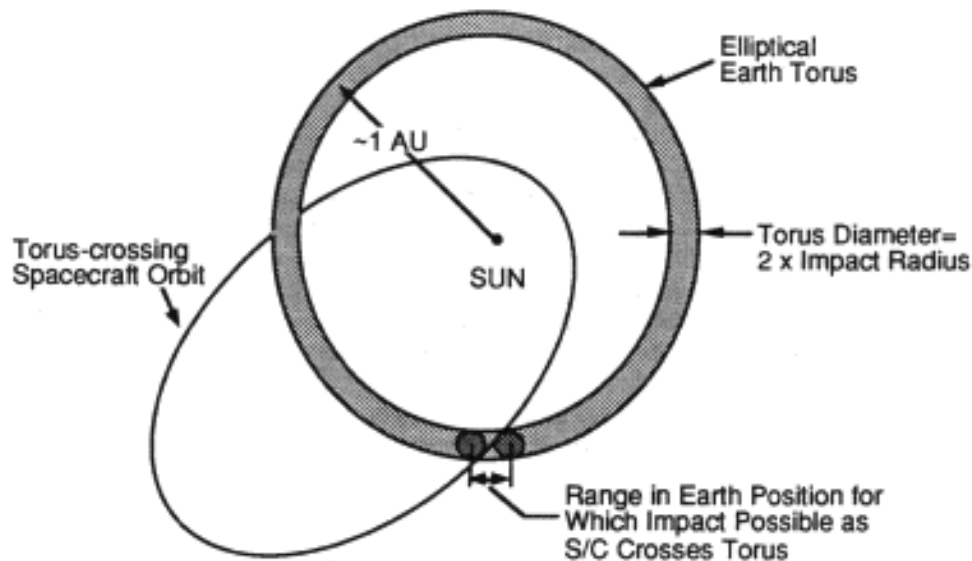
$\sum_{\text{TIME}}$  = summation over long-term time period (100 years)

$N_{\text{CRX}}$  = number of Earth torus crossings encountered in all Monte Carlo cases propagated 100 years

$N_{\text{CASE}}$  = number of Monte Carlo cases (initial trajectory states at spacecraft failure times) propagated 100 years

$P_{I/\text{CRX}}$  = probability of Earth impact given that spacecraft has passed through torus

#### LONG-TERM EARTH TORUS CROSSINGS



$$1 \text{ AU} = 1.495 \times 10^8 \text{ km} \quad (9.295 \times 10^7 \text{ mi})$$

Figure 5-1 Orbit Geometry And Phasing Required For Earth Impact

The first term,  $N_{CRX}/N_{CASE}$ , in Equation 5-2 yields the expected number of torus crossings per Monte Carlo case. The second term,  $P_{I/CRX}$ , is the probability that the Earth occupies the same portion of the torus as the spacecraft at the time the spacecraft crosses the torus. Substitution of Equation 5-2 into Equation 5-1 yields Equation 5-3, which is used to compute the long-term Earth impact probability. Since  $P_{NR}=1$  for the long-term, this term is omitted from Equation 5-3.

$$P_I = \sum_{FAIL} \sum_{TIME} P_F(i) (N_{CRX} / N_{CASE}) P_{I/CRX} \quad (5-3)$$

The process for computing the required data for the  $N_{CASE}$  Monte Carlo cases is illustrated in Figure 5-2. The process for computing the trajectory initial conditions depicted in the top half of Figure 5-2 has already been briefly discussed and is treated in more detail in Subsection 5.2.2. The process for computing best estimates of  $N_{CRX}$  and  $P_{I/CRX}$  is described below.

The number of torus crossings for all cases were computed by propagating the initial conditions for each case using a high-precision numerical integration program, and counting each passage through the Earth torus. This procedure was used rather than the analytical model for long-term orbital motion used in most Earth-crossing asteroid analyses, since the assumptions inherent in the analytical expressions proved inadequate for the Cassini time frame and orbital characteristics. An uncertainty on the number of torus crossings per case was determined and a distribution for the  $N_{CRX}/N_{CASE}$  term was constructed assuming a normal (Gaussian) distribution.

Standard Earth-crossing asteroid theory was used to compute the  $P_{I/CRX}$  term. The value of  $P_{I/CRX}$  is slightly different for each torus crossing and thus an average value was used to compute a best estimate value representative of all torus crossings. An uncertainty in the value of  $P_{I/CRX}$  was estimated and a distribution for this term constructed assuming a log-normal distribution.

The distributions for the  $N_{CRX}/N_{CASE}$  and  $P_{I/CRX}$  terms were combined with the distributions for the  $P_F(i)$  term to yield a p.d.f. for the long-term Earth impact probability,  $P_I$ . The velocity vector of the spacecraft

relative to the Earth was estimated at each torus crossing assuming that the Earth was in the position required for impact.

Portions of the above methodology are described in greater detail in the following subsections.

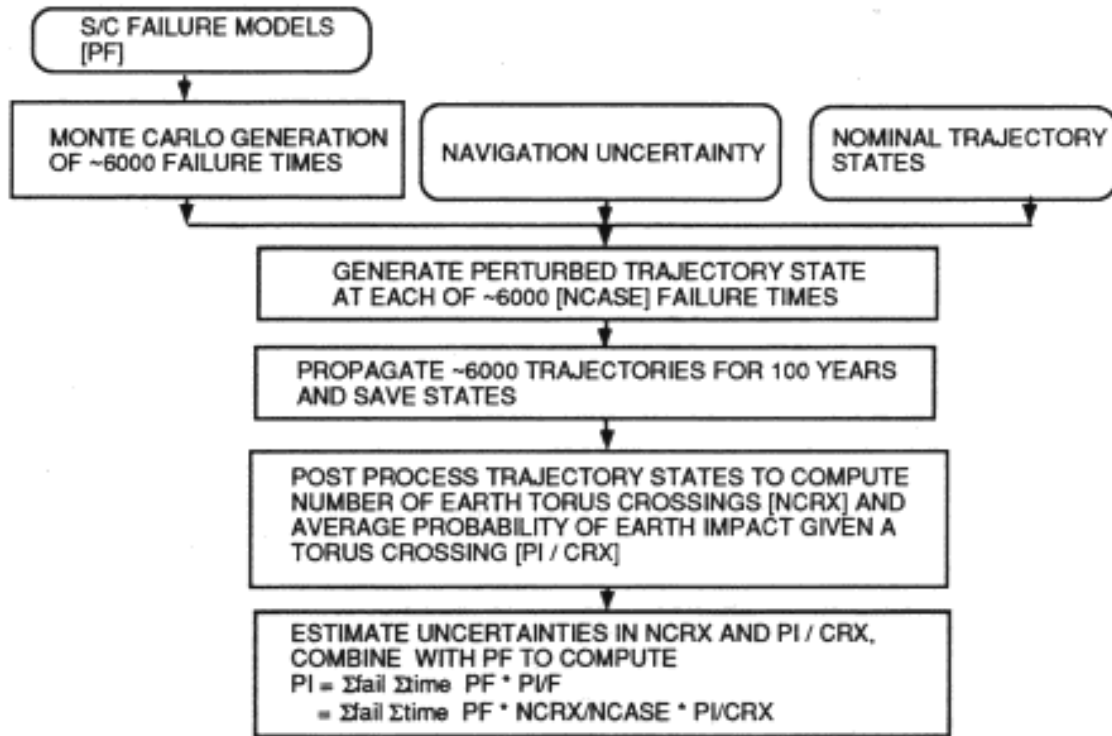


Figure 5-2 Process for Computing Long-Term Earth Impact Probability for Each Mission

### 5.2.1 Trajectory Design Strategy

Each maneuver targets the spacecraft to a nominal aimpoint at the next planetary swingby whose coordinates are usually expressed in terms of B-plane parameters (see Figure 4-1). The location of these nominal aimpoints affects both the short and long-term impact probabilities. An aimpoint biasing strategy was employed to minimize the short-term impact probability as detailed in Subsection 4.2. Since there exists some flexibility in the aimpoint biasing scheme used for the short-term analysis, iteration of the nominal aimpoint targets was performed, when deemed appropriate, to minimize both the short and long-term

impact probabilities. This iteration only occurred for aimpoints which tended to place the spacecraft on a trajectory which would eventually cross in the vicinity of the Earth torus. For the initial iteration, an aimpoint biasing scheme which considered only the short-term impact probability was used.

If the spacecraft fails during interplanetary cruise, it will still swingby the next targeted planet at an aimpoint within the last maneuver's orbit determination uncertainty mapped to the swingby planet B-plane. The spacecraft usually receives a very strong gravity assist from the planet due to its close proximity to the planet. This aimpoint therefore determines the initial heliocentric state of the spacecraft which is then monitored for the next 100 years to determine the number of Earth torus crossings. Since the first gravity assist following spacecraft failure is generally by far the largest perturbation the spacecraft will receive over the next 100 years, the swingby aimpoint greatly influences the long-term impact probability. For example, an aimpoint which places the spacecraft on a trajectory which initially crosses near the Earth torus is likely to have more torus crossings over 100 years than an aimpoint which places the spacecraft on a trajectory which is initially further away from the Earth torus.

It is not sufficient, however, just to examine the initial spacecraft state following the first planetary swingby after failure, since the spacecraft could continue on to the next targeted planetary swingby and the trajectory is always significantly perturbed in a difficult to predict manner by the third-body gravitational effects of Venus, Earth, and Jupiter. Since the third-body gravitational effects are not well predicted using analytic theory, numerical integration was used to propagate the spacecraft trajectory to better model the effects of these perturbations.

To first order, the short-term impact probability depends on the miss distance ( $B$ , see Figure 4-1) and is not sensitive to small variations (i.e., tens of degrees) in the  $\delta$ -plane angle. However, the gravity assist supplied by the planetary swingby and the resulting heliocentric spacecraft trajectory are sensitive to the B-plane angle. Therefore, if other state variables are fixed, the B-plane angle selected determines the initial spacecraft distance from the Earth torus. A typical strategy employed to minimize the long-term impact probability was for a given miss distance ( $B$ ), to select a B-plane angle which maximized the initial spacecraft distance from the Earth torus. If modifying the B-plane angle did not produce the desired geometry, then the miss distance,  $B$ , was also modified. Hundreds to thousands of sets of initial

conditions (i.e., Monte Carlo cases described in Subsection 5.2.2) were then propagated 100 years using numerical integration to examine the effects of third-body gravitational effects on the closest approach distance to the Earth torus. Hundreds of cases are required to adequately examine the dispersion about the nominal aimpoint due to navigation uncertainty. If too many of the Monte Carlo cases crossed in the vicinity of the Earth torus, a nominal aimpoint modification was performed to increase the initial distance from the Earth torus and the process was repeated

### 5.2.2 Monte Carlo Case Formulation

If exact knowledge of the spacecraft state at failure were available and the ability to precisely predict the spacecraft trajectory 100 years into the future existed, to determine if the spacecraft were to impact the Earth, the trajectory would simply be propagated 100 years beyond the failure time and checked for Earth impact. However, exact knowledge of the spacecraft state is never available due to orbit determination uncertainty and maneuver execution errors. In addition, the ability to accurately model the physical universe for such long time spans does not exist, since the long-term trajectory is extremely sensitive to small differences in the initial spacecraft state and the force modeling used to propagate the trajectory does not exactly model the actual perturbations experienced by the spacecraft. The time at which a failure could occur is specified in a probabilistic sense and thus a failure could occur anytime during cruise although failures are more likely at certain times than others.

Therefore, a small number of trajectories is not representative of the range of possible spacecraft trajectories which could result given a failure anytime during the interplanetary cruise. The solution adopted in this analysis is to perform a Monte Carlo analysis of thousands of trajectories. The primary and secondary Cassini trajectories were each evaluated using more than 6000 failure cases. The failure probability distribution was obtained by randomly sampling the cumulative failure probability distributions as many times as required until ~6000 failure times during cruise were obtained. The ~6000 cases resulted in sufficient numbers of torus crossings and sampling of the navigation aimpoint dispersions to provide confidence in the results. The influence of the number of cases run is discussed further in Subsection 5.3.1. Associated with each Monte Carlo case is an initial spacecraft orbital state which has been perturbed by navigation uncertainty.

Given a failure time, the initial conditions for the spacecraft state were obtained in the following manner. Navigation uncertainty encompassing both orbit determination and maneuver execution errors is typically expressed in terms of  $1\sigma$  B-plane aimpoint dispersions mapped to the next targeted planetary swingby. Different aimpoint dispersion data was supplied for each maneuver and perturbations in all 6 state variables as well as swingby epoch are modeled. Aimpoint dispersion data corresponding to the last maneuver before the failure time was randomly sampled to yield a perturbed swingby state which was then used as the initial state for the trajectory propagation. Each aimpoint dispersion was sampled at least 200 times and often up to 1000 times regardless of the likelihood of spacecraft failure on that maneuver segment to avoid undersampling the dispersion.

The initial conditions for the Monte Carlo cases therefore always occur at planetary swingbys. The perturbed aimpoint coordinates could have been mapped backward in time to the failure epoch, but the resulting trajectories would be the same. Furthermore, examination of perturbed planetary swingby states yields more intuitive information. For failure times between a planetary swingby and the next maneuver, the dispersion data from the last maneuver before the swingby was sampled. The only exception to this procedure is the initial conditions generated for the time period between Earth injection and the first maneuver. For these Monte Carlo cases whose failure time occurs before the first maneuver is performed, the perturbed initial conditions at Earth injection were created by sampling the injection covariance data, and the initial conditions were generated at Earth injection instead of at the next planetary swingby.

For failures on a trajectory leg where the next targeted swingby was not Earth, impact with the targeted body sometimes occurred. Most of these impacts occurred at the first Venus encounter of each mission. These cases were identified but not propagated. Impact with targeted Earth encounters is avoided by the strategy described in Subsection 4.2.

### 5.2.3 Orbital Geometry Required For Impact

For a given spacecraft trajectory corresponding to a failure event, several conditions are required for Earth impact to occur. The most likely outcome is that the spacecraft will never reencounter the Earth in 100 years. The orbital geometry of the spacecraft is used to compute the long-term Earth impact probability using theory used to estimate the probability of impact by Earth-crossing asteroids.

In order for any chance of Earth impact, the spacecraft must be present in the solar system. For nearly all failures during the second half of the interplanetary cruise, the spacecraft is ejected from the solar system by the strong Saturn gravity assist, precluding any possibility of Earth impact.

If the spacecraft is present in the solar system, in order for an Earth impact to occur, the spacecraft must at some time be present at Earth's orbital distance from the Sun. For this to occur, the periapsis (closest approach) distance of the spacecraft orbit with respect to the Sun must be less than the orbital distance of the Earth which is approximately 1 AU [=  $1.495 \times 10^8$  km ( $9.295 \times 10^7$  mi)] For many portions of the spacecraft trajectory, the periapsis distance is greater than 1 AU precluding any possibility of Earth impact except in the extremely unlikely event that a future accidental planetary encounter would alter the trajectory.

If the periapsis distance of the spacecraft after failure is less than 1 AU, crossings through the Earth torus are possible but uncommon since the spacecraft must be precisely on a trajectory which crosses through the Earth torus whose diameter (typically ~16,000 km (10,000 mi)) is quite small relative to the scale of the spacecraft's orbit whose dimensions are typically described in terms of 1 AU. The spacecraft may be on an Earth torus-crossing orbit at the failure time or may eventually be put on one by orbital perturbations such as gravitational perturbations by the planets and solar radiation pressure. Distant non-targeted gravity assists are actually quite common for some trajectory legs. For the ~6000 sets of initial conditions propagated for 100 years (600,000 years of trajectory data), on the order of several hundred torus crossings occurred.

In order for impact to occur, if the spacecraft does pass through the Earth torus, at the time the spacecraft crosses through the Earth torus, the Earth and spacecraft must occupy the same space in the torus at the same time - another highly unlikely event since the Earth's diameter is about 5 orders of magnitude smaller than its orbital circumference. To more precisely determine the probability of Earth impact given a torus crossing ( $P_{I/CRX}$  (i) in Equation 5-3), use was made of theory used to estimate the probability of impact by Earth-crossing asteroids. The value of  $P_{I/CRX}$  is on the order of  $10^{-5}$ .

5.2.3.1 Application of Earth-Crossing Asteroid Theory. If the spacecraft crosses through the Earth torus, Earth-Crossing asteroid theory is applied to compute the probability of impact. A fundamental paper was written in 1951 on the subject by Opik (ref.5-1), who subsequently revised and extended his work (refs.5-2 and 5-3). Further research was done by Arnold (refs.5-4 and 5-5) in the 1960's and more recently this topic has been addressed by Shoemaker, Wetherill, and others (refs.5-6 to 5-10). In this theory, the probability that the spacecraft is within the torus swept out by the Earth as it orbits the Sun is used to compute the probability of Earth impact. An advantage to this method is that passage of the spacecraft through the Earth torus is a more likely event than an actual collision with the Earth and thus provides a statistically significant set of data. A prohibitive number of Monte Carlo cases would probably have to be evaluated in order for a single Earth impact to result within 100 years. No Earth impacts were detected for any of the -6000 trajectory propagations conducted for each of the missions investigated.

In Earth-crossing asteroid theory, the average probability that the spacecraft is within the Earth torus over extremely long time spans is computed using very approximate analytical expressions (equivalent to the  $N_{CRX}/N_{CASE}$  term in Equation 5-3). This probability is multiplied by the probability that the Earth is in the correct position in its orbit at the time the spacecraft crosses through the Earth torus ( $P_{I/CRX}$ ) to compute the probability of Earth impact. This intersection geometry was discussed in Subsection 5.2.3 and is illustrated in Figure 5-1. The diameter of the Earth torus is twice the impact radius of the Earth, which is slightly larger than the Earth radius due to gravitational focusing. The Earth impact radius is a function of the velocity of the spacecraft relative to the Earth and the mass of the Earth.

Figure 5-1 shows that in order for an impact to occur, the spacecraft must cross through the Earth torus, and at the time of the crossing, the Earth must be at a position within the torus to cause impact. The probability that the spacecraft passes through the torus is computed differently than in the referenced Earth-crossing asteroid theories since the analytical expressions used to model the long-term orbital motion proved inadequate for the Cassini time frame and orbital characteristics. The analytic expressions used in these theories are only valid when considering time spans approaching millions of years for a restricted class of orbits and do not accurately depict what is likely to occur for Cassini trajectories in 100 years. In this analysis, the probability that the spacecraft passes through the Earth torus was computed by

numerically integrating each of the Monte Carlo cases using a high-precision trajectory propagation program and then counting the number of times the spacecraft actually passed through the Earth torus during these propagations. The total number of torus crossings ( $N_{CRX}$ ) divided by the total number of Monte Carlo cases ( $N_{CASE}$ ) yields the likelihood that the spacecraft will be within the torus during the interplanetary cruise. The estimated uncertainty in this torus-crossing frequency is discussed in Subsection 5.3.1.

Numerical integration of the trajectory provides the most realistic model of long-term orbital motion. Forces modeled included the gravity of all the planets and solar radiation pressure. Trajectory states were archived at least every 3 months and at every time the spacecraft's orbital distance from the Sun was equal to 1 AU for each 100-year propagation, and then post-processed to determine the number of spacecraft crossings through the Earth torus. The impact radius assumed for each torus crossing was different and was based on the velocity of the spacecraft relative to the Earth assuming that the Earth was in an impact position for that crossing. An elliptical torus was used whose shape was identical to that of the osculating orbit of the Earth at the torus crossing epoch. Passages through the Earth torus were detected using a root search algorithm which examined all closest approaches by the spacecraft to the Earth torus.

Earth-crossing asteroid theory was used to analytically compute  $P_{I/CRX}$  for each torus crossing. The  $P_{I/CRX}$  term is a function of the velocity vector of the spacecraft relative to the Earth at impact and is slightly different for each torus crossing; therefore, an average value was used to compute a best estimate value representative of all torus crossings. The theory may be used to compute  $P_{I/CRX}$  because no assumptions about long-term perturbations are made in this calculation. A basic assumption in the computation is that the Earth is equally likely to be anywhere in its orbit at the time of the crossing (ref.5-1). This assumption is valid for the long-term time period and is discussed in Subsection 5.3.1. Derivation of the analytic expression used is provided in the following Subsection 5.2.3.2.

5.2.3.2 Derivation of  $P_{I/CRX}$  Expression . The following derivation assumes that the spacecraft will pass through the Earth torus during a particular orbit. For spacecraft orbits inclined with respect to the Earth's orbit, an elliptical intersection region is formed by the intersection of the plane of the spacecraft's orbit and the Earth torus (see Figure 5-3). The velocity of the spacecraft relative to the Earth orbit node determines the

time spent by the spacecraft within this intersection ellipse during a spacecraft orbit, which contributes to the probability of Earth impact.

The average probability of impact,  $P$ , for passage through the elliptical intersection zone by the spacecraft per spacecraft revolution is:

$$P = \pi/4 P' \quad (5-4)$$

where  $P'$  is the average probability of collision with the Earth for a spacecraft trajectory which passes through the center of the elliptical intersection zone. It is assumed that the relative probability of a collision is proportional to the length of the chord of the intersection ellipse (which determines the time spent in the intersection zone). The average chord length is  $\pi/4$  times the maximum chord length, which is the distance traversed by the spacecraft if it passes through the center of the ellipse.

For a collision to occur, the Earth and spacecraft must be present within the intersection ellipse at the same time. The average probability of collision,  $P'$ , is proportional to the arc distance measured along the Earth's orbit for which any part of the Earth lies within the intersection ellipse (see Figure 5-4). This arc distance normalized by the heliocentric distance of the Earth is:

$$\eta = \tau |U| / \text{sqrt}[U_x^2 + U_z^2] \quad (5-5)$$

where  $\tau$  is the impact radius divided by the heliocentric distance of the Earth,  $|U|$  is the magnitude of the velocity of the spacecraft relative to the Earth divided by the heliocentric velocity of the Earth,  $U_x$  is the radial (Sun to Earth direction) component of  $U$ , and  $U_z$  is the component of  $U$  normal to the Earth orbit plane direction. For these calculations, the Earth is assumed to be at an impact position. The value  $\eta$  defines the range in Earth motion for which an impact is possible. The average probability of collision is simply  $2\eta$  divided by the circumference of the Earth's orbit, which when normalized by the Earth's  $c$  heliocentric distance is:

$$P' = |\eta|/\pi \quad (5-6)$$

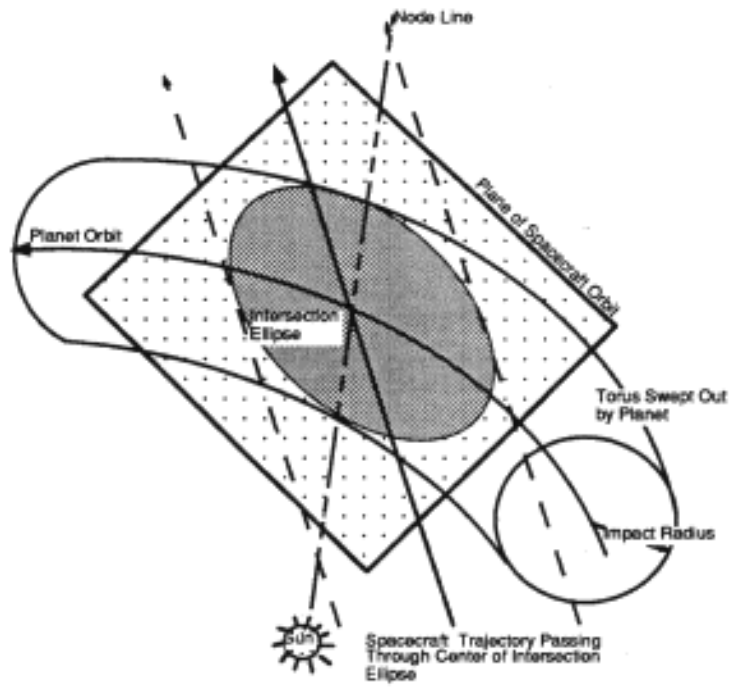


Figure 5-3 Spacecraft and Earth Orbit Intersection Geometry

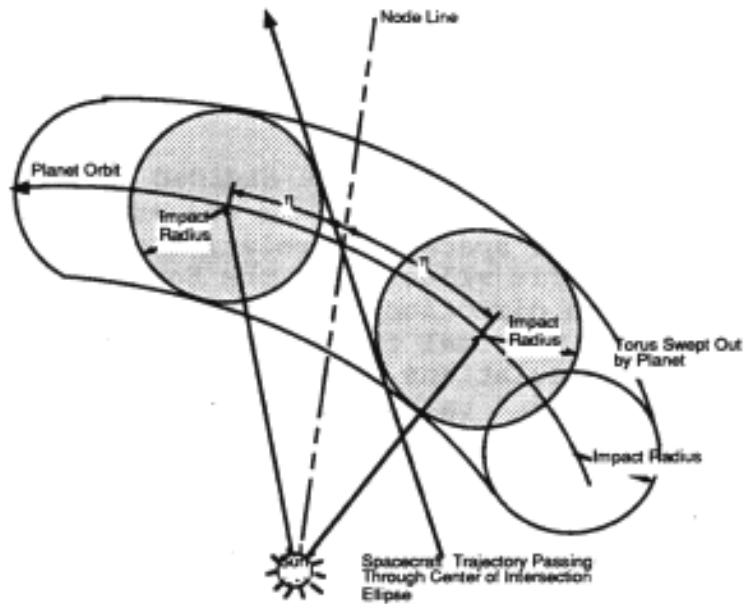


Figure 5-4 Range of Planet Motion for Which Intersection Is Possible

Equation 5-5 assumes that the Earth is equally likely to be anywhere in its orbit at the time of a torus crossing. For the long time spans considered in Earth-crossing asteroid theory and in this long-term analysis, this assumption is valid. Resonance between the spacecraft orbital period and that of the Earth can sometimes cause the Earth to be more or less likely to be in certain portions of its orbit at a torus crossing. These effects were studied as part of the uncertainty analysis presented in Subsection 5.3.1.

If the spacecraft's orbit partially crosses the Earth's orbit, collision is only possible within the fraction of the Earth's orbit crossed by the spacecraft. The spacecraft's orbit "partially crosses" the Earth's orbit if the spacecraft's perihelion or aphelion lies between Earth's perihelion and aphelion. In this case, the value of  $P'$  obtained from Equation 5-6 must be multiplied by this fraction,  $f$ , to obtain the probability of impact per spacecraft revolution.

By combining Equations 5-4, 5-5, and 5-6, the probability of impact within a spacecraft revolution is obtained:

$$P_{I/CRX} = f \tau |U| / ( 4 \text{ sqrt} [U_x^2 + U_z^2] ) \quad (5-7)$$

Passage of the spacecraft through the intersection ellipse often occurs for multiple revolutions of the spacecraft until orbital perturbations move the spacecraft orbit away from the Earth torus.

### 5.3 RESULTS

The probability of long-term Earth impact is presented and discussed in this subsection. Other long-term characteristics pertinent to the Earth impact analysis are also presented.

An uncertainty analysis is first described which yields uncertainties for the torus-crossing frequency ( $N_{CRX}/N_{CASE}$ ) and probability of Earth impact given a torus crossing ( $P_{I/CRX}$ ) terms which are required to compute the long-term Earth impact p.d.f. (see Equation 5-3). The contribution to Earth impact probability will be shown to be influenced by the interplanetary trajectory characteristics at the failure time.

### 5.3.1 Uncertainty Analysis

Several parameter and model uncertainties enter into the long-term impact probability calculation. They are the spacecraft system internal failure uncertainty, the micrometeoroid failure model uncertainty, the Earth torus-crossing frequency uncertainty, and (given a torus crossing) the Earth impact probability uncertainty. All of the uncertainties take the form of a log-normal distribution, except the torus-crossing frequency uncertainty, which is a normal (Gaussian) distribution. Probability distributions for each term in the long-term Earth impact Equation 5-3 are combined to yield a single long-term p.d.f. as described in Subsection 5.3.2. Probability distributions for the probability of failure,  $P_F(i)$ , are detailed in Subsection 3 for each failure mode. Probability distributions for the  $N_{CRX/NCASE}$  and  $P_{I/CRX}$  terms were constructed as follows using empirical analysis and engineering judgment.

The mean value of  $N_{CRX/NCASE}$  was computed by counting the torus crossings detected for all Monte Carlo cases. A normal distribution for this torus-crossing frequency was constructed by estimating a sigma due to all uncertainties. The dominant uncertainties in the computation of the torus-crossing frequency are listed in Table 5-1. One  $\sigma$  uncertainties are listed in terms of the percentage of the mean value of  $N_{CRX/NCASE}$  and were root-sum-squared to yield a final sigma.

Navigation uncertainty results from orbit determination and maneuver execution uncertainty, and enters into the computation of the initial trajectory states for each Monte Carlo case as described in Subsection 5.2.2. The contribution due to navigation uncertainty was estimated by evaluating trajectory legs which had significant numbers of torus crossings using 10%, 50%, and 90% navigation uncertainties to generate the initial states. One  $\sigma$  variations in the number of torus crossings were then computed by comparing the difference in the torus-crossing counts for each navigation uncertainty. The analysis showed that the  $1\sigma$  variation in the number of torus crossings approaches 20% of the mean total. The 50% navigation uncertainty was used to compute the mean torus-crossing frequency for the nominal study. The uncertainty due to solar radiation pressure force modeling in the trajectory propagation was computed in a similar manner. The nominal solar radiation pressure force was scaled to higher and lower values and certain trajectory legs propagated again. The variation in the number of torus crossings was then used to compute the uncertainty.

Table 5-1 Dominant Contributors to  
NCRX/NCASE and P<sub>I</sub>/CRX Uncertainties

Term	Source of Uncertainty	VVEJGA Uncertainty	VEEGA Uncertainty
NCRX/NCASE		Uncert.= 1 sigma / mean	
	Navigation	0.2	0.2
	Solar Radiation Pressure	0.15	0.15
	Sample Size	0.05	0.03
P <sub>I</sub> /CRX		5% Confidence= Median/Uncert. 95% Confid.= Median x Uncert.	
	Random Earth Location at Torus Crossing	5	6

The uncertainty in the number of torus crossings due to the number of Monte Carlo cases considered is roughly equal to the square root of the number of torus crossings detected. For example, if 100 torus crossings were detected in 300 cases, the uncertainty would be  $\sim 10/300$ . Examining the sensitivity of the torus crossing frequency to the number of Monte Carlo cases propagated was another method used to estimate the effect of sample size.

The median value of the probability of Earth impact given a torus crossing, P<sub>I</sub>/CRX, was computed as the average of all values computed at each torus crossing. A sigma for this term was estimated in order to construct a log-normal distribution. The dominant uncertainty in P<sub>I</sub>/CRX is due to the assumption that the Earth is equally likely to be anywhere in its orbit at the time of a torus crossing. Uncertainties due to navigation, solar radiation pressure, and sample size were found to be negligible compared to the random Earth location assumption.

For the long time spans considered in Earth-crossing asteroid theory and in this long-term analysis, the assumption that Earth is equally likely to be anywhere in its orbit is valid. The trajectory can be predicted for the first few years, but predictive accuracy quickly degrades due to lack of precise knowledge of the initial spacecraft state and an inability to exactly model the

physical universe. Resonance between the spacecraft orbital period and that of the Earth can sometimes cause the Earth to be more or less likely to be in certain portions in its orbit at a torus crossing. These effects were studied as part of the uncertainty analysis. The uncertainty analysis did not invalidate the relation but resulted in the specification of a large uncertainty for the  $P_{I/CRX}$  term. The uncertainty is slightly different for each mission since the degree to which orbital resonance plays a role is a function of the trajectory characteristics. Uncertainty values are listed in Table 5-1 as a multiplication or division factor to the mean. For example, for the VVEJGA trajectory, 5% of the  $P_{I/CRX}$  values are estimated to possibly be beyond 5 times the median value and 5% are estimated to be below the median value divided by 5. The uncertainty values were based both on empirical analysis of the location of the Earth in its orbit at each torus crossing and engineering judgment as to the accuracy of the Earth-crossing asteroid theory used.

### 5.3.2 Long-Term Earth Impact Probability

Distributions for each term in Equation 5-3 used to compute  $P_I$  were combined to yield a long-term probability density function (p.d.f.) for the primary VVEJGA and secondary VEEGA trajectories. All of the uncertainties take the form of a log-normal distribution, except for the torus-crossing frequency, which is a normal (Gaussian) distribution. A log-normal distribution is expected to arise when several variables with independent distributions are multiplied, especially when most of those distributions are themselves log-normal. These distributions were combined using a Monte Carlo simulation (separate from the Monte Carlo analysis which produced the data) of 1000 points for both the primary and secondary trajectories. 1000 points are sufficient to generate a distribution within the accuracy of the analysis. A maximum-likelihood fit was made to a log-normal distribution. The simulation data was used to produce p.d.f. and complementary cumulative distributions for each mission as shown in Figures 5-5 to 5-8. The points plotted are fractions of the 1000 simulations of the long-term impact probability, and the solid curves are the fit log-normal distributions. The mean value of the long-term Earth impact probability,  $P_I$ , is  $1.4 \times 10^{-7}$  for the primary and  $3.5 \times 10^{-7}$  for the secondary mission.

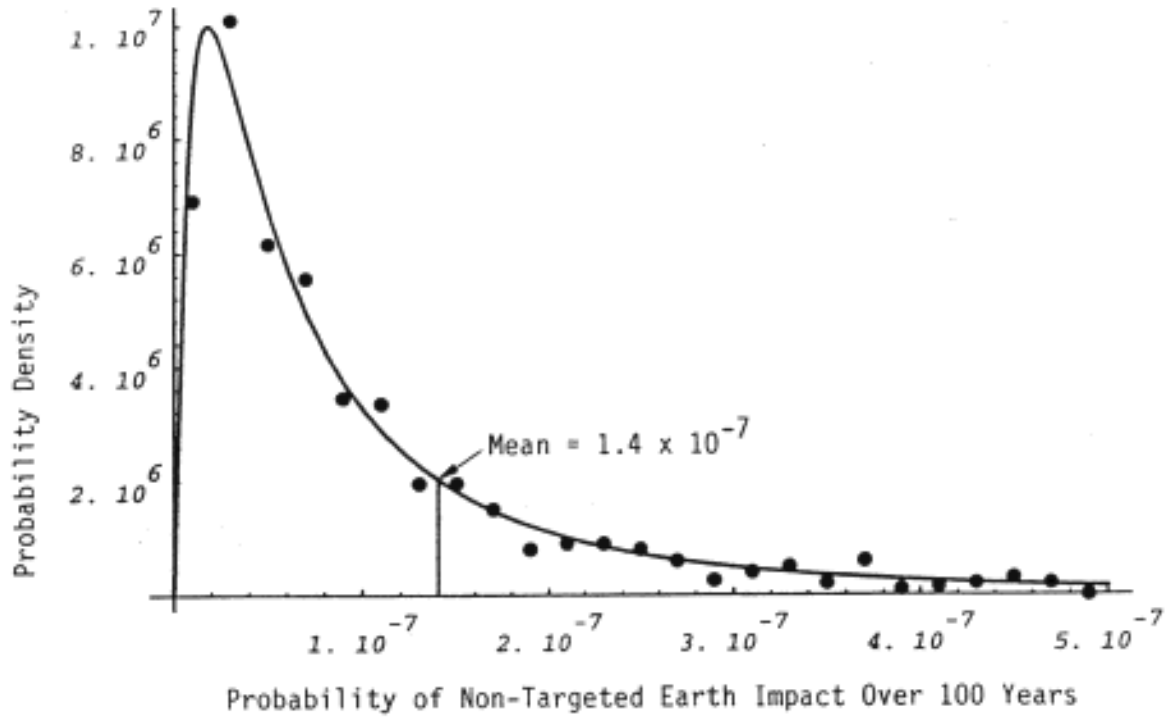


Figure 5-5 Long-Term Earth Impact Probability Density Function for Primary Mission

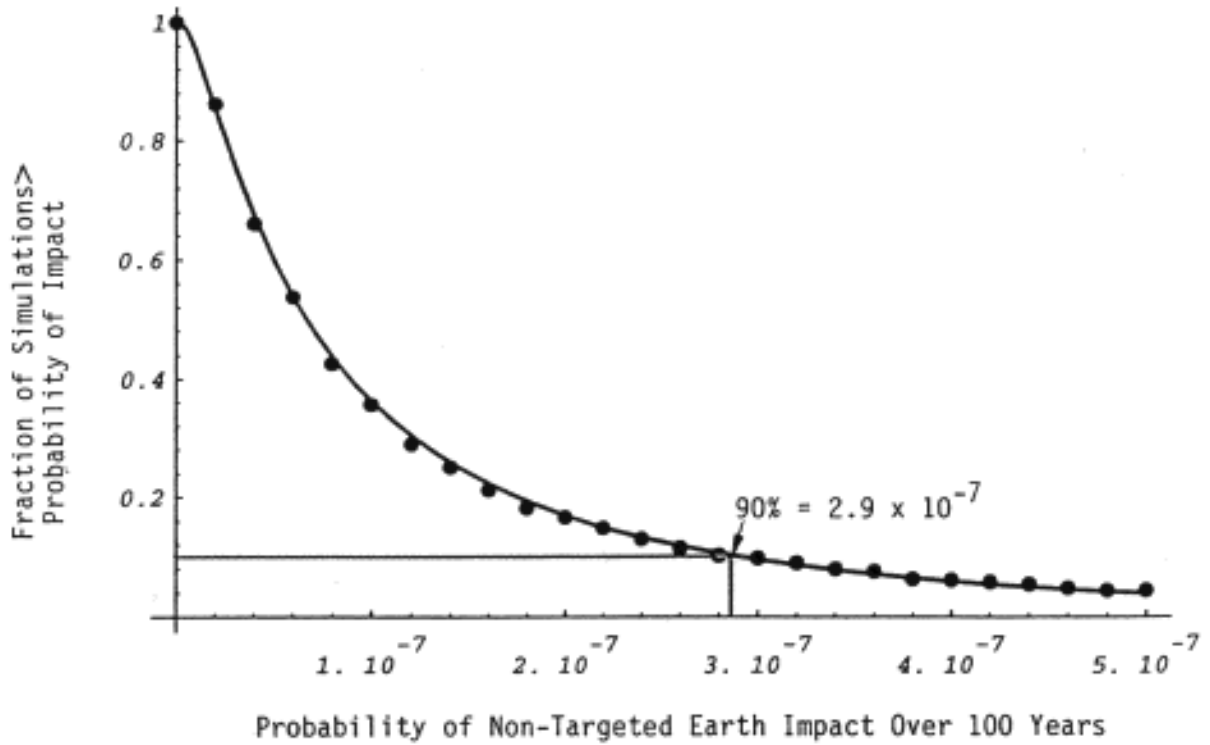


Figure 5-6 Long-Term Earth Impact Complementary Cumulative Distribution for Primary Mission

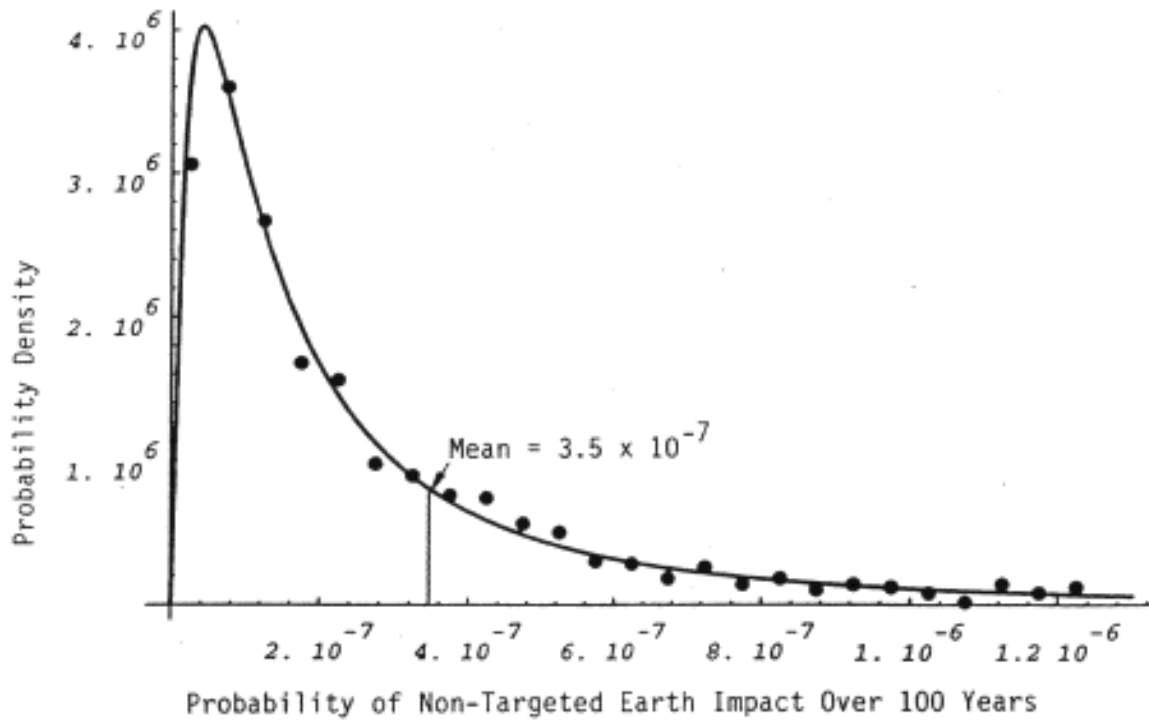


Figure 5-7 Long-Term Earth Impact Probability Density Function for Secondary Mission

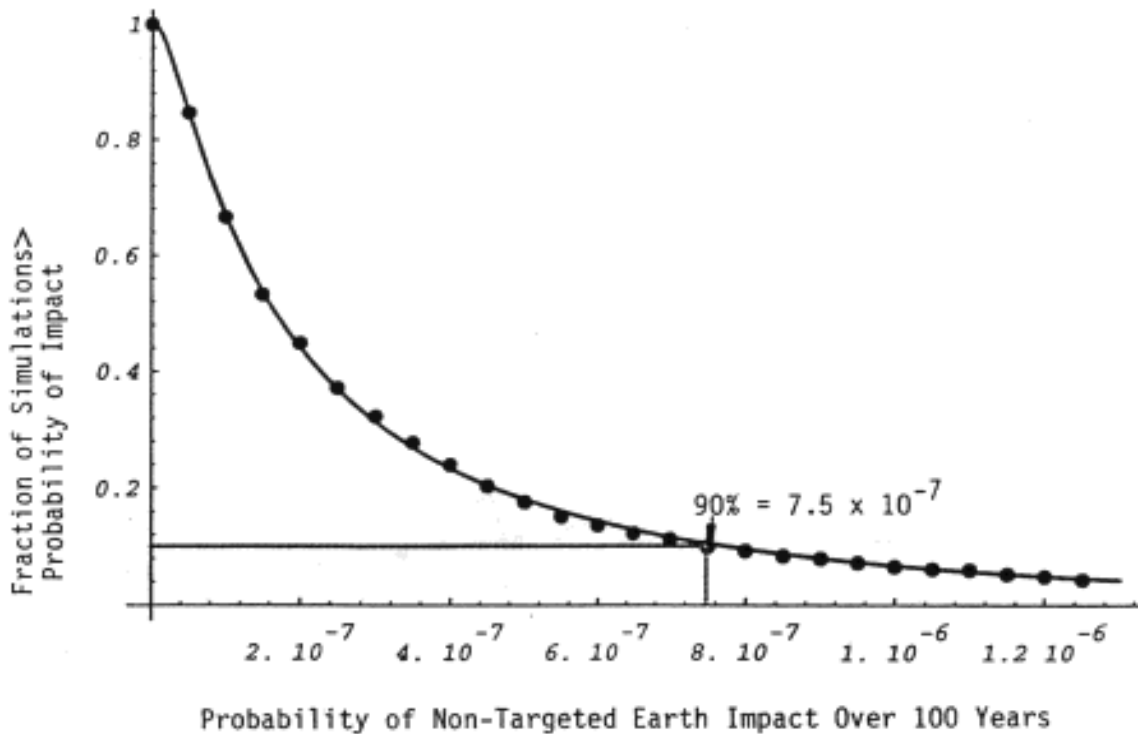


Figure 5-8 Long-Term Earth Impact Complementary Cumulative Distribution for Secondary Mission

### 5.3.3 Influence of Trajectory Characteristics on Long-Term Earth Impact Probability

The probability of Earth impact is a function of the spacecraft trajectory characteristics at failure and their evolution over the next 100 years. The spacecraft trajectory orbital characteristics change significantly at targeted planetary swingbys or after major maneuvers. Recall that targeted swingbys are those planetary swingbys which are part of the nominal sequence of planned swingbys during cruise. Over a 100 year time period, the third-body gravitational effects of primarily Venus, Earth, and Jupiter can also significantly alter the spacecraft trajectory.

The number of torus crossings is influenced by the trajectory geometry at failure. If the spacecraft fails during interplanetary cruise, it will usually continue to swingby the next targeted planet at an aimpoint within the aimpoint dispersion corresponding to the last maneuver before failure. The size of the aimpoint dispersion at the next targeted planetary swingby determines the scatter in the post-swingby trajectories and is due to navigation uncertainty. Aimpoint dispersions tend to be smaller when the next targeted swingby is Earth rather than another planet in order to ensure the short-term (i.e., targeted Earth swingby(s)) Earth impact probability is controlled to an acceptably low level. The spacecraft can receive multiple targeted gravity assists even after failure if no major maneuvers are required and the aimpoint dispersions are sufficiently small, but such occurrences are rare.

Although torus crossings may occur within the first 100 years, the mean time to impact is much greater. A rough estimate of the mean time to impact can be computed using theory presented in Reference 1. The mean time to impact is a function of the spacecraft orbit's semi-major axis, the torus crossing frequency ( $N_{CRX/NCASE}$ ), and the probability of impact given a torus crossing ( $P_{I/CRX}$ ). The mean time to impact was estimated for each trajectory segment and ranges from 105 to beyond 106 years. Within the first few thousand years, the likelihood of torus crossings is greater since the spacecraft is targeted for at least one Earth swingby during the interplanetary cruise, resulting in a spacecraft orbit which is initially in the vicinity of Earth's orbit. Long-term perturbations tend to move the spacecraft orbit away from its initial orientation, but over millennia the torus crossing geometry can be reestablished by long-term orbital perturbations.

Failures on legs targeted to Venus or Earth swingbys tend to result in trajectories for which a portion of the orbit remains in the vicinity of Earth's orbit. To determine the vicinity to the Earth torus, the spacecraft orbit's ascending and descending node distance with respect to the Earth's orbital plane (i.e., the ecliptic plane) are examined. If the spacecraft orbit inclination with respect to the ecliptic is nonzero and the node crossing distances are well away from 1 AU [= 1.495x10<sup>8</sup> km (9.295x10<sup>7</sup> mi)] , then future torus passages are unlikely since third-body gravitational perturbations do not radically alter the spacecraft orbit. If the ascending or descending node distance is in the vicinity of 1 AU, the effects of third-body gravitation perturbations over 100 years are studied and an iterative aimpoint strategy which maximizes the initial node distance from the Earth torus may be employed using the trajectory design strategy described in Subsection 5.2.2.

Most torus crossings occur on legs for which the next targeted planetary swingby after spacecraft failure places the spacecraft orbit in the vicinity of the Earth torus. Even if this initial spacecraft orbit does not pass through the Earth torus, third-body gravitational effects can cause the spacecraft to pass through the torus at a later date. In general, for spacecraft orbits whose heliocentric apoapsis distance (farthest point in the spacecraft orbit from the Sun) is less than about 1 AU [= 1.495x10<sup>8</sup> km (9.295x10<sup>7</sup> ml)] , third-body gravitational perturbations by Venus and Earth are the dominant long-term perturbations to the spacecraft orbit. For spacecraft orbits whose heliocentric apoapsis distance is well beyond 1 AU, the third-body effects of Jupiter are the dominant long-term orbital perturbation. Even though Jupiter is always many AUs distant from the spacecraft, it can still significantly perturb the spacecraft orbit due to its large mass.

Failures on legs targeted to Jupiter or Saturn result in trajectories which never return to the vicinity of Earth's orbit. The Jupiter gravity assist on the primary trajectory raises the spacecraft orbit periapsis (closest approach distance to the Sun) well above the distance of the Earth torus precluding any torus crossings. The periapsis radius remains above this initial value for the duration of the long-term analysis. For both the primary and secondary trajectories, when failures occur on legs targeted to Saturn, the Saturn aimpoint dispersion is located such that ejection from the solar system by the Saturn swingby occurs more than 99.5% of the time. The few trajectories whose arrival conditions are outside the ejection region have their orbit periapses raised above 5

AU [ $7.49 \times 10^8$  km ( $4.55 \times 10^8$  ml)] by the Saturn swingby thereby precluding any torus crossings on legs targeted to Saturn.

The relation between the spacecraft trajectory geometry at failure and the long-term Earth impact probability is discussed in greater detail for the primary and secondary missions in the following two Subsections. Since torus crossings must occur in order to have a nonzero long-term Earth impact probability, the likelihood of torus crossings as a function of the spacecraft failure time and the resulting trajectory are discussed.

#### 5.3.3.1 Primary VVEJGA Long-Term Behavior.

The total number of torus crossings resulting from the ~6000 sets of Monte Carlo initial states, each propagated 100 years (a total time period of ~600,000 years), was 228 for the primary mission. Torus crossings are therefore a rare event. The probability of Earth impact given a torus crossing ( $P_{I/CRX}$  in Equation 5-3) varies slightly with the spacecraft geometry at crossing but averaged about  $1.6 \times 10^{-5}$ .

For the primary VVEJGA trajectory, few torus crossings occur on the Earth injection to Venus-1 leg, since for failures on this leg, the subsequent Venus-1 gravity assist places the initial spacecraft orbit sufficiently far away from the Earth torus that long-term perturbations do not cause the spacecraft orbit to pass through the torus at a later date. This behavior results because the nominal aimpoint at Venus-1 is designed to send the spacecraft to a second targeted Venus swingby and therefore not to the vicinity of the Earth torus. For failure times between Venus-1 and the large deep space maneuver (between Venus-1 and Venus-2), few torus crossings occur for similar reasons since without the large deep space maneuver, the Venus-2 swingby never occurs, keeping the spacecraft on a trajectory far away from the Earth torus.

Most torus crossings occur due to failures occurring between the large deep space maneuver (between Venus-1 and Venus-2) and the Venus-2 swingby. For failures on this leg, a small fraction of the trajectories receive the required geometry at the Venus-2 swingby to send the spacecraft to the vicinity of Earth torus. This is expected since the purpose of the Venus-2 swingby is to target the spacecraft to the targeted Earth swingby. Almost no torus crossings occur due to failures on the short (<2 months) Venus-2 to Earth leg of the trajectory where significant aimpoint bias is employed to reduce the short-term impact probability (see Subsection 4.2). The

biased Earth aimpoints are also favorable for the long-term since if the spacecraft should fail, the subsequent Earth gravity assist places the spacecraft sufficiently far away from the torus that third-body perturbations over the next 100 years do not result in torus passages (see aimpoint design strategy discussion in Subsection 5.2.1). Failures just before the targeted Earth swingby receive an Earth gravity assist which sends the spacecraft on to the targeted Jupiter swingby, where the Jupiter gravity assist virtually assures no torus crossings can ever occur.

For failures between the targeted Earth swingby (-1.8 years after launch) and Jupiter, the spacecraft is always targeted to the vicinity of Jupiter where it receives a powerful gravity assist that raises the distance at the nearest point in the spacecraft orbit to the Sun (i.e., orbit periapsis) to greater than 1.4 AU [ $2.09 \times 10^8$  km ( $1.30 \times 10^8$  mi)]. The periapsis radius remains above this initial value for the duration of the long-term analysis precluding any torus crossings. No torus crossings occur due to failures on the Jupiter to Saturn leg either since, as discussed above (Subsection 5.3.3), Saturn usually ejects the spacecraft from the solar system or raises spacecraft orbit periapsis to the point where no torus crossings are possible. Note that these trajectory legs occupy a considerable portion of the entire cruise duration. Gravity assists by Jupiter and Saturn virtually assure that failures during the last 72% of the primary mission will not result in Earth impact.

#### 5.3.3.2 Secondary VEEGA Long-Term Behavior.

The total number of torus crossings resulting from the -6000 sets of Monte Carlo initial states, each propagated 100 years (a total time period of -600,000 years), was 465 for the secondary mission. Torus crossings are therefore a rare event. The probability of Earth impact given a torus crossing (PI/CRX in Equation 5-3) varies slightly with the spacecraft geometry at crossing but averaged about  $1.5 \times 10^{-5}$ .

For the VEEGA secondary trajectory, few torus crossings occur on the Earth injection to Venus leg even though the purpose of the Venus swingby on the secondary mission is to target the spacecraft to the Earth-1 swingby. The number of torus crossings is small since the nominal Venus swingby aimpoint was designed to result in post-swingby trajectories which did not cross near the Earth torus. The spacecraft is not targeted to the vicinity of the Earth until after the large deep space maneuver at 100 days before Earth-1 swingby

Most torus crossings occurred on the Venus to Earth-1 leg of the trajectory where significant aimpoint biasing is employed to reduce the short-term impact probability (see Subsection 4.2). The biased Earth-1 aimpoints were designed to minimize the long-term impact probability using the aimpoint iteration strategy described in Subsection 5.2.1. Failures on this leg of the trajectory tend to place the spacecraft orbit in the vicinity of Earth torus since the next targeted swingby is Earth-1, but judicious selection of biased aimpoints insures that most failure cases will never cross through the torus for the duration of the long-term analysis.

Almost no torus crossings occur on the Earth-1 to Earth-2 leg of the trajectory due to the adoption of two trajectory design strategies. First, the inclination of the spacecraft orbit with respect to the Earth's orbital plane (i.e., the ecliptic plane) was increased from near zero to  $0.2^\circ$  by expending additional  $\Delta V$  at the large deep space maneuver between Earth-1 and Earth-2. Without this inclination change, passage through the Earth torus is a much more likely event following spacecraft failure. Secondly, the biased Earth-2 aimpoints were also designed to minimize the long-term impact probability using the aimpoint iteration strategy described in Subsection 5.2.1.

For failures between the targeted Earth-2 swingby (-4.7 years after launch) and Saturn, just as in the primary mission, Saturn usually ejects the spacecraft from the solar system or raises spacecraft orbit periapsis to the point where no torus crossings are possible. Note that the Earth-2 to Saturn leg comprises ~50% of the total cruise duration, and thus for the last half of secondary mission interplanetary cruise, failures do not result in Earth impact.

#### 5.4 CONCLUSIONS

This analysis computed the probability of Earth impact by a non-targeted Earth swingby within 100 years following a possible spacecraft failure during cruise. p.d.f.s for the long-term probability of Earth impact were generated for the primary and secondary missions. The mean probability of Earth impact for the long-term is  $1.4 \times 10^{-7}$  for the primary mission and  $3.5 \times 10^{-7}$  for the secondary mission. For trajectories for which long-term impact is possible, the mean time to impact is estimated to range from  $10^5$  to beyond  $10^6$  years.

The significant spacecraft failure mode for the long-term is spacecraft system internal failure. The probability of impact given failure is influenced by the

trajectory characteristics of the spacecraft at the time of failure and long-term third-body gravitational effects primarily by Venus, Earth, and Jupiter. Gravity assists by the massive outer planets virtually assure that failures during the last 72% of the primary and last 50% of the secondary interplanetary cruise do not result in Earth impact.

## REFERENCES

- 5-1 Opik, E.J, "Collision Probabilities With the Planets and Distribution of Interplanetary Matter", Proceedings of the Royal Irish Academy vol. 54A, 1951.
- 5-2 Opik, E.J, "The Dynamical Aspects of the Origin of Comets", Liege Mem. vol. 8, Ser. 5, 12 (Armagh Observatory Contributions, vol. 53), 1966.
- 5-3 Opik, E.J., Interplanetary Encounters: Close-Range Gravitational Interactions, Scientific Publishing Company, Amsterdam, 1976.
- 5-4 Arnold, J.R., The Origin of Meteorites as Small Bodies, in Isotopic and Cosmic Chemistry, Craig, H., S.L., Miller and G.J. Wasserburg, ea., North Holland Publishing Co., Amsterdam, pp. 347-364, 1964.
- 5-5 Arnold, J.R., The Origin of Meteorites as Small Bodies, II and III, Astrophysical. J. 141: 1536-1547; 1548-1556, 1965.
- 5-6 Shoemaker, E.M., J.G. Williams, E.F. Helin, and R.F. Wolfe, "Earth Crossing Asteroids: Orbital Classes, Collision Rates With Earth, and Origin", in Asteroids, T. Gehrels, ea., University of Arizona Press, Tucson, 1979.
- 5-7 Shoemaker, E.M., R.F. Wolfe, and C.S. Shoemaker, "Asteroid and Comet Flux in the Neighborhood of Earth", Geological Society of America special paper 247, 1990.
- 5-8 Wetherill, G.W. and Shoemaker, E.M, "Collision of Astronomically Observable Bodies with the Earth", Geological Society of America Special Paper 190, in Geological Implications of Impacts of Large Asteroids and Comets on the Earth, Silver, L.T., and H.T. Schultz, eds., Boulder, CO, 1982.
- 5-9 Friedlander, A.L., and D.R. Davis, "Long-Term Risk Analysis Associated with Nuclear Waste Disposal in Space", AAS Paper 79-175, presented at the AAS/AIAA Astrodynamics Specialist Conference, Provincetown, MA, 1979.
- 5-10 Greenberg, R. and M.C. Nolan, "Delivery of Asteroids and Meteorites to the Inner Solar System", in Asteroids 2, T. Gehrels, ea., University of Arizona Press, Tucson, 1989.

## SECTION 6

### EARTH IMPACT PROBABILITY ASSESSMENT

The short-term probability of Earth impact and the long-term probability of Earth impact were combined probabilistically for both the primary and secondary trajectories. The data from the 1000 Monte Carlo simulations for the short-term impact probability on the primary trajectory calculated in Section 4 were added point-by-point to the data from the 1000 Monte Carlo simulations for the long-term impact probability on the primary trajectory calculated in Section 5. This provided a 1000-point Monte Carlo simulation for the total probability distribution for Earth impact on the primary trajectory. The same procedure was used for the secondary trajectory.

The p.d.f. and complementary cumulative probabilities for the primary and secondary trajectories are presented in Figures 6-1 thru 6-4. The mean values of these distributions are  $7.6 \times 10^{-7}$  for the primary trajectory and  $8.3 \times 10^{-7}$  for the secondary trajectory. Since the means of both distributions are less than  $10^{-6}$ , the Project Earth impact requirement is satisfied for both missions. For reference, Figures 6-2 and 6-4 also indicate values below which 90% of the possible Earth impact probabilities lie.

As the probability distributions for the short-term and long-term probabilities were largely but not completely independent, Monte Carlo simulations were run to test the effects of correlation. Correlation was demonstrated to have no significant effect on the results.

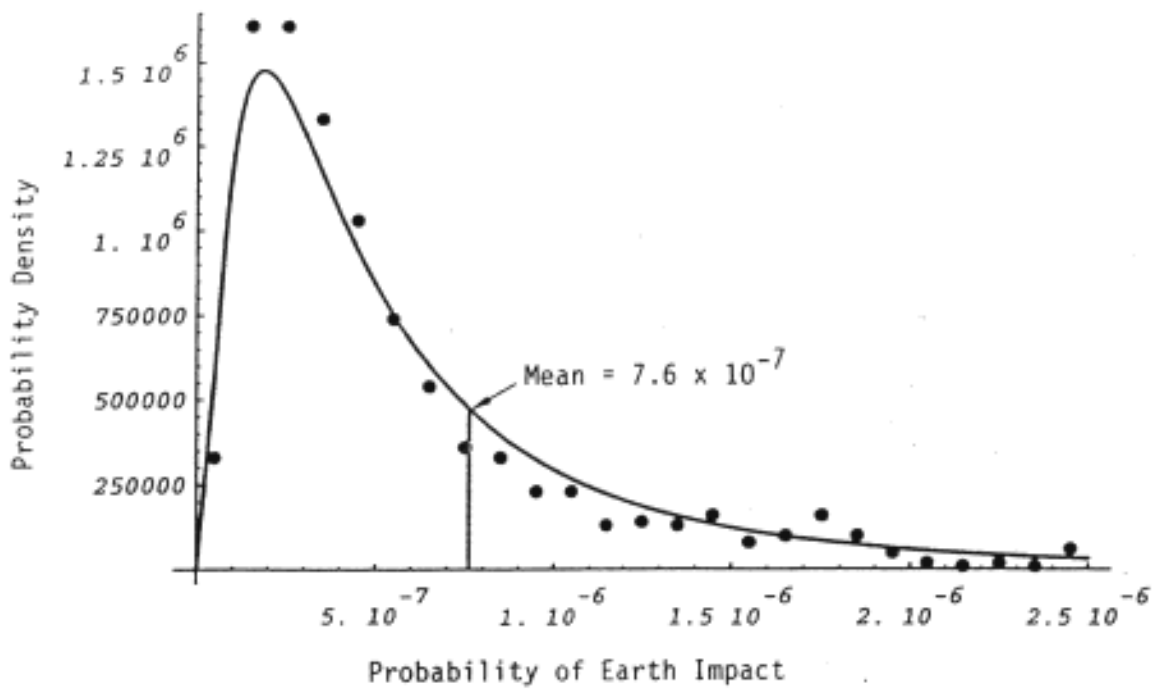


Figure 6-1 Primary Mission Probability Density Function

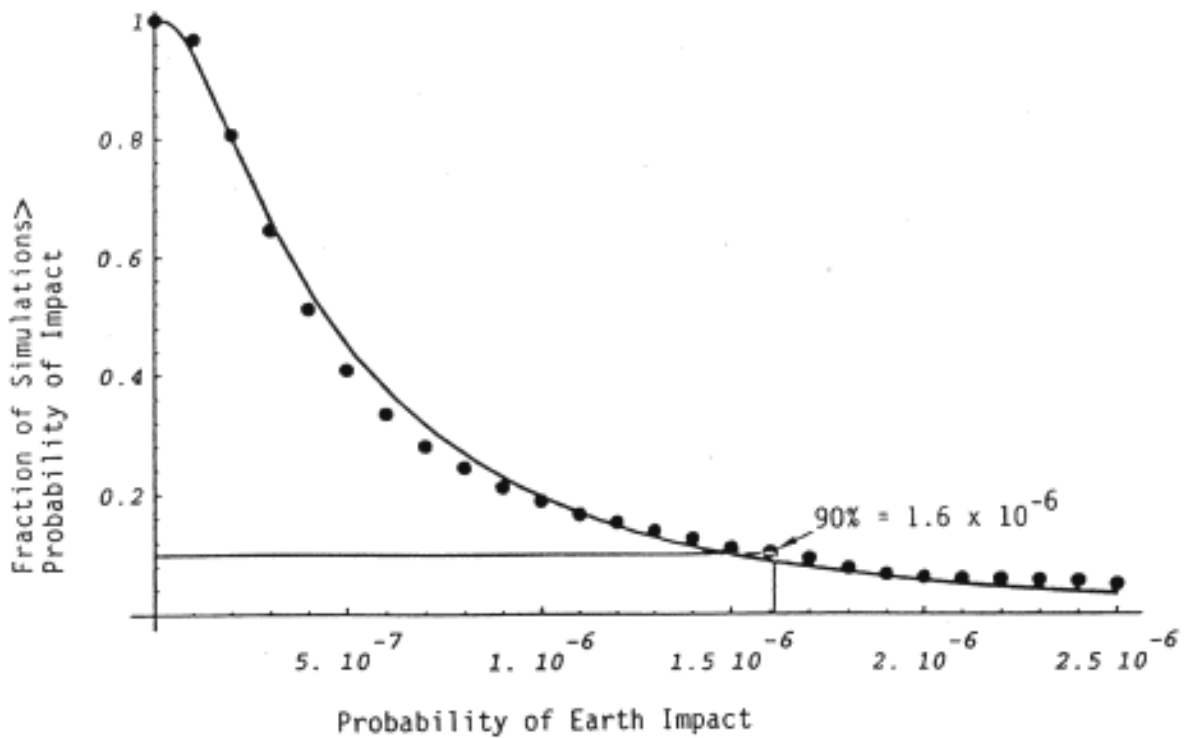


Figure 6-2 Primary Mission Complementary Cumulative Probability

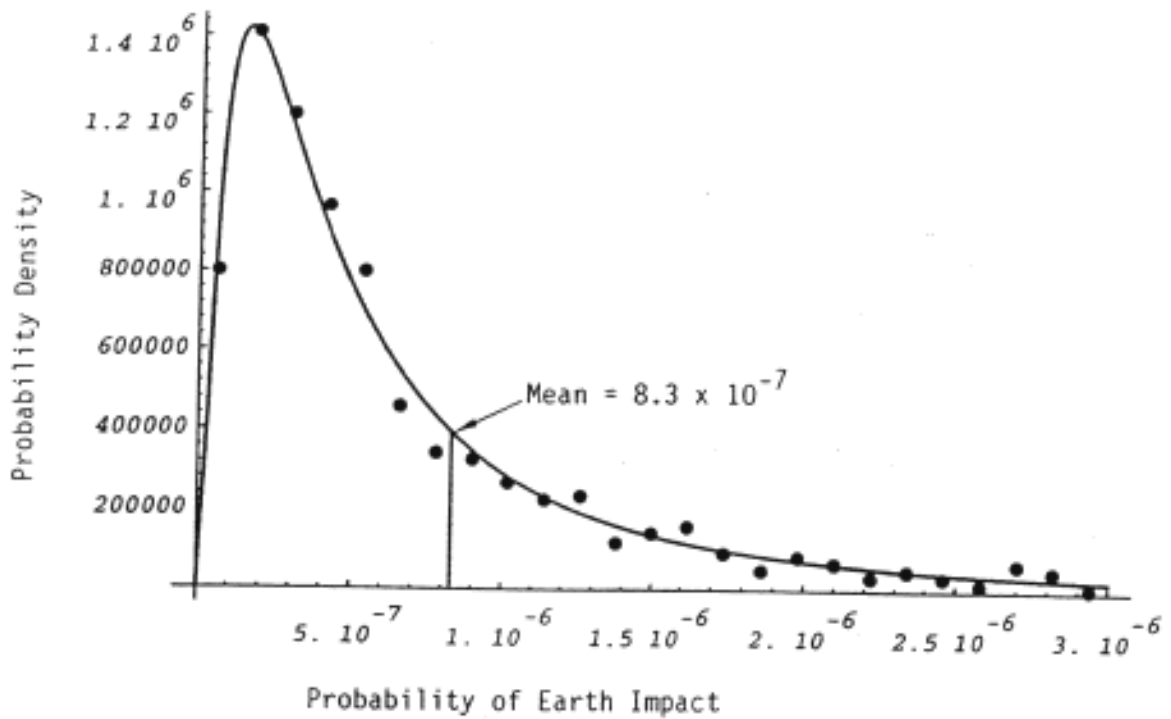


Figure 6-3 Secondary Mission Probability Density Function

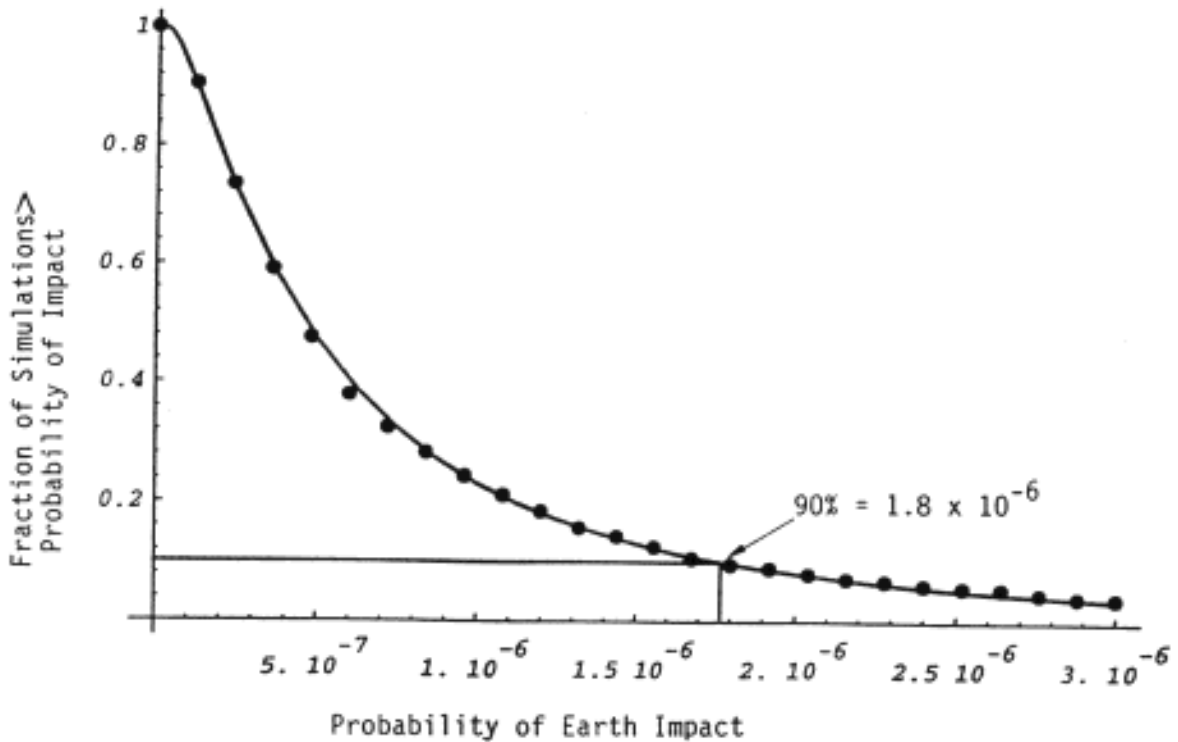


Figure 6-4 Secondary Mission Complementary Cumulative Probability

## **Cassini Environmental Impact Statement Supporting Studies**

Executive Summary

Volume 1 - Program Description

Volume 2 - Alternate Mission and Power Study

Volume 3 - Earth Swingby Plan

Earth Swingby Plan Supplement